

Lawrence Berkeley National Laboratory

Recent Work

Title

A MULTI-FEEDZONE GEOTHERMAL WELLBORE SIMULATOR

Permalink

<https://escholarship.org/uc/item/4fj9533v>

Author

Bjornsson, G.

Publication Date

1987-05-01



Lawrence Berkeley Laboratory

UNIVERSITY OF CALIFORNIA

EARTH SCIENCES DIVISION

RECEIVED
LAWRENCE
BERKELEY LABORATORY

A Multi-Feedzone Geothermal Wellbore Simulator FEB 15 1989

G. Bjornsson
(M.S. Thesis)

LIBRARY AND
DOCUMENTS SECTION

May 1987

TWO-WEEK LOAN COPY

*This is a Library Circulating Copy
which may be borrowed for two weeks.*



LBL-23546
c.2

DISCLAIMER

This document was prepared as an account of work sponsored by the United States Government. While this document is believed to contain correct information, neither the United States Government nor any agency thereof, nor the Regents of the University of California, nor any of their employees, makes any warranty, express or implied, or assumes any legal responsibility for the accuracy, completeness, or usefulness of any information, apparatus, product, or process disclosed, or represents that its use would not infringe privately owned rights. Reference herein to any specific commercial product, process, or service by its trade name, trademark, manufacturer, or otherwise, does not necessarily constitute or imply its endorsement, recommendation, or favoring by the United States Government or any agency thereof, or the Regents of the University of California. The views and opinions of authors expressed herein do not necessarily state or reflect those of the United States Government or any agency thereof or the Regents of the University of California.

A Multi-Feedzone Geothermal Wellbore Simulator

Grimur Bjornsson
(M.S. Thesis)

Earth Sciences Division
Lawrence Berkeley Laboratory
1 Cyclotron Road
Berkeley, California 94720

May 1987

Table of Contents

LIST OF FIGURES	iii
LIST OF TABLES	v
NOMENCLATURE	vi
ACKNOWLEDGEMENTS	x
1.0 INTRODUCTION	1
2.0 BACKGROUND	5
3.0 FLUID FLOW IN GEOTHERMAL WELLS	8
3.1 Introduction	8
3.2 General Governing Equations	8
3.3 Single Phase Flow	9
3.4 Two Phase Flow	10
3.4.1 Basic Definitions	10
3.4.2 Two-Phase Flow Regimes	12
3.4.3 Frictional Pressure Drop	13
3.4.4 Velocities of Individual Phases	17
3.5 Heat Losses	18
4.0 THE WELLBORE SIMULATOR HOLA	21
4.1 Introduction	21
4.2 Basic Architecture of the Model	21
4.2.1 Interzonal Flow	22
4.2.2 Multiple Feedzones	24
4.3 Flow Diagrams and Major Subroutines	25
4.4 Computational Options	30
5.0 VALIDATION OF THE SIMULATOR	31

5.1 Cerro Prieto, Wells M-51, M-90, M-91 and M-39	32
5.2 East Mesa, Well 6-1	33
5.3 Krafla, Wells KW-2, KJ-7 and KJ-9	34
5.4 Nesjavellir, Well NJ-14	34
5.5 Svartsengi, Well 4	35
5.6 Summary	35
6.0 PREDICTING INTERNAL FLOWRATES IN WELLS	37
6.1 Nesjavellir, Well NJ-7	38
6.2 Krafla, Well KJ-11	39
6.3 Olkaria, Well OW-201	40
6.4 Olkaria, Well OW-15	41
7.0 WELLBORE PERFORMANCES	43
7.1 Wellhead Output Curves	43
7.2 Formulating Flow from the Reservoir	45
7.3 A Solution Algorithm for Wells with Two Feedzones	46
7.4 A Limited Sensitivity Study	48
7.5 Field Application: Well KJ-11 in Krafla, Iceland	50
7.5.1 Feedzones and Flow Characteristics of Well KJ-11	50
7.5.2 Simulating the Output Curves	51
7.5.3 Some General Comments on the Results	55
8.0 CONCLUSIONS	57
REFERENCES	59
FIGURES	64
APPENDIX A: Input Data for HOLA	97

LIST OF FIGURES

Figure 1.1	A simplified sketch of a geothermal well with two feed-zones and related surface equipment.	64
Figure 3.1	The flow regimes in vertical gas-liquid flow (from Orkiszewski, 1967).	65
Figure 4.1	A feedzone in the grid. The imaginary node ξ is infinitely close to node j , where the feedzone is.	66
Figure 4.2	The six possible flow cases at a feedzone in the well. ξ is an imaginary node defined in Figure 4.1.	67
Figure 4.3	A flow diagram for the main routine HOLA.	68
Figure 4.4	Flow diagram for the subroutine VINNA1	69
Figure 5.1	Calculated and measured pressures in well M-51, Cerro Prieto.	70
Figure 5.2	Calculated and measured pressures in well M-90, Cerro Prieto.	71
Figure 5.3	Calculated and measured pressures in well M-91, Cerro Prieto.	72
Figure 5.4	Calculated and measured pressures in well M-39, Cerro Prieto.	73
Figure 5.5	Calculated and measured downhole profiles in well 6-1, East Mesa	74
Figure 5.6	Calculated and measured downhole profiles in well KW-2, Krafla.	75
Figure 5.7	Calculated and measured downhole profiles in well KJ-7, Krafla.	76
Figure 5.8	Calculated and measured downhole profiles in well KJ-9, Krafla.	77
Figure 5.9	Calculated and measured downhole profiles in well NJ-14, Nesjavellir. Solid lines in between data points at each depth indicate the range of measured pressures, dashed lines are for the range in measured temperatures.	78
Figure 5.10	Calculated and measured pressure in well no. 4, Svartsengi.	79
Figure 6.1	Calculated and measured downhole profiles in well NJ-7, Nesjavellir.	80

Figure 6.2	Calculated and measured downhole profiles in well KJ-11, Krafla. Negative flowrates are present in the lower part of the well.	81
Figure 6.3	Calculated and measured downhole profiles in well KJ-11, Krafla. Positive flowrates are found in the well and the feedzones.	82
Figure 6.4	Calculated and measured downhole profiles in well OW-201, Olkaria.	83
Figure 6.5	Calculated and measured downhole profiles in well OW-15, Olkaria. Two feedzones are assumed for the well.	84
Figure 6.6	Calculated and measured downhole profiles in well OW-15, Olkaria. Single feedzone is assumed for the well.	85
Figure 7.1	Wellhead output curves for (a) well 2 in the Loz Azufres field, Mexico and (b) from well 1 in the Miravalles field, Costa Rica (from Gudmundsson, 1986.)	86
Figure 7.2	Wellhead delivery curves for wells in the Svartsengi (SG-4,SG-10) and Krafla (KG-10) fields (from Palmason 1983, Parlaktuna 1985, and Sigurdsson 1985).	87
Figure 7.3	Calculated wellhead conditions as a function of bottomhole pressure for the standard well discussed in text. Wellhead pressure is indicated by dotted line, wellhead enthalpy by solid line and wellhead flowrate by dashed line.	88
Figure 7.4	Wellhead output curves for the standard well discussed in text. The wellhead enthalpy is indicated by solid line and the wellhead flowrate by dotted line.	89
Figure 7.5	Discharge ranges for the standard well. The reservoir pressure at the upper feedzone is 80 bars. Dashed lines indicate solution boundaries for $1 \times 10^{-12} \text{ m}^3$ feedzone productivity indices, whereas the solid lines are for $5 \times 10^{-13} \text{ m}^3$ productivity indices.	90
Figure 7.6	A simplified model of the Krafla reservoir (from Stefansson, 1981).	91
Figure 7.7	Estimated reservoir temperatures and pressures in the vicinity of well KJ-11. The geometry of the well and location of feedzones for the well are also shown (from Steingrimsson, 1986, personal communication).	92
Figure 7.8	Measured wellhead output curves from well KJ-11 (from Stefansson and Steingrimsson, 1980).	93

Figure 7.9	Calculated downhole pressures in well KJ-11, using the measured wellhead data in Figure 7.8. Case A represents 5.0 bars wellhead pressure and 34 kg/s flowrate, Case B is for 5.6 bars and 23.8 kg/s and Case C is for 6.6 bars and 14.9 kg/s. The wellhead enthalpy is 915 kJ/kg for all cases.	94
Figure 7.10	Measured and calculated wellhead output curves for well KJ-11. The lower feedzone is at 1600 m depth. See Table 7.1 for the feedzone parameters.	95
Figure 7.11	Measured and calculated wellhead output curves for well KJ-11. The lower feedzone is at 2000 m depth. See Table 7.1 for the feedzone parameters.	96

LIST OF TABLES

Table 3.1	Different flow regimes and the criteria to determine when each one is applicable.	14
Table 3.2	Values of B_s for smooth pipes.	16
Table 3.3	Equations for the Armand coefficients.	20
Table 7.1	Calculated productivity indices for well KJ-11.	54

NOMENCLATURE

A	-	Cross sectional area of the well, m^2
A_g	-	Cross sectional area occupied by steam, m^2
A_l	-	Cross sectional area occupied by liquid, m^2
B_S	-	A semi-empirical coefficient for calculation of two-phase friction in smooth pipes.
B_R	-	A semi-empirical coefficient for calculation of two-phase friction in rough pipes.
C_A	-	Armand coefficient
D	-	Depth to a grid node in the well, m
E_t	-	Total energy flux in the well, J/s
f	-	Friction factor
F_1	-	A nonlinear function in the variable $\mathbf{y} = (y_1, y_2)$
F_2	-	A nonlinear function in the variable $\mathbf{y} = (y_1, y_2)$
G	-	Mass velocity in the well, $kg/(m^2 s)$
g	-	Acceleration of gravity, $9.82 m/s^2$
h	-	Enthalpy of the phases, J/kg
H	-	Total fluid enthalpy, J/kg
\tilde{H}	-	Distance between the two feedzones in the well, m
I	-	Feedzone productivity, $kg/(Pa s)$
i	-	A general node in the grid
j	-	A node which includes a feedzone
k	-	Ambient thermal conductivity, $W/(m^\circ C)$
K	-	Ratio of the steam and the liquid velocity.
k_{rl}	-	Relative permeability of the liquid phase
k_{rg}	-	Relative permeability of the steam phase
\tilde{k}	-	Absolute permeability of the reservoir rock, m^2
L	-	The thickness of the permeable horizon
L_M	-	An empirical variable defined in Table 3.3
L_S	-	An empirical variable, defined in Table 3.3
L_w	-	Total length of the well, m
m	-	Total mass flow, kg/s
M	-	A Jacobian matrix, used in the Newton-Raphson iteration

MF	-	Total momentum flux in the well, Pa
n	-	Exponent in the Blasius equation
\mathbf{p}	-	The vector (p_1, p_2) which makes $F_1(\mathbf{p}) = F_2(\mathbf{p}) = 0$.
P	-	Pressure, Pa
P_{bott}	-	Bottomhole pressure, Pa
P_r	-	Reservoir pressure, Pa
P_{r1}	-	Reservoir pressure at upper feedzone, Pa
P_{r2}	-	Reservoir pressure at lower feedzone, Pa
P_w	-	Wellbore pressure, Pa
P_{w1}	-	Wellbore pressure at upper feedzone, Pa
P_{w2}	-	Wellbore pressure at lower feedzone, Pa
$(\frac{dP}{dz})_{\text{acc}}$	-	Accelerational pressure drop, Pa/m
$(\frac{dP}{dz})_{\text{fri}}$	-	Frictional pressure drop, Pa/m
$(\frac{dP}{dz})_{\text{pot}}$	-	Potential pressure drop, Pa/m
$(\frac{dP}{dz})_{2p}$	-	Two-phase frictional pressure drop, Pa/m
$(\frac{dP}{dz})_{\text{LO}}$	-	Frictional pressure drop if all the fluid flows as liquid only, Pa/m
$(\frac{dP}{dz})_{\text{GO}}$	-	Frictional pressure drop if all the fluid flows as steam only, Pa/m
PI	-	Productivity index, m^3
Q	-	Ambient heat flux, W/m
Q_g	-	Volumetric flow of steam, m^3/s
Q_l	-	Volumetric flow of liquid, m^3/s
r	-	Radial distance from the well, m
r_w	-	Radius of the well, m
R	-	Radial distance to the reservoir pressure P_r , m
Re	-	Reynolds number
S	-	Steam saturation
t	-	Time, seconds
T	-	Temperature, $^{\circ}\text{C}$
T_w	-	Fluid temperature inside the well, $^{\circ}\text{C}$
T_{∞}	-	Ambient initial temperature, $^{\circ}\text{C}$
\hat{T}_w	-	Mean fluid temperature of two adjacent grid nodes, $^{\circ}\text{C}$
\hat{T}_{∞}	-	Mean ambient temperature of two adjacent grid nodes, $^{\circ}\text{C}$

u	- Average fluid velocity, m/s
u_b	- Velocity of a bubble relative to the mean fluid velocity, m/s
u_{ch}	- Choked velocity, m/s
u_{chg}	- Choked velocity of steam, m/s
u_{chl}	- Choked velocity of liquid, m/s
u_{ch2p}	- Choked velocity of two-phase mixture, m/s
u_g	- Average velocity of the steam, m/s
u_l	- Average velocity of the liquid, m/s
u_{gs}	- Superficial steam velocity, m/s
u_{gl}	- Superficial liquid velocity, m/s
u_H	- Homogeneous fluid velocity, m/s
u_T	- Velocity of a Taylor bubble relative to the mean fluid velocity, m/s
v_{gd}	- An empirical variable
x	- The mass fraction of steam to the total flow
z	- Depth coordinate, m
α	- Thermal diffusivity, m^2/s
β	- The ratio of gas volumetric flowrate to the total volumetric flowrate
γ	- The Euler's number, 0.577216...
γ_1	- Fluid mobility in the upper feedzone
γ_2	- Fluid mobility in the lower feedzone
Γ	- A physical property coefficient
ϵ	- Pipe roughness, m
κ	- Incompressibility, Pa
κ_g	- Incompressibility of steam, Pa
κ_l	- Incompressibility of liquid, Pa
κ_m	- Mean mixture incompressibility, Pa
μ	- Fluid viscosity, kg/m/s
ξ	- An imaginary grid node, right below a feedzone in the well
ρ	- Density, kg/m^3
ρ_{mix}	- Density of a two-phase mixture, kg/m^3
σ	- Surface tension of a steam-liquid mixture, N/m
ψ_{FLO}	- A two phase multiplier
Ω	- Ambient thermal conductance, $W/m/^\circ C$

SUBSCRIPTS

g	-	steam (gas)
l	-	liquid
i-1	-	upper grid node
i	-	lower grid node
r	-	reservoir
w	-	well
1	-	shallower feedzone
2	-	deeper feedzone

ACKNOWLEDGEMENTS

I would like to thank Dr. Gudmundur Bodvarsson for his patience, guidance and very helpful suggestions during this study. I would also like to thank Dr. Paul A. Wither-
spoon, my advisor, for his overall supervision and support.

I am indebted to Benedikt Steingrimsson and his colleagues at the Icelandic National Energy Authority for providing data used in this report and for cooperation during this work. Thanks are also due to Mary Bodvarsson for carefully reading and improving the English of this thesis.

This work was supported through U.S. Department of Energy Contract No. DE-AC03-76SF00098 by the Assistant Secretary for Conservation and Renewable Energy, Office of Renewable Technology, Division of Geothermal Technology.

1.0 INTRODUCTION

In June 1783, a large volcanic eruption began on the 25 km long Laki fissure in S-E Iceland. During a 9 month period, over 11 km³ of lava flowed from the fissure, along with large amounts of volcanic gases, which partially blocked sunlight to the northern hemisphere and caused a temporary change in climate. This eruption came as a major surprise to the ruling Danish government, which sent representatives to Iceland to find the burning underground coals that were causing this earth fire (Thorarinsson, 1967). Since that time knowledge and understanding of the earth's internal forces and their consequences have developed rapidly, allowing earth scientists to explain volcanic eruptions and natural occurrences. The acquired knowledge is of great importance in many industries, such as mining of metals, coals and fluids from the underground, and in the case of geothermal energy it has turned the mystery of "burning underground coals" into an economically feasible and exploitable natural resource.

For centuries geothermal water has been used for bathing and cooking, and sulphur was mined in geothermal areas as early as the 18th century. In 1904 electrical power was generated for the first time from geothermal steam in Italy; since then the geothermal power industry has expanded rapidly. Today 4800 MW of electricity are produced worldwide (DePippo, 1985). In addition around 7000 MW of heat energy, extracted from low enthalpy geothermal fluids, are used for space heating, bathing and agriculture (Gudmundsson, 1985). The rapid growth of geothermal energy utilization is still continuing, promising to be a significant source of energy in many countries.

Geothermal research requires knowledge from a wide range of science and engineering disciplines. Knowledge of geology, geochemistry, geophysics, drilling technology, oil and gas engineering and hydrology are needed in the exploration, definition and exploitation of a geothermal resource. In recent years geothermal reservoir engineering has emerged as a specialized field borrowing experience from Petroleum Engineering, Hydrology and Heat Transfer. The primary objective of geothermal reservoir engineering is to use all the hydrological, thermal and chemical data available about a

geothermal reservoir to construct a model which simulates the past, and hopefully the future response of the reservoir to production. When such a model is available, the planning of appropriately sized power plants and other surface facilities are made with greater confidence.

The most reliable way of exploring a geothermal reservoir is well drilling. Common logging techniques provide information on reservoir temperatures and pressures, the location of aquifers and some other general information which are used to improve the constantly evolving, conceptual model of the reservoir. Well testing will yield important information regarding the hydrological characteristics of the resource.

Energy is withdrawn from a geothermal reservoir by discharging fluid from wells. The fluid flows in the wellbore as either single-phase liquid or steam or as a mixture of both. The steam phase is usually separated at the surface and piped to a turbine which rotates an electrical generator (Figure 1.1). The name of the game is to generate as much power as possible from the geothermal well(s). The maximum power output of the turbine occurs when the momentum drop across the turbine is maximized. Hence one wants to maximize both the rate of steam flow and the pressure gradient over the turbine. The turbine outlet pressure is always 1 bar or less, but the inlet pressure is directly related to the wellhead pressure. Wellhead pressure, on the other hand, is a complicated function of wellbore geometry, wellbore flow and enthalpy, number of feedzones and their reservoir pressures, enthalpies and productivity. It is of engineering interest to predict the thermodynamic variables describing two-phase flow in the well, given the source terms and the boundary conditions of the system. This is a rather complicated problem since the formulation of two-phase flow is highly non-linear and must be solved numerically. Mixed analytical and empirical formulations do exist for various types of flow. They have been used by several authors in their development of wellbore models for numerically predicting downhole pressures, given the well design and either wellhead or bottomhole flow conditions. These predictions usually compare fairly well with measured data. All of the present available codes assume that fluid only enters at the wellbottom.

The numerical wellbore codes have various applications, such as in determining the well design that optimizes the energy transfer from a well to a power plant, or detecting the minimum wellhead pressure that prevents scaling in the well; they can also be coupled with geothermal reservoir simulators to predict the flow history of a well/reservoir system with time.

Most geothermal reservoirs are characterized by fractured, volcanic rocks of low porosity. Wells drilled in such reservoirs receive fluids through localized production zones, called feedzones. Between the feedzones there are usually long, nonproducing sections. The feedzones are associated with different layers (aquifers) in the geothermal reservoir, each one having its own pressure potential and flow characteristics. When a multi-feedzone well is discharged its wellhead flow and enthalpy can vary greatly with wellhead pressure, reflecting the different nature of the feedzones and their response to pressure changes in the well during discharge. These wellhead flow conditions can not be reproduced by a single-feedzone simulator.

The main objective of this work is to develop a multiple feedzone wellbore model for single- or two-phase flow in vertical wells. It has been demonstrated in various fields (e.g. oil and gas and geothermal) that multiple feedzones with different pressure potentials can significantly effect the well performance in the long run. Very little work in this subject has been done to date, but the importance of the subject is becoming more and more evident.

This study concentrates on the following aspects:

1. Review of existing work: Several authors have developed geothermal wellbore simulators and presented their application to field data. These papers are reviewed and the main results are described.
2. Development of a general wellbore simulator: A computer program is developed to simulate one or two phase flow in a vertical well with multiple feedzones. The governing flow equations are solved numerically by finite difference

methods, assuming steady state flow in the well. Either wellhead or wellbottom flowrates, enthalpies and pressures are given as boundary conditions, also the well geometry and the feedzone properties. The simulator can handle variable diameter wells, injection and production and internal flow.

3. Validation of the program by comparing calculated and measured downhole conditions in the literature. There are numerous temperature and pressure profiles from discharging geothermal wells which show definite signs of two or more feedzones. By adding fluid sources (feedzones) to the numerical code, these profiles can be simulated. The matching is performed by guessing the flow and temperature at each feedzone until the calculated curve fits the measured one.

4. Coupling of the simulator to the geothermal reservoir. Instead of specifying the flowrate at each feedzone, it is of interest to find the total flow and enthalpy from a well for a given wellhead pressures. This can be done by specifying productivity indices and reservoir fluid enthalpies and pressures at each feedzone. The simulator will then compute flowrates and enthalpies at the wellhead for the given set of feedzone conditions.

2.0 BACKGROUND

Two-phase flow of fluid occurs extensively in nature and in man made structures. Examples range from a coffee percolator to the large cooling systems of nuclear power plants. Two-phase flow is common in geothermal reservoirs and can be an important driving discharge mechanism of geothermal wells. The prediction of downhole flow conditions in geothermal wells is therefore of great importance and interest to people in the geothermal sciences.

In the present context two-phase flow is defined as the flow of gas-liquid mixtures. The mixture is generally referred to as the fluid (Chisholm, 1983). The two-phase fluid can be either single component, as in the flow of liquid water/steam mixtures, or two or more components, as in the flow of seawater and air, where the three fluid components are pure water, salt and gas.

The earliest method, used in the prediction of two phase flow conditions assumed that the fluid was flowing as a homogeneous mixture of the two phases. These models are called homogeneous flow models. Since the gas phase generally flows faster than the liquid phase, the concept of separated flow models was introduced (Wallis, 1969). In the separated flow models the phases are assumed to flow concurrently. Separate governing equations are written for each phase and the interaction between the phases is considered by coupling terms. This type of a flow model has proven to be more reliable for predictive purposes in two-phase flow.

Systematic studies of two phase flow were first conducted during the 1940s. Martinelli and Nelson (1948) did pioneering work on the prediction of pressure drops in two-phase flow. The oil industry had an early interest in the subject because two phase flow is common in oil and gas pipelines. Orkiszewski (1967) analyzed data from 148 oil wells and presented methods to predict pressure drops in two-phase wells. His formulation is frequently used in two-phase wellbore simulations. The nuclear power industry relies also heavily on two-phase flow in the combined processes of cooling of the reactors and generating power (Chisholm, 1983).

Electrical power from geothermal steam was first generated in 1904 at the Lardarello field in Italy, and later at The Geysers, California. Both fields are characterized by wells that discharge superheated steam. Wells discharging a mixture of steam and liquid were not used for electrical power production until the early 1950s, when the steam phase was separated at the surface in the Wairakei field, New Zealand (Grant et.al., 1982).

The first numerical code capable of simulating two-phase flow in a geothermal wellbore was developed by Gould (1974). Gould applied methods used in the petroleum industry and compared his predicted pressure drops to actual field data. Upadhyay (1977) used several different methods of predicting pressure drop in two-phase flow in his wellbore simulator. He concluded that the relations proposed by Orkiszewski (1967) provide, on the average, the most accurate predictions. Goyal et al. (1980) simulated measured downhole pressures in Cerro Prieto wells by using a program developed by Miller (1980). The paper studied the importance of measured wellhead parameters on the calculated downhole profiles and concluded that wellbore diameter and wellhead pressures were the most sensitive parameters affecting the curves.

The first transient wellbore simulator was developed by Miller (1981) to study the effects of wellbore storage on transient flowing tests. Steady state wellbore simulators which accounted for noncondensable gases and dissolved solids were described by Barelli et al. (1982) and Parlactuna (1985). The effects of these additional fluid components were shown to be considerable in a few special field cases. Gudmundsson (1986) reviewed the literature on geothermal wellbore simulators. He discussed the different discharge characteristics of geothermal wells with wellhead pressure and the positive effects of increased wellbore diameter on maximum flowrates from geothermal wells.

Internal effects of feedzones in geothermal wells have been observed in many fields. Examples in the literature include wells in Iceland (Stefansson and Steingrimsson, 1980), Kenya (Haukwa, 1984) and New Zealand (Grant et al. 1982,1983).

In our knowledge, all existing wellbore simulators consider only one fluid source to the well. This is a reasonable assumption in some geothermal wells. However, most geothermal wells discharge fluid from two or more feedzones. These wells are often said to have "strange" output characteristics and their measured downhole curves cannot be matched using the conventional single feedzone wellbore simulators.

3.0 FLUID FLOW IN GEOTHERMAL WELLS

3.1 Introduction

In this chapter analytical and empirical relations that are used to compute steady-state one- or two-phase flow in geothermal wells are given. In this treatment the conventional approach involving a single feedzone with constant mass flowrate and constant well radius is assumed. All of these assumptions are released in a subsequent chapter (Chapter 4). First fluid flow under single-phase conditions is considered, then the several empirical relations used under two-phase flow conditions are introduced. Finally it is shown how heat losses from the well to ambient are calculated.

3.2 General Governing Equations

The governing steady-state differential equations for mass, momentum and energy in a vertical well are respectively

$$\frac{d\dot{m}}{dz} = 0 \quad (3.1)$$

$$\frac{dP}{dz} - \left[\left(\frac{dP}{dz} \right)_{\text{fri}} + \left(\frac{dP}{dz} \right)_{\text{acc}} + \left(\frac{dP}{dz} \right)_{\text{pot}} \right] = 0 \quad (3.2)$$

$$\frac{dE_t}{dz} \pm Q = 0 \quad (3.3)$$

where \dot{m} is the total mass flow, P is pressure, E_t is the total energy flux in the well and z is the depth coordinate. Q denotes the ambient heat loss over a unit distance. The plus and minus signs indicate downflow and upflow respectively. The pressure gradient is composed of three terms: wall friction, acceleration of the fluid, and the change in gravitational load over dz . These terms are described in section 3.3 for single-phase flow and in sections 3.4.3 and 4.2.1. for two-phase flow.

3.3 Single Phase Flow

The flow of single phase fluid in vertical pipes is treated extensively in the fluid mechanics literature (see for example White, 1979). The flow calculations are carried out with linear equations, assuming the fluid physical properties are constant. These classical equations are used here, but modified to include the pressure and the temperature dependence of the fluid properties. The pressure and energy gradients are given by

$$\left(\frac{dP}{dz}\right)_{\text{fri}} = \pm \frac{f G^2}{4 r_w \rho} \quad (3.4)$$

$$\left(\frac{dP}{dz}\right)_{\text{acc}} = \frac{d(G u)}{dz} \quad (3.5)$$

$$\left(\frac{dP}{dz}\right)_{\text{pot}} = \rho g \quad (3.6)$$

$$\frac{dE_t}{dz} = \dot{m} \frac{d}{dz} \left\{ \left[h + 0.5 u^2 + g (L_w - D) \right] \right\} \quad (3.7)$$

where f is the friction factor, G is the mass velocity, ρ is the fluid density, u is the average fluid velocity, h is the fluid enthalpy and g is the acceleration of gravity. L_w is the total length of the well, r_w is the well radius and D is the depth to the node in question, measured from the wellhead. Again, upward and downward flow are represented by plus and minus signs respectively.

The friction factor, f , is given by (White, 1979)

$$f = \frac{64}{\text{Re}} \quad \text{if } \text{Re} < 2400 \quad (3.8)$$

$$\frac{1}{f^{0.5}} = -2.0 \log_{10} \left[\frac{\epsilon / 2 r_w}{3.7} + \frac{2.51}{\text{Re } f^{0.5}} \right] \quad \text{if } \text{Re} > 2400 \quad (3.9)$$

where Re is the Reynolds number and ϵ is the pipe roughness.

Inserting (3.4) - (3.7) into (3.2) and (3.3) gives two nonlinear, differential equations. The fluid properties are given by any two independent thermodynamical variables of the fluid. In this work pressure and temperature are used for single-phase flow.

3.4 Two-Phase Flow

When two-phase flow is considered, it is customary to treat the flow of liquid water and steam separately, and then combine the equations for the two phases by simultaneously solving the governing equation using some empirical correlations. This is called the method of separated flow models. All the physical properties of the steam and the liquid are given as a function of pressure. The additional parameters needed to fully describe the flow are the total mass flowrate, the well geometry and x , the mass fraction of steam.

3.4.1 Basic Definitions

In this section some basic correlations used to interrelate the flow parameters are introduced. These formulas are taken from Chisholm (1983), and his notation is generally followed.

The mass fraction of steam, x , often called the dryness, is given as

$$x = \frac{\dot{m}_g}{\dot{m}} = \frac{\dot{m}_g}{\dot{m}_g + \dot{m}_l} \quad (3.10)$$

where the subscripts g and l stand for steam (gas) and liquid, respectively.

The mass velocity, G , is

$$G = \frac{\dot{m}}{A} = \frac{\dot{m}_g + \dot{m}_l}{A_g + A_l} \quad (3.11)$$

where A is the well cross-sectional area, and A_g and A_l denote the cross-sectional areas occupied by steam and liquid.

The steam saturation, S , is given as

$$S = \frac{A_g}{A} = \frac{A_g}{A_g + A_l} \quad (3.12)$$

The continuity equations for steam and liquid are respectively

$$\dot{m}_g = u_g \rho_g A_g = u_g \rho_g S A \quad (3.13)$$

$$\dot{m}_l = u_l \rho_l A_l = u_l \rho_l (1 - S) A \quad (3.14)$$

where u_g and u_l are the average velocities of steam and liquid. The velocity ratio is defined as

$$K = \frac{u_g}{u_l} \quad (3.15)$$

and then combining equations (3.10) - (3.15) gives the following relations:

$$S = \left[1 + K \frac{1-x}{x} \frac{\rho_g}{\rho_l} \right]^{-1} \quad (3.16)$$

$$u_g = G \left[\frac{x}{\rho_g} + \frac{K(1-x)}{\rho_l} \right] \quad (3.17)$$

$$u_l = \frac{G}{K} \left[\frac{x}{\rho_g} + \frac{K(1-x)}{\rho_l} \right] \quad (3.18)$$

The definition of a superficial gas or liquid velocity is frequently used in the two-phase literature. This is the velocity the phases would have if they flowed alone in the pipe. They are given as

$$u_{gs} = \frac{x \dot{m}}{\rho_g A} \quad (3.19)$$

$$u_{ls} = \frac{(1-x) \dot{m}}{\rho_l A} \quad (3.20)$$

Note that all the quantities on the right hand side of (3.19) and (3.20) are easily measurable. This is why two-phase flow data are often presented in terms of the superficial velocities.

The volumetric flow rates of steam and liquid are

$$Q_g = A_g u_g = \frac{x G A}{\rho_g} \quad (3.21)$$

$$Q_l = A_1 u_1 = \frac{(1-x)GA}{\rho_l} \quad (3.22)$$

The ratio of gas volumetric flowrate to the total flowrate, β , is

$$\beta = \frac{Q_g}{Q_g + Q_l} = \left[1 + \frac{1-x}{x} \frac{\rho_g}{\rho_l} \right]^{-1} \quad (3.23)$$

The density of a steam/liquid mixture is

$$\rho_{\text{mix}} = S \rho_g + (1-S) \rho_l \quad (3.24)$$

and by combining (3.16) and (3.24) gives

$$\rho_{\text{mix}} = \frac{x + K(1-x)}{\left[\frac{x}{\rho_g} + \frac{K(1-x)}{\rho_l} \right]} \quad (3.25)$$

3.4.2 Two-Phase Flow Regimes

Two-phase flow is generally divided into four flow regimes, depending on the macroscopic behavior of the flow (Orkiszewski, 1967). The regimes are classified as bubble, slug, transition (or churn), and mist (or annular);(see Figure 3.1).

An example of a bubble flow is the rise of bubbles in beer. The gas bubbles move upwards because of buoyancy, but are restrained by the viscous liquid phase. The velocity, u_b , of such a bubble, relative to the average fluid velocity, is (Govier and Aziz, 1972)

$$u_b = 1.53 \left[\frac{g \sigma (\rho_g - \rho_l)}{\rho_l^2} \right]^{0.25} \quad (3.26)$$

where σ is the surface tension of steam/water.

Slug flow occurs when the small steam bubbles coalesce and form large, bullet shaped bubbles with almost the same diameter as the well. The liquid phase is still continuous. Slug flow occurs, for example, in a coffee percolator. The regularly shaped bubbles in slug flow are called "Taylor" bubbles. Their velocity, u_T , relative to the mean

fluid velocity, is (Chisholm, 1983)

$$u_T = 0.35 \left[2 r_w g \left(1 - \frac{\rho_g}{\rho_l} \right) \right]^{0.5} \quad (3.27)$$

Transition flow occurs when the continuous liquid phase breaks up into irregular clusters of gas and liquid. The flow is chaotic and is likely to be unpredictable by any empirical relations.

Annular or mist flow occurs when the gas phase is continuous in a flowing well. The liquid can flow both as entrained droplets in the steam and in a film on the pipe walls. Rain is an example of mist flow.

Orkiszewski (1967) reviewed the available literature on two-phase flow and compared different flow methods by analyzing flowing pressure profiles from 148 oil wells. He developed empirical relations which can be used to classify the different flow regimes. These relations are given in Table 3.1.

3.4.3 Frictional Pressure Drop

The pressure drop for single phase liquid flow is given by

$$\left(\frac{dP}{dz} \right)_{LO} = \frac{f_{LO} G^2}{4 r_w \rho_l} \quad (3.28)$$

where the subscript LO stands for "liquid only". The friction factor, f_{LO} , is given by (3.8) and (3.9).

Martinely and Nelson (1948) introduced the concept of the "two phase multiplier"

$$\psi_{FLO}^2 = \frac{\left(\frac{dP}{dz} \right)_{2p}}{\left(\frac{dP}{dz} \right)_{LO}} \quad (3.29)$$

where $(dP/dz)_{2p}$ is the actual pressure drop for two-phase flow, and $(dP/dz)_{LO}$ is the pressure drop that would occur if all the fluid flowed as liquid only, with the properties

TABLE 3.1 Different flow regimes and the criteria to determine when each one is applicable (from Orkiszewski, 1967)

Flow regime	Limits
Bubble	$\beta < L_B$
Slug	$\beta > L_B$ and $v_{gD} < L_S$
Transition	$L_S < v_{gD} < L_M$
Mist	$L_M < v_{gD}$

$$v_{gD} = \frac{x G}{\rho_g} \left(\frac{\rho_l}{g \sigma} \right)^{0.25}$$

$$v_t = G \left[\frac{x}{\rho_g} + \frac{1-x}{\rho_l} \right]$$

$$L_B = 1.071 - 0.676 \frac{v_t^2}{2 r_w} \quad \text{and} \quad L_B > 0.13$$

$$L_S = 50 + 36 v_{gD} \frac{Q_l}{Q_g}$$

$$L_M = 75 + 84 \left(v_{gD} \frac{Q_l}{Q_g} \right)^{0.75}$$

$$\beta = \frac{Q_g}{Q_g + Q_l}$$

of the liquid phase.

Chisholm (1973, 1983) correlated available pressure drop data and obtained a generalized expression for the two-phase multiplier ψ_{FLO}^2 , independent of flow regime:

$$\psi_{FLO}^2 = 1 + (\Gamma^2 - 1) \left[B_S x^{(2-n)/2} (1-x)^{(2-n)/2} + x^{(2-n)} \right] \quad (3.30)$$

where n is the exponent in the Blasius equation, B_S is a semi-empirical coefficient given in Table 3.2 and Γ is a physical property parameter, given as

$$\Gamma^2 = \frac{\left(\frac{dP}{dz} \right)_{GO}}{\left(\frac{dP}{dz} \right)_{LO}} = \left(\frac{\mu_g}{\mu_l} \right)^n \left(\frac{\rho_l}{\rho_g} \right) \quad (3.31)$$

where μ is viscosity and GO represents "gas only".

The coefficient B_S in Table 3.2 is only valid for flow in smooth pipes. To correct for the surface roughness of the pipe, Chisholm (1983) suggested the relation

$$\frac{B_R}{B_S} = \left\{ 0.5 \left[1 + \left(\frac{\mu_g}{\mu_l} \right)^2 + 10^{(-300\epsilon)/r_w} \right] \right\}^{\frac{0.25-n}{n}} \quad (3.32)$$

where B_R stands for rough surfaces and B_S for smooth ones.

The Blasius exponent, n , takes the value 0.25 in smooth pipes but is zero in fully rough flow (geothermal wells). Inserting those two values into Table 3.2 and equation (3.30) respectively, gives for the two-phase multiplier

$$\psi_{FLO}^2 = 1 + (\Gamma^2 - 1) \left[B_r x (1-x) + x^2 \right] \quad (3.33)$$

The two-phase pressure drop can now be predicted by rearranging (3.29) as

$$\left(\frac{dP}{dz} \right)_{2p} = \psi_{FLO}^2 \left(\frac{dP}{dz} \right)_{LO} \quad (3.34)$$

with the quantities on the right hand side computed using equations (3.29) and (3.33).

TABLE 3.2 Values of B_s for smooth pipes (from Chisholm, 1983)

Γ	$G \left(\frac{\text{kg}}{\text{m}^2 \text{ s}} \right)$	B_s
≤ 9.5	≤ 500	4.8
	$500 \leq G \leq 1900$	$\frac{2400}{G}$
	≥ 1900	$\frac{55}{G^{0.5}}$
$9.5 < \Gamma < 28$	≤ 600	$\frac{520}{\Gamma G^{0.5}}$
	> 600	$\frac{21}{\Gamma}$
≥ 28		$\frac{15000}{\Gamma^2 G^{0.5}}$

3.4.4 Velocities of Individual Phases

Two methods for calculating the average phase velocities of steam and water are presented. These methods are based on semi-empirical equations, discussed to some extent in section 3.4.2.

One possibility for calculating phase velocities is to use the flow regime definitions of Orkiszewski (1967), given in Table 3.1. Defining the homogeneous velocity of the fluid as

$$u_H = G \left[x / \rho_g + (1-x) / \rho_l \right] \quad (3.35)$$

Chisholm (1983) shows that

$$u_g = u_H + \begin{cases} u_b \\ \text{or} \\ u_T \end{cases} \quad (3.36)$$

where u_b and u_T are the bubble and slug velocities given in (3.26) and (3.27), respectively. The flow is assumed homogeneous (velocities of both phases are equal) in the mist regime (Miller, 1980). A linear interpolation between bubble velocities in slug and mist flow is used in the transition regime, yielding

$$u_b = \frac{L_M - v_{gd}}{L_M - L_S} u_T \quad (3.37)$$

where the empirical factors L_M , L_S and v_{gd} are given in Table 3.1.

By combining (3.10), (3.11), (3.13) and (3.14), we have

$$S = \frac{G x}{u_g \rho_g} \quad (3.38)$$

$$u_l = \frac{G - u_g \rho_g S}{\rho_l (1 - S)} \quad (3.39)$$

The average phase velocities can now be calculated by initially identifying the proper flow regime (Table 3.1), inserting the appropriate bubble velocity function into (3.36) and solving (3.38) and (3.39) simultaneously.

Another possibility for calculating the phase velocities is to use the method of Armand coefficients. Armand (1946) correlated data for the saturation, S , during air/water flow in pipes. He proposed the relation

$$S = C_A \beta \quad (3.40)$$

where C_A is called the Armand coefficient.

Chisholm (1983) reviewed Armand's approach and recommended several equations for calculation of C_A , depending on β , r_w , m and the physical properties of the two phases. These equations are given in Table 3.3.

Combining equations (3.16), (3.23) and (3.40) we can solve for the velocity ratio, K :

$$K = \left[\frac{1}{C_A \beta} - 1 \right] \frac{x \rho_l}{(1-x) \rho_g} \quad (3.41)$$

The phase velocities are then given by (3.17) and (3.18).

3.5 Heat Losses

The ambient heat flux, Q , in (3.3) is calculated as follows. Assuming that all the heat is conducted horizontally to rocks of thermal conductivity, k , and thermal diffusivity, α , the equation for heat conduction is

$$\frac{1}{r} \frac{\delta}{\delta r} \left(r \frac{\delta T}{\delta r} \right) = \frac{1}{\alpha} \frac{\delta T}{\delta t} \quad (3.42)$$

where T is temperature and r is the radial distance from the well. The boundary conditions are

$$\begin{aligned} T(r_w, t) &= T_w \\ T(r, 0) &= T_\infty \\ T(\infty, t) &= T_\infty \end{aligned} \quad (3.43)$$

where r_w is the well radius, T_w is the temperature of the wellbore fluid and T_∞ is the initial temperature of the well surroundings. A solution to the heat flux problem, valid

when the term $\alpha t/r_w^2 \gg 1$, is given by Carslaw and Jaeger (1959) as

$$Q \approx 4 k \pi (T_w - T_r) \left[\ln \left(\frac{4\alpha t}{r_w^2} - 2\gamma \right) \right]^{-1} \quad (3.44)$$

where $\gamma = 0.577216\dots$ is the Euler's constant.

Equation (3.6) is only an approximation of the actual heat flux. Complications such as varying well temperature during the production history and additional heat losses due to fluid convection in the vicinity of the well are neglected. However, this approximation is probably reasonable since the term dE_t/dz in (3.3) is usually much larger than Q .

Table 3.3 Equations for the Armand coefficients (from Chisholm, 1983).

$\beta > 0.9$

$$\frac{1}{C_A} = 1 + \frac{23}{u_H} \left[\frac{\mu_l u_{ls}}{2 r_w \rho_g} \right]^{0.5} \left(1 - \frac{\rho_g}{\rho_l} \right)$$

$\beta < 0.9$ and $u_H > \frac{u_{wd}}{1/C_{Ah} - 1}$

$$C_A = C_{Ah}$$

$\beta < 0.9$ and $u_H < \frac{u_{wd}}{1/C_{Ah} - 1}$ and $D > D_{crit}$

$$\frac{1}{C_A} = 1 + \frac{W u_b}{u_H}$$

$\beta < 0.9$ and $u_H < \frac{u_{wd}}{1/C_{Ah} - 1}$ and $D < D_{crit}$

$$\frac{1}{C_A} = 1 + \frac{W u_T}{u_H}$$

$$\frac{1}{C_{Ah}} = \beta + \frac{1 - \beta}{\left[1 - \beta \left(1 - \frac{\rho_g}{\rho_l} \right) \right]^{0.5}}$$

$$W = 1.4 \left(\frac{\rho_l}{\rho_g} \right)^{0.2} \left(1 - \frac{\rho_g}{\rho_l} \right)^5$$

$$D = 2 r_w$$

$$D_{crit} = 19 \left[\frac{\sigma}{g (\rho_l - \rho_g)} \right]$$

$$u_{wd} = u_g - u_l$$

4.0 THE WELLBORE SIMULATOR HOLA

4.1 Introduction

The wellbore simulator HOLA (the Icelandic word for a well) solves numerically the differential equations that describe mass, momentum and energy flow in a vertical pipeline. The flow is assumed to be steady state. Calculations either start at the wellhead and continue downwards in a finite difference grid, or at the wellbottom and precede upwards. The governing equations are nonlinear and are solved by using an iteration procedure. Pure water is the flowing fluid, but can be either in single- or two-phase conditions. All physical properties are assumed uniform at any given depth within the well.

The program HOLA allows for multiple feedzones, variable grid spacing and well radius. Feedzones are assumed to occur at single grid points in the well, which appears to be a reasonable assumption for wells in fractured, geothermal reservoirs. Two-phase mixtures are always assumed to flow upwards whereas single-phase fluid can flow either up or down. The solution algorithm is explicit, giving one unique solution for each set of wellhead/wellbottom conditions, as long as there are no fluid sources/losses in the well. Calculations are made in SI-units. The program language is FORTRAN 77.

4.2 Basic Architecture of the Model

The one-dimensional nature of flow in pipelines allows one to compute the flow conditions by either forward or backward solution methods. This requires fully defined flow conditions at one end of the system (inlet conditions), and fully defined boundaries (wellbore geometry, lateral mass and heat flow). The governing equations are then solved in small but finite steps along the the pipe, either in the direction of flow (forward calculations) or against the flow direction (backward calculations). Whenever a feedzone is encountered the mass and energy inflow (or outflow) are given, allowing the

calculation to continue further in the wellbore.

HOLA performs its computations in two major steps. They are:

- (1) Balance given wellbore and feedzone mass and energy fluxes at the grid node where the feedzone is encountered. Find the inlet conditions for the next, unknown section of the well.
- (2) Calculate the flowing conditions in the well between feedzones.

These two steps are repeated until the program reaches the other end of the grid (the well). The second step is a conventional, single-feedzone wellbore simulator, similar to the ones discussed in chapter 2. The effects of multiple feedzones are introduced to the simulator by step one, which only re-initializes the inlet conditions for the next, unknown nodes in the grid.

4.2.1 Interzonal Flow

In this section we show how the governing equations are solved between feedzones in the well. With a constant mass flux, the governing equations written in discrete form are

$$\frac{P_i - P_{i-1}}{\Delta z} - \left[\left(\frac{\Delta P}{\Delta z} \right)_{fri} + \left(\frac{\Delta P}{\Delta z} \right)_{acc} + \left(\frac{\Delta P}{\Delta z} \right)_{pot} \right] = 0 \quad (4.1)$$

$$\frac{E_{t i} - E_{t i-1}}{\Delta z} \pm Q = 0 \quad (4.2)$$

where the subscripts $i-1$ and i refer to an upper and a lower grid node, respectively, at a distance Δz apart. All properties in node $i-1$ are known when the calculations proceed down the well, whereas the properties of node i are known in upward calculations. The acceleration and potential pressure drop terms can be discretized as,

$$\left(\frac{\Delta P}{\Delta z} \right)_{acc} = \frac{MF_{i-1} - MF_i}{\Delta z} \quad (4.3)$$

$$\left(\frac{\Delta P}{\Delta z} \right)_{pot} = 0.5 (\rho_{mix i-1} + \rho_{mix i}) g \quad (4.4)$$

where MF denotes the momentum flux of the fluid and is given by

$$MF = G (x u_g + (1-x) u_l) \quad (4.5)$$

The frictional pressure losses in single phase flow are given by

$$\left(\frac{\Delta P}{\Delta z} \right)_{fri} = \pm 0.5 \left[\frac{f_{i-1} G_{i-1}^2}{4 r_{w i-1} \rho_{i-1}} + \frac{f_i G_i^2}{4 r_{w i} \rho_i} \right] \quad (4.6)$$

and in two phase flow by

$$\left(\frac{\Delta P}{\Delta z} \right)_{fri} = 0.5 \left[\left(\frac{\Delta P}{\Delta z} \right)_{2p i-1} + \left(\frac{\Delta P}{\Delta z} \right)_{2p i} \right] \quad (4.7)$$

where $(\Delta P/\Delta z)_{2p}$ is defined by (3.34).

The total energy flux at any cross section in the well is

$$E_t = \dot{m} \left[x h_g + (1-x) h_l + 0.5 (x u_g^2 + (1-x) u_l^2) + g (L_w - D) \right] \quad (4.8)$$

Inserting (4.3)-(4.8) into (4.1) and (4.2) gives a set of two nonlinear equations in terms of two unknowns: P_i and x_i in the case of two-phase flow, or P_i and T_i in the case of single-phase flow. These two sets of independent variables were chosen because of convenience in developing the code HOLA. For example, steam tables most generally give the properties of single-phase steam and liquid as a function of pressure and temperature. The steam fraction, x , is also frequently used as a dependent variable in formulation of two-phase flow relations. The total fluid enthalpy, H , can replace both x_i and T_i as dependent parameters. However, this change is expensive in computer time and was therefore not considered.

The wellbore simulator HOLA solves equations (4.1) and (4.2) by Newton-Raphson iteration (Burden et.al., 1981). The method is based on the following. Consider twice differentiable and continuous functions $F_1(\mathbf{y})$ and $F_2(\mathbf{y})$ for the two variables y_1 and y_2 . We want to find a solution $\mathbf{p} = (p_1, p_2)$ which makes $F_1(\mathbf{p}) = F_2(\mathbf{p}) = 0$. By initially guessing $\mathbf{y} = \mathbf{y}^* = (y_1^*, y_2^*)$, a new iterative value of \mathbf{y} is given by

$$\begin{bmatrix} y_1 \\ y_2 \end{bmatrix} = \begin{bmatrix} y_1^* \\ y_2^* \end{bmatrix} - \mathbf{M}^{-1} \begin{bmatrix} F_1(\mathbf{y}^*) \\ F_2(\mathbf{y}^*) \end{bmatrix} \quad (4.9)$$

where \mathbf{M} is the Jacobian matrix:

$$\mathbf{M} = \begin{bmatrix} \frac{\delta F_1(\mathbf{y}^*)}{\delta y_1} & \frac{\delta F_1(\mathbf{y}^*)}{\delta y_2} \\ \frac{\delta F_2(\mathbf{y}^*)}{\delta y_1} & \frac{\delta F_2(\mathbf{y}^*)}{\delta y_2} \end{bmatrix} \quad (4.10)$$

If there is a solution \mathbf{p} to our problem, and all the first and second derivatives of F_1 and F_2 are bounded, then \mathbf{y} will converge quadratically to \mathbf{p} .

The derivatives in (4.10) are discretized as

$$\frac{\delta F_1(y_1^*, y_2^*)}{\delta y_1} \approx \frac{F_1(y_1^* + \Delta y_1, y_2^*) - F_1(y_1^*, y_2^*)}{\Delta y_1} \quad (4.11)$$

where Δy_1 is a small fraction of y_1^* ($1 \times 10^{-6} y_1^*$). The other derivatives are similar.

The functions F_1 and F_2 are equations (4.1) and (4.2) respectively. Their dependent variables are either (P_i, x_i) in two-phase flow or (P_i, T_i) in single-phase flow. In geothermal wells, P_i increases steadily downwards while x_i decreases. T_i , on the other hand, remains relatively stable. This gives "good behavior" of the functions F_1 and F_2 and rapid convergence. The routine assumes the iteration is successful when the numerical values of F_1 and F_2 are less than 10^{-6} of the pressure and total energy in the previous node.

4.2.2 Multiple Feedzones

The numerical algorithm discussed in the previous section assumes constant mass flow in the well. The solution is unique between feedzones. The following method is used to account for additional feedzones. It assumes that the feedzone flowrates and the fluid enthalpies are given.

Suppose a feedzone occurs at node j in the well (Figure 4.1). All flow conditions are known in node $j-1$ and the conditions in node j are calculated by (4.9). It is assumed that the wellbore and the feedzone fluids mix instantaneously at the node. Furthermore, it is assumed that there exists an imaginary node ξ below but infinitely close to

node j , having the same pressure as in node j . The flow conditions in node ξ are then given by balancing mass and energy as

$$P_{\xi} = P_j \quad (4.12a)$$

$$\dot{m}_{\xi} = \dot{m}_j - \dot{m}_f \quad (4.12b)$$

$$H_{\xi} \dot{m}_{\xi} = H_j \dot{m}_j - H_f \dot{m}_f \quad (4.12c)$$

where the mass flow, \dot{m} , has two possible direction and is therefore given a vector symbol; the subscript f denotes the feedzone and H is the total fluid enthalpy given by

$$H = x h_g + (1-x) h_l \quad (4.13)$$

Equation (4.12) gives the necessary initial conditions (e.g. new fluid mass rate and enthalpy) for continuing computations, either to the wellhead/wellbottom or to the next feedzone.

There are 6 possible flow directions and conditions in the wellbore close to the feedzone, depending on the characteristics of the feedzones (inflow or outflow) and the type of well flow behavior (production or injection). In the formulation, positive flowrates imply upward flow in the well or flow from the feedzone to the well, whereas negative flowrates imply downward flow or flow from the well to the feedzone. Figure 4.2 shows these possible flow directions.

4.3 Flow Diagrams and Major Subroutines

This section describes briefly the architecture of the wellbore simulator HOLA. The main paths of calculations are shown by flow diagrams and some of the major subroutines are briefly described.

The main routine HOLA reads in input data, calls routines to calculate the wellbore conditions and writes the results to an output file. Figure 4.3 shows a flow diagram for HOLA. The non-simultaneous nature of the computations in HOLA requires a complicated structure of logical statements, that guide the calculations as they proceed from one end of the well to the other. These logical statements are dependent on the

problem under consideration. The program HOLA is therefore composed of five major, independent subroutines, each designed to perform a special set of calculations, depending on the problem at hand. These subroutines are:

- (1) VINNA1 calculates pressure, temperature and saturation profiles from given wellhead conditions and given flowrates and enthalpies at each feedzone except the lowest one. The calculations proceed from the wellhead down the grid to the bottom of the well. All profiles shown in Chapters 5 and 6 are calculated by this subroutine.
- (2) ITHEAD iterates for a required wellhead pressure, given the productivity indices, reservoir pressures and enthalpies at each feedzone (detailed examples are given in chapter 7). The feedzones can either have positive or zero flowrates, so that cases with injection into feedzones are not considered. There is no restriction of the number of feedzones.
- (3) ITHEAD2 is similar to ITHEAD, except that the feedzones can both accept or discharge fluid. The routine assumes that there are only two feedzones in the well. This routine is described in detail in Chapter 7.
- (4) ITHEAD3 iterates for the bottomhole pressure that satisfies a specified positive wellhead flowrate. This option is limited to two feedzones and only positive or zero flow is allowed from the feedzones.
- (5) ITHEAD4 is similar to ITHEAD3 except that fluid injection into the well is considered. The routine allows a maximum of two feedzones and only negative flowrates (i.e. injection). This routine and the routines ITHEAD and ITHEAD3 were developed for a future integration with reservoir simulators.

Input data (wellhead or wellbottom conditions, well design, reservoir temperatures, number and locations of feedzones, reservoir conditions near the feedzones and computational option) are read in from a file by the subroutine INPUT (The input guide is

given in Appendix A). The subroutine develops the wellbore grid and calculates the reservoir temperature at each grid node by linear extrapolation between the inputted reservoir temperatures at specified depths. Also calculated for each node is the thermal conductance of the well surroundings Ω , given as

$$\Omega = 4k\pi \left[\ln \left(\frac{4\alpha t}{r_w^2} - 2\gamma \right) \right]^{-1} \quad (4.14)$$

The heat loss Q can then be computed as

$$Q = \Omega (\hat{T}_w - \hat{T}_r) \quad (4.15)$$

where \hat{T}_w and \hat{T}_r are the mean fluid and reservoir temperatures, respectively, of the two adjacent nodes.

After the wellhead/wellbottom data and the wellbore grid are specified, the calculations can proceed with the appropriate solution algorithms, discussed above. These calculations are conducted by the subroutine VINNA1 (Figure 4.4) or similar subroutines. First, all the wellhead parameters are assigned by the subroutine TOP. The conditions of the neighboring node are calculated by initially assuming the same steam fraction as in the wellhead node. Equation (4.9) is then solved by one of the three routines ITERATE1, 2 or 3, depending on the previous value of x . The calculations for the other nodes proceed in the same manner.

The following methods are used to check for phase transitions in the nodes.

- (1) Single phase steam {liquid} to a mixture flow: After new values are calculated at grid node i for P_i and T_i , one determines if

$$P_i \approx P_{\text{sat}}(T_i) \quad (4.16)$$

where $P_{\text{sat}}(T_i)$ is the saturation pressure at T_i . When this occurs, x is assigned the value 0.999995 {0.000005} and the iterations proceed.

- (2) Two-phase to single-phase liquid {steam} flow: This transition will happen when the subroutine ITERATE1 calculates $x < 0$ { $x > 1$ } for the grid node i . When this occurs the program returns to node $i-1$ and assumes $x = 0$ { $x = 1$ }. The energy flux in the well is conserved by calculating a new liquid {steam} temperature T_{i-1} such that

$$h_l(T_{i-1}, P_{i-1}) = H_{2p}(P_{i-1}, x_{i-1}) \quad (4.17)$$

and x_{i-1} is then set equal to zero {equal to one}. The calculations then continue in the usual manner.

There are several other checkpoints in the program. Negative pressures are sometimes calculated if the flow is changing phases or if the water level in the well is below the wellhead. This makes the program return to the previous node and add a new node to the grid, halfway between the current node and the unsuccessful node. The same procedure is used when one of the subroutines ITERATE1, 2 or 3 uses more than 10 iterations without converging. The program can calculate negative temperatures if the flowrate and the fluid temperature are low, but the formation temperature is high. This is physically impossible and will result in termination of the compilations.

All properties of steam and water are calculated using the program library STEAM (Bjarnason, 1985), which is based on formulas given by the International Formulation Committee (1967). These formulas are continuous (within numerical limits) over a large section of the phase diagram (0.1–1000 bars-a and 0–800 °C). The continuity condition is necessary for rapid convergence of the Newton-Raphson iteration method. Although STEAM covers most of the phase diagram, calculations are terminated if pressures or temperatures rise above the critical point ($P = 221.2$ bar-a and $T = 374$ °C). This is done because of observed instability in HOLA, close to the critical point.

The subroutine CHOKED checks for choked flow in the well. The sonic velocity, u_{ch} , in single phase fluid is (Zemansky et.al., 1975)

$$u_{ch} = \left[\frac{\Delta P}{\Delta \rho} \right]^{0.5} \quad (4.18)$$

The sonic velocity in two-phase flow is estimated as (Kjaraan and Eliasson, 1983)

$$u_{ch} = \left[\frac{\kappa_m}{\rho_{mix}} \right]^{0.5} \quad (4.19)$$

where κ_m is the "mean" incompressibility of the fluid, given as

$$\frac{1}{\kappa_m} = \frac{S}{\kappa_g} + \frac{1-S}{\kappa_l} \quad (4.20)$$

and the incompressibility is calculated in general as

$$\kappa = \Delta P \frac{\rho}{\Delta \rho} \quad (4.21)$$

In the program choked velocity is compared to the homogeneous fluid velocity and the flow is assumed choked when $u_{ch} > u_H$.

The incompressibility of water is much higher than that for steam, and the mixture density ρ_{mix} is governed by the water density at low to moderate saturations. This gives a κ_m value of the mixture close to κ_g but fluid density close to the water density and therefore drastically reduces sonic velocities for two-phase mixtures. For example, the sonic velocities in the water and steam phases and in the two-phase mixture, calculated by using the above equations and the numerical values $P=33.5$ bar and $S=0.3$ (Kjaraan and Eliasson, 1983), are

$$u_{ch_l} = 1110 \text{ m/s} \quad u_{ch_g} = 555 \text{ m/s} \quad u_{ch_{2p}} \approx 140 \text{ m/s} \quad (4.22)$$

When the simulator calculates sonic conditions in the well, a warning message is printed to a log-file but execution continues. The calculations are terminated if the calculated fluid velocities exceed twice the sonic velocities. This criteria was adopted because equation (4.19) is only an approximation for sonic velocities in two-phase mixtures. A well chokes when the total pressure gradient (dP/dz) is required to overcome the change in the momentum flux (dMF/dz). Chisholm (1983) gives methods based on

this equality, but they are not used here because of their complexity.

When the computations are completed over the entire well length the results are written to an output file with either the routine OUTPUT1 or OUTPUT2. The simulator also creates a log-file which stores information on phase changes, sonic velocities, additional grid nodes used in the simulations or iteration difficulties.

4.4 Computational Options

The simulator HOLA is a tool designed to compute flowing conditions in wellbores. The program is general and offers several options in the computations. They are as follows:

- (1) **Curve Fitting:** Flowing downhole pressure and temperature logs exist for many geothermal wells. The simulator can be used to match this field data, given the wellhead conditions, reservoir temperatures and the wellbore geometry. This is especially valuable in wells with multiple feedzones, allowing one to estimate the relative strength of the feedzones.
- (2) **Optimum Well Design:** The simulator can be used to find the wellbore geometry which maximizes wellhead pressures and flowrates, given the average expected fluid enthalpy and depth to the feedzone(s).
- (3) **Wellhead Output Curves:** It is of interest to predict the wellhead flowrate and enthalpy with wellhead pressure. The simulator is capable of performing these calculations, given the wellbore geometry and properties and thermodynamic conditions near feedzones.
- (4) **Coupling with Reservoir Simulators:** Large scale, integrated finite difference codes such as PT (Bodvarsson, 1982) simulate fluid discharge by giving a wellbore pressure and productivity indices at some nodes in the grid. HOLA can be coupled with these simulators and used to predict changes in well flowrates and enthalpies with time, or to interpret data from flowing well tests. These calculations are performed by specifying a constant value of either the wellhead pressure or the wellhead flowrate. HOLA will then iterate for the wellbore conditions that satisfy all the given wellhead and feedzone conditions.

5.0 VALIDATION OF THE SIMULATOR

In this chapter calculated and measured pressure and temperature profiles in flowing wells with a single, dominant feedzone are analyzed using the simulator HOLA. The purpose is to test the simulator as a tool for predicting downhole conditions in a flowing well. Wells which show effects of two or more feedzones are discussed in the next chapter.

The profiles analyzed are from wells located at Cerro Prieto, Mexico; East Mesa, California; and the Krafla, Nesjavellir and Svartsengi fields in Iceland.

Measuring downhole conditions in a flowing well is a difficult task. The measuring gauges are sensitive devices, which are severely stressed when introduced to the turbulent environment existing in a flowing geothermal wellbore. The pressure and temperature meters are usually mechanical, limiting the number of recorded data points and the time of measurements. Available downhole data from flowing wells are therefore scarce.

An additional problem with flowing pressure and temperature data is the question of how stable the thermodynamic conditions in the well are when the data is collected. The well has to be shut-in, then the device is placed in the well and then the well is discharged again. This causes some initial transients in the wellbore flow which may last for hours, hence the true, steady-state flow conditions in the well may not be measured.

In matching the pressure and temperature profiles from the wells, the wellhead conditions are specified and then the calculations proceed down to the bottom of the well (option 1 in Chapter 4.3). Also inputted are the wellbore geometry and (for some cases) the reservoir temperature with depth. The phase velocities are always calculated using the method of Armand coefficients, since this method was found to lead to more continuous and monotonic derivatives than those obtained through use of the

Orkiszewski flow methods; hence more rapid convergence in the Newton-Raphson formulation. A 25 m grid spacing was used in all the simulations, except for cases with variable well diameter. In regions of changing well diameter nodal point distances down to 1 m were used.

The wellbore simulator accounts for the pipe roughness in the well. The roughness values used here are between 0.2–2 mm, which is common for cast iron (White, 1979). The roughness factor was found to be insignificant in single liquid and two-phase flow conditions but was varied to match flowing pressures in wells discharging superheated steam. It should also be noted that inner diameters of the casing and liner are used to specify the wellbore geometry. This neglects flow in the annulus between the liner and the well and may cause some uncertainties in single-phase steam and two-phase flow predictions, but should not be significant for single-phase liquid flow where the liquid density dominates the pressure gradient.

5.1 Cerro Prieto Wells M-51, M-90, M-91 and M-39

Flowing pressure profiles for wells at Cerro Prieto, Mexico include wells M-39, M-51, M-90 and M-91. The data for wells M-51, M-90 and M-91 are discussed in paper by Goyal et al. (1980), from which the data were taken. The data for well M-39 was provided by Lippmann (1986, personal communication).

Figure 5.1 shows calculated and measured pressure profiles for well M-51, the geometry of the well (to the right) and specified wellhead parameters. The match is satisfactory. The simulator predicts two-phase, slug flow along all the well interval shown, which is in agreement with the results of Goyal et al. (1980).

Figure 5.2 shows downhole pressure profiles in well M-90. The calculated pressure is underestimated at the wellhead and overestimated at the wellbottom. This discrepancy is most likely due to transient conditions within the wellbore, suggested by the sharp pressure drop between the two measured pressure values closest to the wellhead. A temperature profile would help determine if the well was in transient state

during the measurements.

Figure 5.3 shows measured and calculated flowing pressures in well M-91. The match is reasonably good. The simulator predicts slug flow in most of the two-phase section (above the depths of 900 m) and bubble flow in the 50-75 m interval above the flashing level. Note that the measured pressures in the single phase flow interval fluctuate around the calculated pressure profile. This may reflect some oscillations in the depth of the flashing level in the well during the discharge.

Figure 5.4 shows calculated and measured pressure profiles in well M-39. For this well the predicted pressure profile agrees very poorly with the measured values. This discrepancy is most likely due to a secondary change in wellbore geometry, caused by scaling (Goyal et al., 1980). The scaling is most likely present at the depth of the flashing level (500 m depth). A reduction in wellbore diameter increases frictional pressure losses and prevents flashing below the scaled interval. An attempt to match the pressure profile using well restriction due to scaling has not been done, basically because of unfamiliarity with the well and the field.

5.2 East Mesa, Well 6-1

Figure 5.5 shows measured and calculated downhole conditions in East Mesa well 6-1. The data are from Gould (1974) and Juprasert and Sanyal (1977). Neither of these papers give the actual wellbore geometry. The wellbore diameter assumed corresponds to a 9 5/8 " outer casing diameter, which is common for geothermal wells. Other well diameters tried did not yield as good match with the measured data. The discharged fluid contained 20-25 g/l total dissolved solids. This increases the liquid density, compared to the pure water relations used in HOLA, but this effect seems to be rather insignificant, as indicated by the good match.

5.3 Krafla, Wells KW-2, KJ-7 and KJ-9

Figure 5.6 shows calculated and measured flowing profiles for Krafla well KW-2. The data was provided by Steingrímsson (1986, personal communication). The measured downhole profiles could only be matched by introducing scaling in the well at approximately 300 m depth. This is a reasonable assumption since scaling has occurred in most other Krafla wells (Stefan Arnórsson, 1978). A trial and error procedure was used to determine a scaling geometry (shown in the figure) that matched the measured profiles. Certainly, with lack of other independent data the determination of the scaling geometry is rather non-unique, but yields a good match.

Figure 5.7 shows calculated and measured downhole pressures in Krafla well KJ-7. The data were provided by Steingrímsson (1986, personal communication). The well was discharging superheated steam during the measurement. The measured pressure profile was easily matched and in addition allows an estimation of actual pipe roughness to be made. The value that yielded the best results was 0.2 mm, which is in good agreement with handbook values.

Figure 5.8 shows calculated and measured profiles for Krafla well KJ-9. The data are from Stefánsson and Steingrímsson (1981) and Steingrímsson (1986, personal communication). The measured pressures and temperatures resemble those from well KW-2 and could not be matched without the introduction of scaling. A trial and error procedure was used to find the scale geometry that matched the measured data. The sharp spike at ≈ 250 m depth in the calculated temperature occurs when the wellbore diameter changes suddenly. This happens because of negative pressure gradient and very high fluid velocities at the upper edge of the scaling. This sharp spike is of no practical importance and can be reduced by appropriate refinements in the grid.

5.4 Nesjavellir Well NJ-14

Figure 5.9 shows calculated and measured downhole conditions in Nesjavellir well NJ-14. The data were provided by Steingrímsson (1986, personal communication). The figure demonstrates the difficulties encountered when a high temperature well is

measured during discharge. The well was shut in prior to measurement, the logging device emplaced and the well was discharged again. Two data points were measured at each depth, at different times. It is evident from the figure that large flow transients occurred during the measurements, especially in the pressure profile. In addition the measured pressure/temperature values do not match saturation conditions, although the well flashes to the bottom. Calculated downhole profiles, based on wellhead data, are also shown in Figure 5.9. Understandingly they match poorly with the measured data. This inconsistency is almost certainly caused by the rapid transients in the measured data, which cannot be matched by a steady state simulator.

5.5 Svartsengi, Well 4

Figure 5.10 shows measured and calculated pressure profiles in Svartsengi well no. 4. The data are from a report by Parlactuna (1985). The well discharges brine, with a total dissolved solids content of about 21 g/l. Silicia scaling is common in Svartsengi wells at the flashing level, and the wells are frequently cleaned in order to maintain production. A caliper measurement was conducted in well 4 in December 1978, indicating scaling at and above the flashing level. Its shape was specified directly in the input data for HOLA. The results are shown in Figure 5.10. The match is satisfactory. It should be noted that there is 2 years difference between the caliper and pressure measurements. It should also be noted that there is a small difference between the calculated and measured pressure gradients in the liquid region below 350 m depth. This reflects the high liquid density caused by the high concentrations of dissolved solids in the fluid and shows that the effects of dissolved solids should be considered if detailed matching is to be done.

5.6 Summary

In summary, the wellbore simulator HOLA has shown the capability of matching pressure and temperatures profiles from single-feedzone, geothermal wells. For most cases reasonable matches were observed and where discrepancies were found, these are most likely due to transient conditions in the wellbore. This emphasizes the need for very

careful measurements of flowing wellbore conditions, since if large transients are present the data may be totally useless for simulation studies.

Some of the measured profiles were not matched without introducing a scaling in the wells, which is reasonable in the fields considered. This shows that the simulator is capable of predicting secondary changes in wellbore geometry, given measured pressure and/or temperature profiles in the well.

6.0 PREDICTING INTERNAL FLOWRATES IN WELLS

One of the most practical applications of a multi-feedzone wellbore simulator is to use it for estimating flowrates and enthalpies of the different feedzones in a well. This information is often difficult to gain by other methods. A possible alternative is to measure the wellbore flowrate by flowmeters, also called spinners (Solbau et al.,1983). Flowmeters measure volumetric flowrates with depth. The main difficulty encountered in the use of a downhole flowmeter (and all other downhole instruments) in high temperature fields is transmitting the data to the surface. Electrically insulated cables which can withstand temperatures on the order of 250–350 °C and pressures in the range 50–200 bars are expensive and rare. The flowmeters themselves are also sensitive devices which tend to break down during measurement.

The wellbore simulator HOLA can be used to estimate internal flowrates in geothermal wells, given the measured downhole pressures and/or temperatures. Simulation begins at the wellhead, where all the flow parameters are known. Unique downhole profiles are then calculated down to the first feedzone. The interpretation begins at that point by specifying the feedzone flowrate and enthalpy. Calculations then proceed to the next feedzone, where new feedzone parameters are specified. This continues down to the lowest feedzone, for which parameters need not be specified since they can be computed from the specified wellhead conditions and the flowrates and enthalpies of all the other feedzones. The flow values and enthalpies of the individual feedzones are then varied until the calculated temperature and pressure profiles match the measured ones.

Even though temperature and pressure profiles in a flowing well have been matched, this does not mean that an unique solution has been obtained. Experience gained when using the simulator HOLA has indicated that the predicted feedzone parameters are generally nonunique. Thus, the interpretations of flowing wellbore profiles will never yield unique parameters without support from other, independent data.

In the following sections (6.1-6.4) interpretations of flowing downhole surveys in geothermal wells in Kenya and Iceland are presented. All of these wells have two or more

major feedzones. The method of interpretation is described briefly and the non-uniqueness of the solutions discussed.

6.1 Nesjavellir Well NJ-7

Figure 6.1 shows calculated and measured downhole profiles for well NJ-7 in the Nesjavellir field, Iceland. The data were provided by Steingrímsson (personal communication, 1987). The well discharged 23 kg/s of steam/liquid mixture during the test, with a total fluid enthalpy of 1360 kJ/kg. Feedzones are located at 1000, 1550 and 1900 m depth. It was believed that most of the fluid is produced from the feedzone at 1900 m depth (Steingrímsson, 1987, personal communication).

The constant, 260 °C temperature at 1100-1600 m depth in well NJ-7 indicates flow of single-phase liquid with an enthalpy of approximately 1150 kJ/kg. This enthalpy is substantially lower than measured at the wellhead, and requires discharge of high enthalpy fluid from the feedzone at 1000 m depth. It also indicates that the liquid water at 1100-1600 m depth is flowing upwards in the well, from feedzone at 1550 m. At depths greater than 1550 m there is a sharp change in the temperature, most likely caused by low flowrate of the deepest feed and hence large effects of ambient heat fluxes on the wellbore fluid temperature.

The initial reservoir pressure and temperature at 1000 m depth in well NJ-7 are approximately 80 bars and 260 °C (Stefánsson, 1985), respectively. For these thermodynamic conditions single phase liquid has an enthalpy of 1100 kJ/kg. In order to match the data, higher enthalpy is required, suggesting two-phase conditions in the reservoir.

The calculated pressure and temperature profiles shown in Figure 6.1 are obtained by assuming an enthalpy of 1500 kJ/kg for the feedzone at 1000 m depth. The calculated solution shows that most of the produced fluids are flowing from the feedzone at 1000 m. The rest is primarily from the feedzone at 1600 m, with negligible flow from below.

The assumed 1500 kJ/kg fluid enthalpy at 1000 m depth is very uncertain; it is only required that this enthalpy must be higher than the wellhead enthalpy, since colder fluid is flowing from below and mixing with the discharge from the uppermost feedzone. This makes the determined feedzone parameters shown in Figure 6.1 nonunique. For example, higher enthalpy at the feedzone at 1000 m would reduce the flow from that feedzone and vice versa. Independent data such as determination of the enthalpy of the upper feedzone, perhaps by geochemical considerations, will make the parameter determinations much more unique.

6.2 Krafla Well KJ-11

Well KJ-11 in the Krafla field, Iceland is a classical example of a well discharging fluids from two or more feedzones with very different characteristics. This well is discussed in detail in a later section. This section presents two different interpretations of the same downhole data, showing that similar calculated downhole pressure and temperature profiles can be obtained for two different sets of feedzone parameters.

The downhole data shown in Figures 6.2 and 6.3 were provided by Steingrímsson (1986, personal communication). The test was done only two weeks after initial discharge of the well. Major feedzones are at 850–1050 m, at 1500 m and below 1800 m depth. The wellhead flowrate and enthalpy were not recorded during the test, but are believed to be on the order 30–40 kg/s and 900 kJ/kg, respectively (Steingrímsson and Gíslason, 1978). The very high measured pressure gradient in the single-phase liquid interval below 1000 m depth, indicative of fluid density of 1040 kg/m³, suggests that flow transients are taking place during the test.

The constant temperature between 1000 to 1750 m depth suggests internal flow between feedzones, but there are no indications of the actual direction of flow. The data were therefore simulated by assuming both upward and downward flow for this interval.

Figure 6.2 shows calculated downhole profiles assuming the feedzone at 1000 m depth

is discharging fluid both to the wellhead and down to the lower feedzones. The match is satisfactory, with the exception of pressure differences at 750–1100 m depth, which probably are due to transients in the measured pressure. The simulation accounts for heat losses to the ambient and gives an estimated 0.2 kg/s flowrate in the lowest section of the well. In this case the uppermost feedzone produces about 40 kg/s to the well, most of which flows upwards to the wellhead.

Figure 6.3 shows, on the other hand, calculated downhole profiles if fluid is assumed to flow upwards in all of the well. This simulation suggests that the majority of the flow is coming from a feedzone at 1775 m depth. There are again differences between calculated and measured pressures but the temperature match is satisfactory.

If the Krafla reservoir temperatures are considered, the interpretation shown in Figure 6.2 is more likely to represent the actual flowing conditions of the well during the test, rather than from what is shown Figure 6.3. The feedzones at 850–1050 m depth have liquid fluid temperatures between 200–220 °C, which corresponds to enthalpy of 850–950 kJ/kg (Stefansson, 1980). The 670 kJ/kg enthalpy assumed for the feedzone at 850 m depth for the results shown in Figure 6.3 is therefore too low. Increasing the feedzone enthalpy would lower the flashing level in the well and reduce the calculated temperatures at 1000–1200 m depth from that shown in the figure.

6.3 Olkaria, Well OW-201

Figure 6.4 shows calculated and measured downhole profiles for well OW-201 in the Olkaria geothermal field, Kenya. The data are taken from Haukwa (1984). Two major feedzones are present in the well, one at 800–900 m and a second one at 1600–1700 m depth.

This test is interpreted in a similar manner to that for well NJ-7. High enthalpy feedzone is present at 850 m depth in the well. Single-phase liquid with 900 kJ/kg enthalpy flows both up and down from a feedzone at 1650 m depth. The enthalpy of the upper feedzone is not precisely known, but should be somewhat higher than the

wellhead enthalpy. It may be higher than that shown in the figure, thus requiring lower flowrate from the uppermost feedzone and increased flowrate from the feedzone at 1650 m, or vice versa. The match between calculated and measured profiles is good and the results indicate that a majority of the discharged fluid is coming from the feedzone at 850 m depth, which is consistent with other well informations (C. B. Haukwa, personal communications, 1986).

6.4 Olkaria Well OW-15

Figures 6.5 and 6.6 show calculated pressure profiles matched with the same measured pressure data in well OW-15 at Olkaria, Kenya. The data are from a report by The Kenya Power Company Limited (1980). There are two major feedzones in the well, at 700 m and 1200 m depth. The fluid enthalpies of the feedzones were estimated as 2400 kJ/kg for the upper one and 1440 kJ/kg for the lower one (GENZL, 1980). The well discharged a two-phase mixture during the measurement and flashed to the bottom of the well. No record was made on the wellhead flowrate or enthalpy during the test.

Figure 6.5 shows calculated bottomhole pressures if known wellhead flowrates and enthalpies prior to the measurement are used as initial wellhead values. The match is poor. Most of the flow comes from the upper feedzone in order to maintain the lower feedzone enthalpy close to the value estimated by GENZL (1980). A sharp change is seen in the pressure gradient at 1150 m depth. This happens when the simulator assumes a change from bubble to slug flow in the well. This causes a rapid acceleration of the liquid phase and requires high pressure gradient. The simulator probably exaggerates the effects of this change in flow regimes, indicating that some kind of smoothing relations might be helpful between the Armand coefficient relations given in Table 3.3.

Figure 6.6 shows the calculated downhole pressure if we assume the wellhead flow to be 8 kg/s and only one feedzone at the wellbottom. The match is good, but is not calculated in accordance with the wellhead data prior to measurement. The suggestion

that the main flow from the well comes from the deeper feed agrees well with results of numerical simulations of the Olkaria field (Bodvarsson et al., 1987a,b).

7.0 WELLBORE PERFORMANCES

Chapters 4 and 5 dealt extensively with the calculations of downhole conditions, given the wellhead flow parameters, wellbore geometry and reservoir temperatures. Flow and enthalpies at individual feedzones were estimated, but the geothermal reservoir did not otherwise play a role in the study. Although the feedzone parameters are of interest to the reservoir engineer, there is also a need to obtain data for accurate design of multiple feedzone wells. Of particular interest is knowledge on how the well responds to different wellhead pressures, what is the maximum possible flowrate, and how much steam the well can produce.

Answers to these questions and others are the subject of this chapter. The methodology involves coupling the wellbore simulator with the geothermal reservoir by use of productivity indices. This also requires wellbore calculations to be made from the bottom of the well to the wellhead. Reservoir pressures and enthalpies are given at each feedzone and the proper option in the HOLA simulator is called to search for possible solutions at the wellhead for different pressures at the wellbottom. Calculated wellhead output curves are presented and the sensitivity of different parameters to flow are discussed. Finally, an interpretation of wellhead performance curves for a multi-feedzone, high-temperature well in Iceland is given.

7.1 Wellhead Output Curves

Before proceeding further, it is worthwhile to discuss some of the parameters of interest at the wellhead, and how they are used to interpret wellbore and reservoir conditions.

The flow characteristics of wells are investigated by changing the wellhead pressure through use of orifice plates of different sizes. Variations in wellhead pressure cause changes in flowrate and sometimes in the fluid enthalpy. It is customary to plot these two parameters as a function of the wellhead pressure. Such plots are referred to as wellhead output curves or wellhead performance curves, or in the case of mass flow

only, delivery curves. Figure 7.1 shows two examples of observed output curves from wells in Costa Rica and Mexico (Gudmundsson, 1986). The Miravalles well is fed by one liquid-dominated feedzone. The flowrate increases with decreasing wellhead pressure but the enthalpy stays essentially constant since there is no boiling in the reservoir, and heat losses in the wellbore are minor (see Figure 7.1b). The Los Azufres well has two-phase flow conditions near its feedzone. As the wellhead pressure decreases, the flowrate and enthalpy increase. The increase in wellhead enthalpy is probably due to the increased flowrate and lower wellhead pressures (O'Sullivan, 1980; Sorey et al, 1980; Bodvarsson et al, 1980).

James (1970, 1980, 1983) studied output curves from several geothermal wells in New Zealand and Italy. He classified their behavior into two categories. One category consists of wells having output curves dominated by the reservoir conditions. In the other category the output curves are controlled by the wellbore geometry. This is an important concept as the objective is to maximize wellhead flowrates without much reduction in wellhead pressure. The reservoir parameters are invariant at each time, leaving the wellbore geometry as the only adjustable parameter. Figure 7.2 shows delivery curves for three Icelandic high temperature wells. These curves demonstrate the importance of reservoir conditions and wellbore geometry on the wellbore performance. Wells SG-4 and SG-10 are located in the Svartsengi field. Both have similar depths to feedzones and there are no great differences in feedzones enthalpies, pressures and calculated productivity indices (Palmason, 1983; Parlaktuma, 1985). The main difference between the wells is in casing design. Well SG-4 has 9 5/8" casing in its uppermost section, whereas well SG-10 has 13 3/8" casing. The figure shows that 40% increase in casing radius doubles the flowrate at similar wellhead pressures, indicating that the wellbore geometry, rather than the reservoir conditions, controls the wellbore flowrate. One must note however, that this is probably only true for reservoirs of high permeability (transmissivity).

Also shown in Figure 7.2 is a delivery curve for well KG-12 in Krafla, Iceland. The well discharges superheated steam and shows no relationship between wellhead

flowrate and pressure. Stefansson and Steingrímsson (1980) consider this flow behavior to be due to large pressure drawdown in the well. The wellbore pressure at the main aquifer during discharge is 19-23 bars, whereas the undisturbed reservoir pressure is 126 bars. A 10 bar change in wellhead pressure is therefore of little significance to the pressure difference between the well and the aquifer and there is a relatively constant flow with wellhead pressure. Another possible explanation of this phenomenon is choked flow at the well-feedzone intersection, a very likely reason considering the large drawdown in the well and the fractured nature of the Krafla reservoir (Bodvarsson, 1987). Whichever explanation is the correct one, it is probably that the reservoir conditions are governing the flow, not the wellbore geometry. A change in the well design would not increase the flow, except possibly if wellbore radius at the feedzone is increased if choked flow exists there.

7.2 Formulating Flow From The Reservoir

The aim of this chapter is to couple the wellbore simulator to the geothermal reservoir. This is done assuming a linear relationship between flowrate and pressure drawdown at the feedzone. The flowrate is then given by a simple relation

$$\dot{m}_{\text{feed}} = I (P_r - P_w) \quad (7.1)$$

where I is the feedzone productivity, P_r is the reservoir pressure at the feedzone and P_w is the wellbore pressure. As before, flow from the reservoir to the well is positive. In order to account for relative permeabilities and variations in the fluid physical properties equation (7.1) can be rewritten

$$\dot{m}_{\text{feed}} = \text{PI} \left[\frac{k_{r1} \rho_1}{\mu_1} + \frac{k_{rg} \rho_g}{\mu_g} \right] (P_r - P_w) \quad (7.2)$$

where k_r is the relative permeability of each of the phases and PI is the productivity index of the feedzone. The relative permeabilities are calculated here by linear relationships.

The productivity index is basically a lumped parameter of the feedzone geometry and

properties. This can be seen from the similarity of equation (7.2) and Darcy's law, which yields the following definition of the productivity index.

$$PI = \frac{k A}{R} \quad (7.3)$$

Here k is the rock permeability, A is the area for flow into the feedzone and R is the distance to the reservoir pressure P_r . As the feedzone discharge continues with time, R increases and PI decreases. Note that equations (7.2) and (7.3) assume laminar flow.

Feedzones in geothermal wells are generally considered as narrow belts of one or more fractures. The fluid velocity in such fractures can become substantial where they intersect the well, causing turbulent or even choked flow at the intersection. This limits the use of equation (7.2) at high flowrates.

7.3 A Solution Algorithm For Wells With Two Feedzones.

Consider a well with two feedzones, where one of them is at the wellbottom. Furthermore it is assumed that the fluid enthalpies, reservoir pressures and productivity indices are given at both feedzones. The flowing conditions at the wellhead can then be calculated by the following method.

- (1) Assume a bottomhole pressure, P_{bott} .
- (2) Use (7.2) to calculate the flowrate of the bottomfeed. If the rate is positive the fluid physical properties are given by the feedzone enthalpy and P_{bott} . Otherwise the fluid properties are assumed to be given by the enthalpy of the shallower feedzone and P_{bott} .
- (3) Solve the governing equations proceeding up the well, until the upper feedzone is reached.
- (4) Use the calculated wellbore pressure and (7.2) to determine the feedzone flowrate. Determine flowrate and enthalpy in the well above the feedzone by the methods

given in Figures 4.1 and 4.2.

- (5) Proceed until the wellhead is reached.

The subroutine ITHHEAD2 in HOLA was coded to incorporate this solution algorithm (see Figure 4.3).

Here it is of interest to find all possible wellhead conditions for a given set of wellbore and reservoir parameters. A rather detailed scanning algorithm in P_{bott} was developed for this purpose. It initially assumes the bottomhole pressure which occurs if the well is filled with a 10°C column of static water (the maximum reasonable reservoir pressure). The wellbore conditions are then calculated by the algorithm described above. The bottomhole pressure is then decreased in steps, and it is checked at every step if solution exists at the wellhead. The computations are terminated only if P_{bott} is lower than the reservoir pressure at the deeper feed and the wellbore pressure is calculated lower than 1 bar.

Since the assumed value of P_{bott} can be far from reality there are several checkpoints present in the program that can stop the calculations. They are:

- (1) Wellbore pressure is calculated lower than 1 bar
- (2) The fluid velocities in the well are twice the sonic velocities, calculated by the methods given in Chapter 4.
- (3) Wellbore pressures/temperatures exceed the critical point or decline below zero.
- (4) There is negative flowrate above the upper feedzone.

For the time being the above solution algorithm is limited to two feedzones in the well. Adding more feedzones is possible but not considered in this work because of the increased number of variables it would add to the already large set of dependent parameters.

7.4 A Limited Sensitivity Study

The program HOLA can be viewed as a function which has a solution for a given set of input parameters and a certain range of bottomhole pressures. There is a minimum of 15 dependent parameters needed in the computations. Using such a high number of parameters in a sensitivity study is an overwhelming task. Setting the rock thermal conductivity at zero will reduce the number of variables to a minimum of 10. The scope of the study is still narrowed by using a standard well geometry and constant depth to the feedzones. The well geometry we use is an 1800 m deep well, 23 cm in diameter down to 750 m and 18 cm in diameter down to the bottom. The feedzones are at 900 and 1800 m depth. Their fluid enthalpies are 900 and 2000 kJ/kg, respectively. The well is henceforth called the "standard" well. Given the above constraint the feedzone pressures and productivity indices are the only variables in a limited sensitivity study.

Figure 7.3 shows calculated wellhead pressure, flowrate and enthalpy as a function of bottomhole pressure for the standard well. The shallower and deeper feedzone pressures are 80 and 140 bars respectively. The productivity index is the same for both feedzones, $1 \times 10^{-12} \text{ m}^3$. The figure shows that HOLA predicts positive wellhead flowrates for 70 bar interval in the bottomhole pressure. This interval is here called the "bottomhole discharge range" or simply "discharge range". The lower feedzone dominates the wellhead flow at 90-120 bars bottomhole pressure. But below 90 bar bottomhole pressure both feedzones discharge into the well, resulting in a reduced wellhead enthalpy and steeper increase in wellhead flowrate. The sharp drop in wellhead enthalpy at approximately 55 bars bottomhole pressure is most likely caused by the transfer of heat energy to kinetic energy as the well chokes (and HOLA terminates computations).

Figure 7.4 shows the same data as in Figure 7.3, but now the wellhead flow and enthalpy are plotted against wellhead pressure. The figure shows that the highest wellhead pressure is obtained when the lower feedzone discharges fluid both to the wellhead and into the upper feedzone. As is generally observed flowrate increases with

decreased wellhead pressure. On the other hand, the wellhead enthalpy is reduced, reflecting increased contribution of low enthalpy fluid from the shallower feedzone.

It is of interest to observe how the bottomhole discharge range changes by using different reservoir pressures at the feedzones. Figure 7.5 shows an example of discharge ranges for the standard well. The productivity indices are $1 \times 10^{-12} \text{ m}^3$ for both feedzones. Reservoir pressure at the shallower feed is kept constant at 80 bars, while the deeper feed pressure varies from 80 to 140 bars. It is inherently assumed here that the permeability of the shallower feedzone is much higher than that of the deeper zone, hence during production the pressure difference between the feedzones will be much less than hydrostatic. The figure shows that the solution space for the bottomhole pressure can be subdivided into low and high enthalpy discharge ranges. The low enthalpy discharge range exists when fluid flows from the shallower feedzone both to the wellhead and down to the deeper feedzone. The high enthalpy range exists when the lower feedzone produces fluid into the well. The fluid discharged at the wellhead is then either a mixture of fluids produced from both of the feedzones, or only from the deeper feed.

The two enthalpy ranges do not coincide in Figure 7.5, indicating that the well will have two distinct output modes for these input parameters. Also marked in the figure are the discharge ranges for a factor of five decrease in the productivity indices (5×10^{-13} instead of $10 \times 10^{-13} \text{ m}^3$). No change is seen in the upper part of the figure, indicating that the wellbore geometry rather than the productivity indices controls the shape of the solution space. On the other hand, the lower portion of the figure shows an increased pressure drawdown for the decreased productivity index. The reason is that this is a boundary of critical mass flow, causing a choked flow at the wellhead. If the productivity index is lowered, an increase in drawdown is needed to obtain the required critical mass flow at the wellhead.

7.5 Field Application : Well KJ-11 in Krafla, Iceland

Instead of proceeding into a detailed study of parameters we will try to use the methods presented in the previous section to interpret an output curve from the two feedzone well KJ-11 in the high temperature Krafla field in NE-Iceland.

The Krafla reservoir has been described by several authors (Stefansson 1981, Bodvars-son et al., 1984 a,b,c, Pruess et al., 1984). Figure 7.6 shows a simplified model of the field. A high enthalpy, two-phase fluid flows from below into a lower reservoir zone. Pressures and temperatures are close to saturation values, but some deviation is detected because of high amounts of noncondensable gases in the fluid. The lower reservoir zone discharges fluid up through the Hveragil gully to an upper reservoir zone, characterized by lower temperatures and liquid phase fluid.

It should be noted that most of the measurements taken in well KJ-11 show some effects of transient flow (Steingrímsson 1987, personal communication). This data may therefore not be appropriate for steady-state simulations. However, these measurements were the only one available for the study, and they certainly serve as a guide to increased understanding of flow conditions in multi-feedzone wellbores.

7.5.1 Feedzones and Flow Characteristics of Well KJ-11

Well KJ-11 was drilled to 2217 m depth in November 1976. The well is deep enough to produce from both layers of the Krafla reservoir. Figure 7.7 shows the geometry of the well, location of feedzones and estimated reservoir temperatures and pressures prior to production. It is evident from the figure that the feedzones at 800-1050 m depth discharge from the upper reservoir zone, whereas the feedzones below 1500 m produce from the lower reservoir layer (Steingrímsson and Gíslason, 1978). Temperature measurements taken during the warmup period indicate that fluid was flowing from feedzones at approximately 1000 m depth down to the deeper feedzones.

Discharge was initiated from well KJ-11 by pumping air into the water column. The wellhead output curves were then measured and are shown in Figure 7.8 (Stefansson

and Steingrímsson, 1980). The figure shows that the well had two discharge modes, a low enthalpy mode for wellhead pressures under 7 bars, and an high enthalpy mode for wellhead pressures above 9 bars. The well tended to flow in the low enthalpy mode. The high enthalpy range was reached by fully opening the well to the atmosphere. The well was then left in this condition for 12-13 hours, but then it switched in a matters of seconds to the high enthalpy output mode (Steingrímsson 1987, personal communication). This output mode was favorable for the power station and the well was connected to surface pipelines in August 1977. Difficulties were observed during operation because the well was very sensitive to pressure changes at the wellhead, causing it to switch to the low enthalpy output mode. As time went by, it also became more and more difficult to induce high enthalpy flow from the well. The upper feedzones in the well were therefore cased off in 1978. After the casing operation the well discharged ≈ 6 kg/s of superheated steam with 2100 kJ/kg enthalpy (Steingrímsson, personal communication, 1986).

7.5.2 Simulating the Output Curves

The sensitivity study in the previous section is applicable for an interpretation of the output characteristics of well KJ-11. Since the well has two distinct discharge modes there is probably a very narrow, no-solution range between the high and low enthalpy bottomhole discharge ranges for the well (similar to what is shown in Figure 7.5). Any slight disturbance in bottomhole pressure is then sufficient to switch the wellbore flow from one enthalpy discharge range to the other, explaining the two different flow characteristics at the wellhead.

Our aim here is to reproduce the measured output curves of well KJ-11. In order to calculate these curves we need to know the feedzone parameters. They can be estimated by available data except for the productivity indices. The following method is used for that purpose.

- (1) Figure 7.7 shows that there are 6 possible feedzones in the well. We will group these feedzones into one feedzone at 1000 m depth and into another one at either

1600 or 2000 m depth. The enthalpy of the upper feed is set at 925 kJ/kg, and the enthalpy of the lower feed is set at 2000 kJ/kg (Armansson, 1980). Reservoir pressure at the upper feed is set at 70 bars but various pressures are tested at the lower feed.

- (2) The total mass flow at the wellhead, \dot{m}_{top} is given by adding the flow from both feedzones and by using (7.2):

$$\dot{m}_{top} = \gamma_1 PI_1 (P_{r1} - P_{w1}) + \gamma_2 PI_2 (P_{r2} - P_{w2}) \quad (7.4)$$

where the subscripts 1 and 2 denote the upper and the lower feedzones, respectively, and γ is the mobility of the fluid, given by

$$\gamma = \frac{k_{r1} \rho_1}{\mu_1} + \frac{k_{rg} \rho_g}{\mu_g} \quad (7.5)$$

- (3) A liquid column existed in well KJ-11 from wellbottom to less than 1000 m depth when it was discharged in the low enthalpy mode (see Figure 6.2). The studies described in section 6.2 also indicated that fluid was flowing down the well at this interval. This causes a near hydrostatic pressure gradient between the feedzones. If we also assume that changes in fluid density and viscosity are negligible between the two feedzones, then (7.4) can be written as

$$\dot{m}_{top} \approx \frac{\rho_1}{\mu_1} \left[PI_1 \{ P_{r1} - P_{w1} \} + PI_2 \{ P_{r2} - (P_{w1} + \rho_1 g \Delta H) \} \right] \quad (7.6)$$

where ΔH is the distance between the two feedzones. Note that downflow can only occur in the well if $P_{r2} \leq P_{w1} + \rho_1 g \Delta H$.

- (4) Equation (7.6) can now be solved for the two unknown productivity indices if we know two values of wellhead flowrate and the corresponding wellbore pressures at the upper feedzone. The wellbore pressure at 1000 m depth is predictable by HOLA, since we know three wellhead pressure, flow and enthalpy values from Figure 7.8. Figure 7.9 shows these three downhole pressure curves, calculated from the measured wellhead data. The figure shows that increased pressure

drawdown follows the combined increase in wellhead flow and decrease in wellhead pressure. An exception is the pressure profile for the lowest wellhead pressure (Case A), showing higher wellbore pressure than the other two cases. This is in contrast with the increase in measured wellhead flow which requires greater drawdown in the well. The wellhead parameters used to calculate this profile are therefore not used for the study.

Equation (7.6) can now be solved for the three unknowns, PI_1 , PI_2 and P_{r2} . The results are shown in Table 7.2.

It should be emphasized that Table 7.2 is constructed by using measured and assumed properties of the low enthalpy discharge mode. The results are governed by the properties of the upper feedzone. The only parameters dependent on the lower feedzone are its pressure and depth. The very low values for the pressure at the lower feedzone suggest that either the data are dominated by transients or that the upper feedzone permeabilities are much greater than the deeper feedzone permeabilities.

When the productivity indices are known we can proceed to the calculation of wellhead output curves. Figure 7.10 shows calculated wellhead flowrates and enthalpies as a function of wellhead pressure. The figure considers two reservoir pressures at the lower feedzone, 71.5 bars and 76.5 bars (see Table 7.2 for the corresponding PI -indices). The low enthalpy discharge mode is "matched perfectly" which is not surprising since the feedzone parameters were designed for these measured values. The well flashes down to the bottom when positive flow occurs from the lower feed. This reduces potential pressure losses in the well and substantially increases the wellhead pressures. The wellhead pressure increases, for example, to 54 bars in the 76.5 bars bottomfeed pressure case. The 71.5 bars case shows on the other hand a curved flowrate profile with wellhead pressure. This behavior is primarily caused by the existence of a single-phase, liquid plug above the upper feed. The length of this liquid plug decreases as the flow from the lower feedzone increases and as it finally disappears, the wellhead pressure declines with increased flowrate, as is generally observed.

TABLE 7.1 Calculated productivity indexes for well KJ-11. $\rho_l = 850 \text{ kg/m}^3$ and $\mu_l = 0.0012 \text{ kg/m/s}$.

Input data				
\dot{m}_{top} (kg/s)	P_{top} (bars)	P_{w1} (bars)	P_{w2} (bars)	ΔH (m)
14.9	6.6	32.1	82.1	1600
-	-	-	115.6	2000
23.8	5.6	27.1	77.1	1600
-	-	-	110.6	2000

Calculated PI-indexes, $\Delta H = 1600 \text{ m}$

P_{r2} (bars)	PI_1 (m^3)	PI_2 (m^3)
76.5	1.3×10^{-12}	2.9×10^{-12}
71.5	1.6×10^{-12}	2.6×10^{-12}
66.5	1.9×10^{-12}	2.3×10^{-12}

Calculated PI-indexes, $\Delta H = 2000 \text{ m}$

P_{r2} (bars)	PI_1 (m^3)	PI_2 (m^3)
110	1.3×10^{-12}	2.9×10^{-12}
105	1.6×10^{-12}	2.6×10^{-12}
100	1.9×10^{-12}	2.3×10^{-12}

Figure 7.11 shows the same type of wellhead output curves as in Figure 7.10, but with the lower feedzone at 2000 m depth. Two reservoir pressures at the lower feedzone are either 105 bars or 110 bars (see Table 7.2 for the corresponding PI-indices). Maximum wellhead pressures are now much higher than previously and the calculated wellhead enthalpies are somewhat higher than measured.

7.5.3 Some General Comments on the Results

Well KJ-11 was never able to discharge at a higher wellhead pressure than 10–15 bars in the high enthalpy mode. On the other hand, the calculated output curves shown in Figures 7.10 and 7.11 predict flowing wellhead pressures far higher than measured. This inconsistency may be caused by one or more of the following reasons:

- (1) Low permeability of the formation.
- (2) The high steam saturation at the deeper feed causes a factor of 1 or 2 increase in volumetric flowrates compared to the case where the same mass is flowing as single-phase liquid. This causes turbulent or even choked flow at the feedzone and reduces maximum flowrates from what is shown in Figures 7.10 and 7.11.
- (3) The productivity index of the lower feedzone depends on the flow direction in the well. The low enthalpy fluid coming from above cools and causes thermal contraction of the reservoir rock, hence an increase in fracture width. As the flow direction is changed the fluid channels in the reservoir warm up again and contract. These changes in the geometry of the fluid channels cause some transients in the productivity index of the feedzone.
- (4) Although the wellbore simulator HOLA calculates a range of steady state solutions at a flowing wellhead, no judgement is made on the dynamic stability of these solutions, or if they can ever show up in the wellhead measurements.

By using the above arguments we can conclude that the simulator HOLA is not capable of predicting the high enthalpy flow characteristics of well KJ-11. The data and

the flow characteristics of the well are probably too transient for the work. However, the low enthalpy discharge studies may be correct and can serve as a future guide for estimating feedzone properties of geothermal wells, given that the fluid flow in the feedzones follows the linear assumptions discussed in Chapter 7.2. A lack of field data prevents further study on this aspect.

8.0 CONCLUSIONS

The purpose of this study was to examine the effects of two or more feedzones on downhole flow conditions in geothermal wells. A wellbore simulator was developed to solve numerically the steady-state nonlinear equations that describe single or two phase flow in a vertical pipeline.

The simulator was validated by comparing computed pressures and temperatures to actual results from ten, single feedzone wells. Most of the measured data were matched reasonably well, but some of the wells necessitated the introduction of scaling in the wellbore. It was also seen that transient effects inherent in some of the wellbore data yields inconsistent results that cannot be analyzed by a steady state simulator.

Experience, gained by using the simulator, showed that 25 m grid spacing was adequate for most calculations. It also showed that the pipe roughness is of the order 0.2-2 mm which is common for cast iron. Phase velocities are always predicted by the method of Armand coefficients, which gives more continuous derivatives in the Newton-Raphson iteration subroutine of the code.

The simulator was used to match flowing profiles in wells which showed effects of two or more feedzones. Flowrates and enthalpies of individual feedzones were estimated and gave important information on reservoir aquifers. The results are found to be rather non-unique and show that the interpretation needs support from independent field data. The results are also found to be sensitive to the accuracy of the measured wellhead data.

The concept of wellhead output curves was introduced. The wellbore simulator was then coupled to the reservoir by using productivity indices at the feedzones and by specifying the reservoir pressure and fluid enthalpy for each feedzone. The wellhead flow conditions were then calculated by varying the initial bottomhole pressure of various fields.

The calculation of wellhead output curves depends on many problem parameters.

Because of this high number of dependent variables a limited scoping study was conducted for the special case of wells which have low fluid enthalpy at the intermediate feedzone and high enthalpy at the bottom. The results showed that these wells discharge in two different output modes, depending on which feedzone is governing the flow. These two output modes were defined as low- and high enthalpy discharge ranges. The discharge ranges showed to be sensitive to variations in the feedzone pressures. A systematic study of different feedzone pressures led to the introduction of low and high enthalpy stagnation points. The high enthalpy stagnation point was shown to give the maximum pressure difference between the two feedzones, required to discharge the lower feedzone.

Variations in the productivity indices of the two feedzones changed the maximum drawdown boundaries of the high enthalpy range. No effects were on the other hand seen on the shape of the low enthalpy discharge range, indicating that the wellbore geometry controls the output behavior of the well.

Field application was made to well KJ-11 in Krafla, Iceland. It was shown that the two different output modes of the well compared to the definition of high and low enthalpy discharge ranges. Measured data in the low enthalpy mode was used to estimate the productivity indices of the two major feedzones in the well. These parameters were then used to calculate output curves for the well. The predicted wellhead pressures were much higher than ever measured, but this inconsistency is assumed to be a consequence of low feedzone permeability, flow transients, choked flow at the deeper feedzone and not least because of unknown dynamic stability of the calculated profiles.

REFERENCES

- Armand A.A., 1945: Resistance to Two-Phase Flow in Horizontal Tubes (in Russian). *Izv. VTI*, 1946, 15(1), 16-23. English Translation NLL M882, Boston Spa, Yorks: National Lending Library.
- Arnorrsson, S., 1978: Framvinduskýrsla um Efnafræði Utfellinga í Borholum við Kroflu (in Icelandic). The National Energy Authority Report No. OS-JHD-7832, Reykjavik, Iceland.
- Armannsson H., G. Gíslason and T. Hauksson, 1982: Magmatic Gases in Well Fluids Aid the Mapping of the Flow Pattern in a Geothermal System. *Geochim. Cosmochim. Acta*, 46, 167-177.
- Barelli A., R. Corsi, G. Del Pizzo and C. Scali, 1982: A Two-Phase Flow Model for Geothermal Wells in the Presence of Non-Condensable Gas. *Geothermics*, Vol. 11, No. 3. pp. 175-191.
- Bjarnason J.O., 1985: Undirforritasafnid Steam (in Icelandic). The National Energy Authority Report No. OS-85069/JHD-09, Reykjavik, Iceland.
- Bodvarsson G.S, M.J. O'Sullivan and C.F. Tsang, 1980: The Sensitivity of Geothermal Reservoir Behavior to Relative Permeability Parameters. *Proc., Sixth Workshop Geothermal Engineering*, Stanford University, Stanford, California, pp. 224-237.
- Bodvarsson G.S, 1982: Mathematical modeling of the behavior of geothermal systems under exploitation, Ph.D. Thesis, University of California, Berkeley, Lawrence Berkeley Laboratory Report LBL-13937, 353 pp.
- Bodvarsson G.S, S.M. Benson, O. Sigurdsson, V. Stefansson and E.T. Eliasson, 1984a: The Krafla Geothermal Field, Iceland. 1. Analysis of Well Test Data. *Water Res. Res.*, Vol 20(11), pp. 1515-1530.
- Bodvarsson G.S, K. Pruess, V. Stefansson and E.T. Eliasson, 1984b: The Krafla Geothermal Field, Iceland. 2. The Natural State of the System. *Water Res. Res.*, Vol 20(11), pp. 1531-1544.
- Bodvarsson G.S, K. Pruess, V. Stefansson and E.T. Eliasson, 1984c: The Krafla Geothermal Field, Iceland. 3. The Generating Capacity of the Field. *Water Res. Res.*, Vol 20(11), pp. 1545-1559.
- Bodvarsson G.S. and K. Pruess, 1987a: East Olkaria Geothermal Field, Kenya. 1. History Match With Production and Pressure Decline Data. *Journ. Geoph. Res.*, vol 92, NO. B1, pp 521-539.
- Bodvarsson G.S., K. Pruess, V. Stefansson, S. Bjornsson and B. Ojiambo, 1987b: East Olkaria Geothermal Field, Kenya. 2. Predictions of Well Performance and Reservoir Depletion. *Journ. Geoph. Res.*, vol 92, NO. B1, pp 541-554.

- Burden L.B., J.D. Faires and A.C. Reynolds, 1981: Numerical Analysis. Second Edition, 591 pp. Prindle, Weber and Schmidt, Boston, USA.
- Carslaw and Jaeger, 1959: Conduction of Heat in Solids. Oxford University Press, second edition.
- Chierici Gian Luigi, G. Giannone and G. Schlocchi, 1981: A Wellbore Model for Two-Phase Flow in Geothermal Reservoirs. Proceedings of the 56nd Annual Fall Technical Conference and Exhibition of the Society of Petroleum Engineers of AIME, San Antonio, Texas, 1981. Paper SPE-10315.
- Chisholm D., 1973: Pressure Gradients Due to Friction During the Flow of Evaporating Two-Phase Mixtures in Smooth Tubes and Channels. Int. J. Heat Mass Transfer. Vol. 16, pp. 347-358.
- Chisholm D., 1983: Two-Phase Flow in Pipelines and Heat Exchangers. George Godwin, London and New York.
- DiPippo R., 1985: Geothermal Electric Power, The State of the World - 1985. The 1985 International Symposium on Geothermal Energy - International Volume. pp. 3-18. Geothermal Resource Council.
- Genzl, 1980: Measurement Reports KCP/GENZL 038 and 039. Prepared for the Kenya Power Company Ltd.
- Govier G.W. and K. Aziz, 1972: The Flow of Complex Mixtures in Pipes. Van Nostrand Rheinhold, New York.
- Gudmundsson J.S., 1985: Direct Uses of Geothermal Energy in 1984. The 1985 International Symposium on Geothermal Energy - International Volume. pp. 19-32. Geothermal Resource Council.
- Gudmundsson J.S., 1986: Two Phase Wells. Geothermal Resource Council Bulletin, pp. 10-16, March.
- Gould Thomas L, 1974: Vertical Two-Phase Steam-Water Flow in Geothermal Wells. Journal of Petr. Tech., vol. 26, pp. 833-842.
- Goyal K.P., C.W. Miller and M.J. Lippmann, 1980: Effect of Wellhead Parameters and Well Scaling on the Computed Downhole Conditions in Cerro Prieto Wells. Proc., Sixth Workshop Geothermal Engineering, Stanford University, Stanford, California.
- Grant M.A., I.G. Donaldsson and P.F. Bixley, 1982: Geothermal Reservoir Engineering. Academic Press.
- Grant M.A., P.F. Bixley and I.G. Donaldsson, 1983: Internal Flow in Geothermal Wells: Their Identification and Effect on the Wellbore Temperature and Pressure Profiles. J. Society Petroleum Engineers, pp. 168-176, May 1983.

- Haukwa C.B., 1984: Recent Measurements Within Olkaria East and West Fields. A Paper for the Kenya Power Company Scientific and Technical Review Meeting, November, 1984. The Kenya Power Company Ltd.
- International Formulation Committee (IFC), 1967: A Formulation of the Thermodynamic Properties of Ordinary Water Substances. Issued by the Sixth International Formulation Committee of the Sixth Conference on the properties of steam, Feb. 1967.
- James R., 1970: Factors Controlling Wellbore Performance. U.N. Symposium on the Development and Utilization of Geothermal Resources, Pisa 1970. Vol. 2, Part 2, pp. 1502-1515.
- James R., 1980: Deductions of the Character of Steam-Water Wells from the Shape of the Output Curve. Proc. 2nd New Zealand Geothermal Workshop. University of Auckland.
- James R., 1983: Locus of Wellhead Pressure with Time Under Production Discharge. Proc. 5th New Zealand Geothermal Workshop. University of Auckland.
- Juprasert S. and S.K. Sanyal, 1977: A Numerical Simulator for Flow in Geothermal Wellbores. Geothermal Resource Council, Transactions, Vol. 1, pp. 159-161.
- The Kenya Power Company Ltd, 1981: Geothermal Project Report ME/OW/15/011 on Shut-In Test on Olkaria Well 15.
- Kjaran S.P. and J. Eliasson, 1983: Geothermal Reservoir Engineering Lecture Notes. Rep. No. 1983-2, The UNU Geothermal Training Programme, Iceland.
- Martinelly R.C. and Nelson D.B., 1948: Prediction of Pressure Drop During Forced Circulation of Boiling Water. Trans. Amer. Soc. Mech. Engrs., 1948, 70(6), 695-702.
- Miller C.W., 1980: Wellbore User's Manual. Lawrence Berkeley Laboratory Report, no. LBL-10910, 48 pp. Berkeley, California.
- Miller C.W., S. Benson, M.J. O'Sullivan and K. Pruess, 1981: Well-Bore Effects in the Analysis of Two-Phase Geothermal Well Tests. Presented at the Society of Petroleum Engineers' California Regional Meeting, Bakersfield, California, March 25-27, 1981.
- Orkiszewski J., 1967: Predicting Two-Phase Pressure Drop in Vertical Pipe. Journal Petroleum Technology, pp. 829-838, June 1967.
- O'Sullivan M.J., 1980: A Similarity Method for Geothermal Well Test Analysis. Water Resour. Res., 17(2), pp. 390-398.
- Palmason G., V. Stefansson, S. Thorhallsson and T. Thorsteinsson, 1983: Geothermal Field Developments in Iceland. Proc., Ninth Workshop Geothermal Engineering,

Stanford University, Stanford, California.

Parlaktuna Mahmut, 1985: Two-Phase Wellbore Simulator and Analysis of ReInjection Data from Svartsengi, Iceland. The UNU Geothermal Training Programme, Iceland, report no. 1985-7.

Pruess K., G.S. Bodvarsson, V. Stefansson and E.T. Eliasson, 1984: The Krafla Geothermal Field, Iceland. 4. History Match and Prediction of Individual Well Performance. Water Res. Res., Vol 20(11), pp. 1561-1584.

Sigurdsson O., S.P. Kjaran, T. Thorsteinsson, V. Stefansson and G. Palmason, 1985: Experience of Exploiting Icelandic Geothermal Reservoirs. The 1985 International Symposium on Geothermal Energy - International Volume. pp. 357-372. Geothermal Resource Council.

Solbau R.D., C.B. Goranson and S.M. Benson, 1983: The Development and Use of a High Temperature Downhole Flowmeter for Geothermal Well Logging. Proc., Ninth Workshop Geothermal Engineering, Stanford University, Stanford, California.

Sorey M.L., M.A. Grant and E. Bradford, 1980: Non-Linear Effects in Two-Phase Flow to Wells in Geothermal Reservoirs. Water Resources Research, 16(4), pp. 767-777.

Stefansson V., 1980: Rannsoknir a Hahitasvaedinu i Kroflu (in Icelandic with English Summary). Natturufraedingurinn, 50 (3-4), pp. 333-359.

Stefansson V., 1981: The Krafla Geothermal Field, Northeast Iceland. In Geothermal Systems: Principles and Case Histories. Edited by L. Rybach and L.J.P. Muffler. John Wiley & Sons Ltd.

Stefansson V. and B. Steingrimsson, 1980: Production Characteristics of Wells Tapping Two Phase Reservoirs at Krafla and Namafjall. Proc., Sixth Workshop Geothermal Engineering, Stanford University, Stanford, California.

Stefansson V. and Steingrimsson, 1981: Geothermal Logging I. The National Energy Authority Rep. No. OS80017/JHD09, 2nd. ed., Reykjavik, Iceland.

Steingrimsson B. and Gislason G., 1978: Krafla - Afmaelingar i Borholum (in Icelandic). The National Energy Authority Report no. OS-JHD-7804, Reykjavik, Iceland.

Thorarinsson S., 1967: Skaftareldar and Lakagigar (in Icelandic with English Summary). Natturufraedingurinn, 37, pp. 27-33.

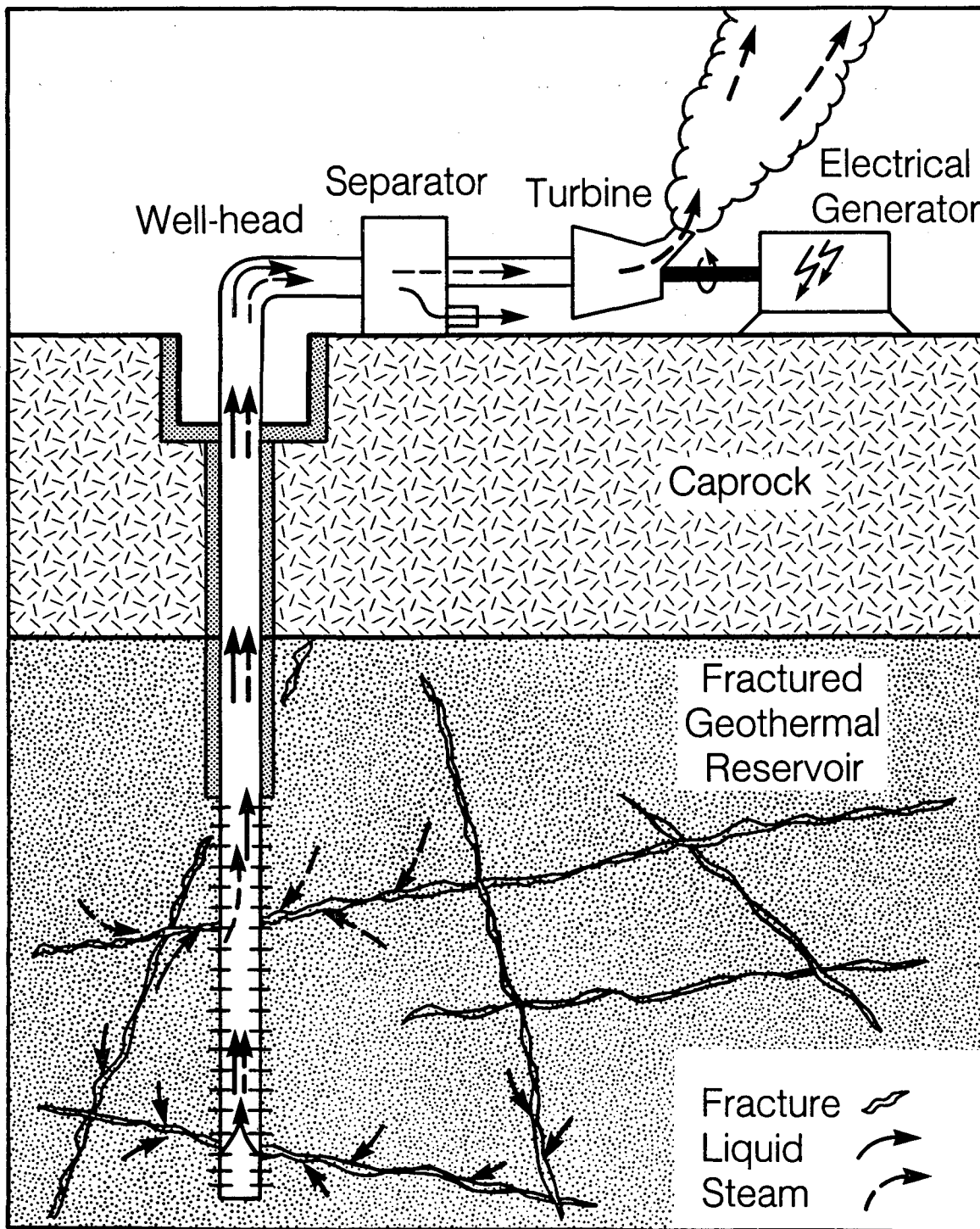
Upadhyay R.N., J.D. Hartz, B.N. Tomkoria and M.S. Gulati, 1977: Comparison of Calculated and Observed Pressure Drops in Geothermal Wells Producing Steam-Water Mixtures. Proceedings of the 52nd Annual Fall Technical Conference and Exhibition of the Society of Petroleum Engineers of AIME, Denver, Colorado,

1977. Paper SPE-6766.

Wallis G.B., 1969: One-Dimensional Two-Phase Flow. McGraw-Hill, USA.

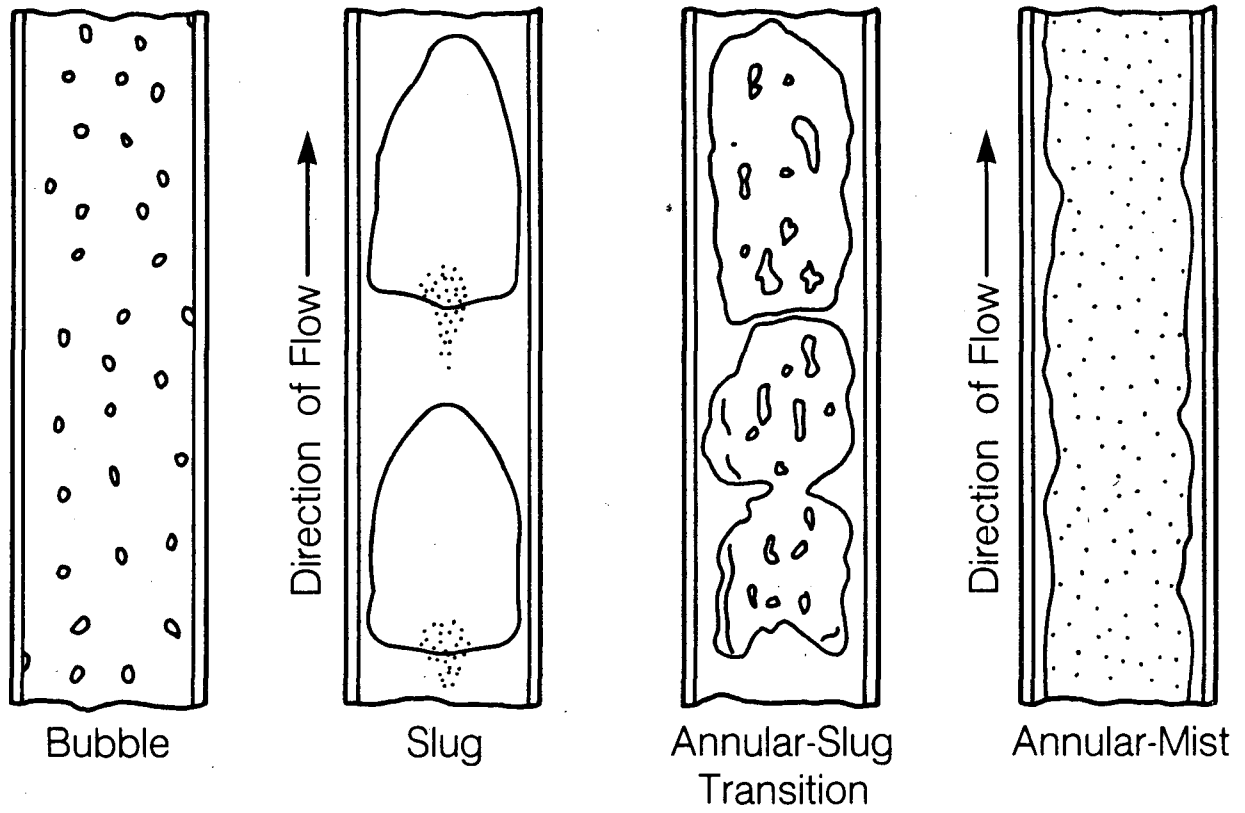
White F.M., 1979: Fluid Mechanics. 693 pp. McGraw-Hill, USA.

Zemanski M.W., M.M. Abbot and H.C. Van Ness, 1975: Basic Engineering Thermodynamics. 2nd. ed., 487 pp. McGraw-Hill.



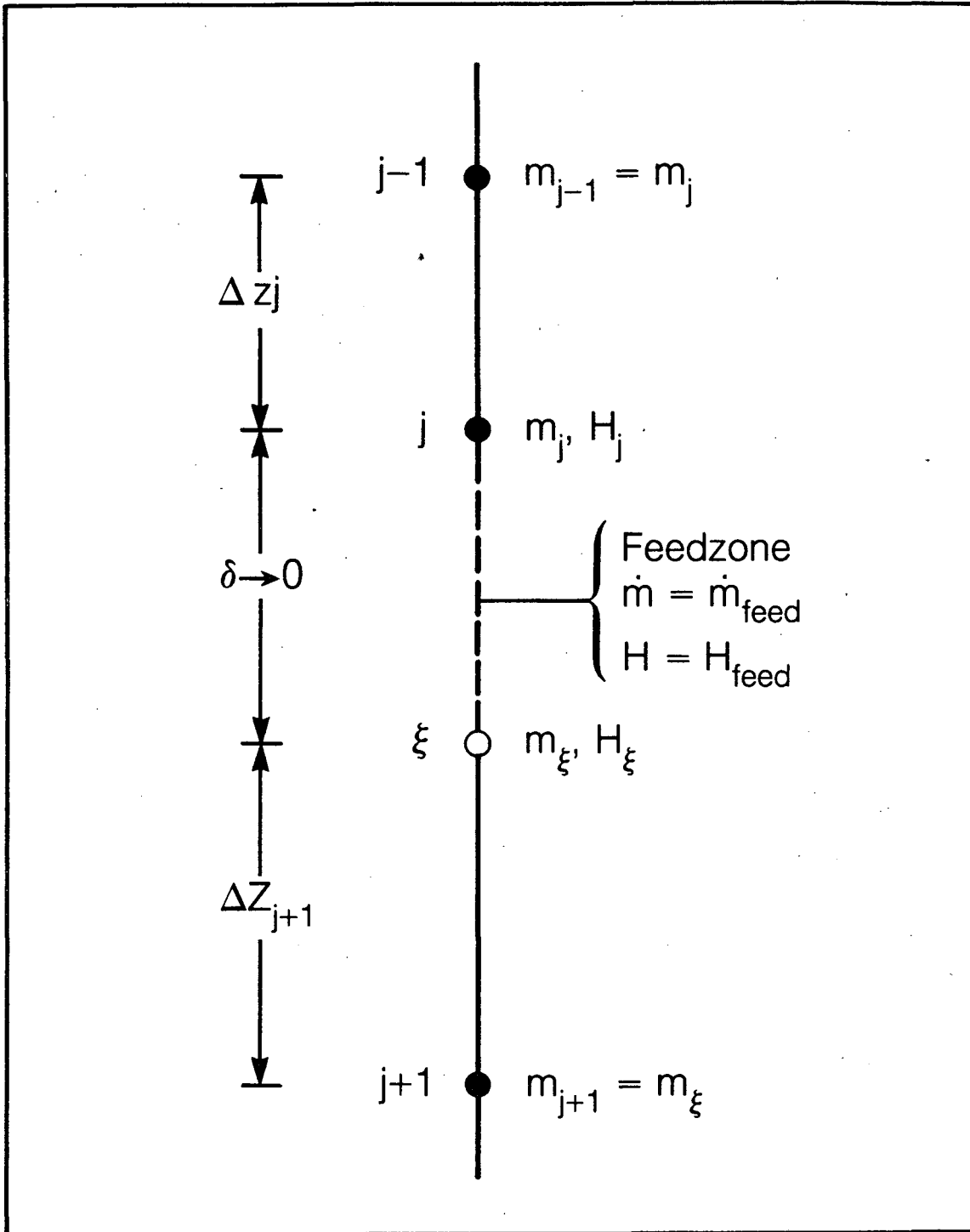
XBL 874-10135

Figure 1.1 A simplified sketch of a geothermal well with two feed-zones and related surface equipment.



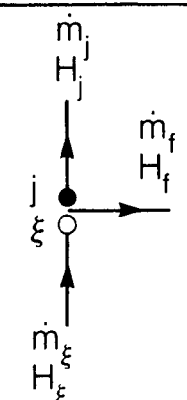
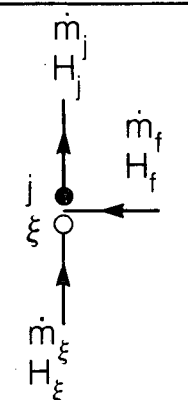
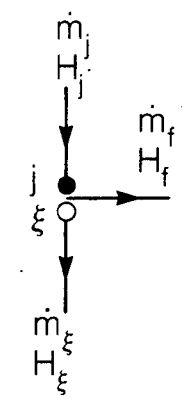
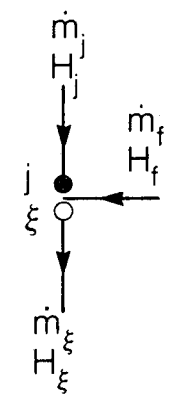
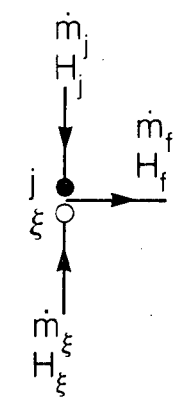
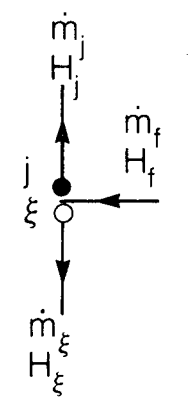
XBL 874-10130

Figure 3.1 The flow regimes in vertical gas-liquid flow. From Orkiszewski, 1967.



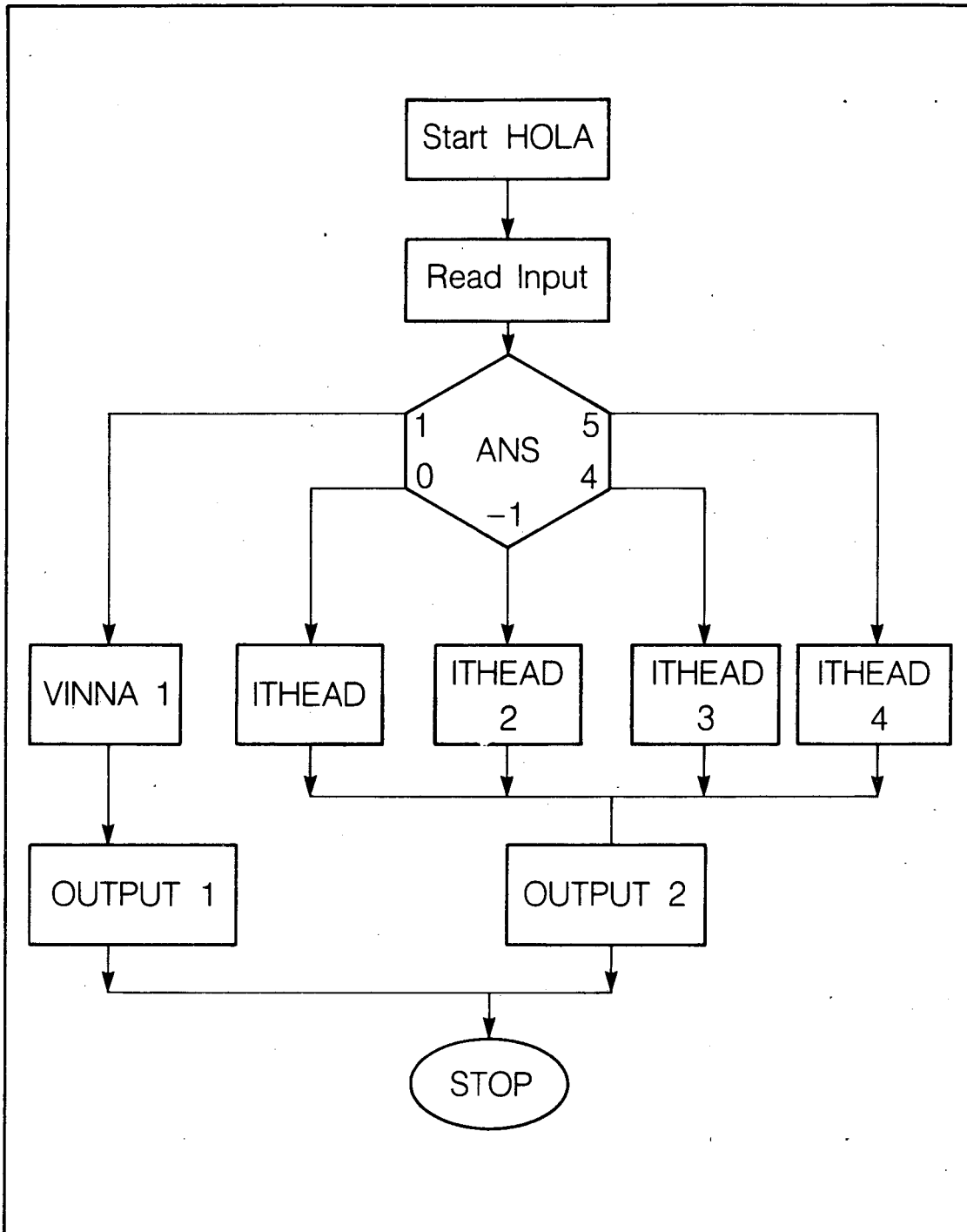
XBL 874-10136

Figure 4.1 A feedzone in the grid. The imaginary node ξ is infinitely close to node j , where the feedzone is.

<p>Case 1 $\dot{m}_j > 0 > \dot{m}_f$</p>  <p>$\dot{m}_\xi = \dot{m}_j - \dot{m}_f$</p> <p>$H_\xi = H_j = H_f$</p>	<p>Case 4 $\dot{m}_j > \dot{m}_f > 0$</p>  <p>$\dot{m}_\xi = \dot{m}_j - \dot{m}_f$</p> <p>$H_\xi = \frac{H_j \dot{m}_j - H_f \dot{m}_f}{\dot{m}_\xi}$</p>
<p>Case 2 $\dot{m}_j < \dot{m}_f < 0$</p>  <p>$\dot{m}_\xi = \dot{m}_j - \dot{m}_f$</p> <p>$H_\xi = H_j = H_f$</p>	<p>Case 5 $\dot{m}_f > 0 > \dot{m}_j$</p>  <p>$\dot{m}_\xi = \dot{m}_j - \dot{m}_f$</p> <p>$H_\xi = \frac{H_j \dot{m}_j - H_f \dot{m}_f}{\dot{m}_\xi}$</p>
<p>Case 3 $\dot{m}_f < \dot{m}_j < 0$</p>  <p>$\dot{m}_\xi = \dot{m}_j - \dot{m}_f$</p> <p>$H_\xi = \frac{H_j \dot{m}_j - H_f \dot{m}_f}{\dot{m}_\xi}$</p>	<p>Case 6 $\dot{m}_f > \dot{m}_j > 0$</p>  <p>$\dot{m}_\xi = \dot{m}_j - \dot{m}_f$</p> <p>$H_\xi = H_f = H_j$</p>

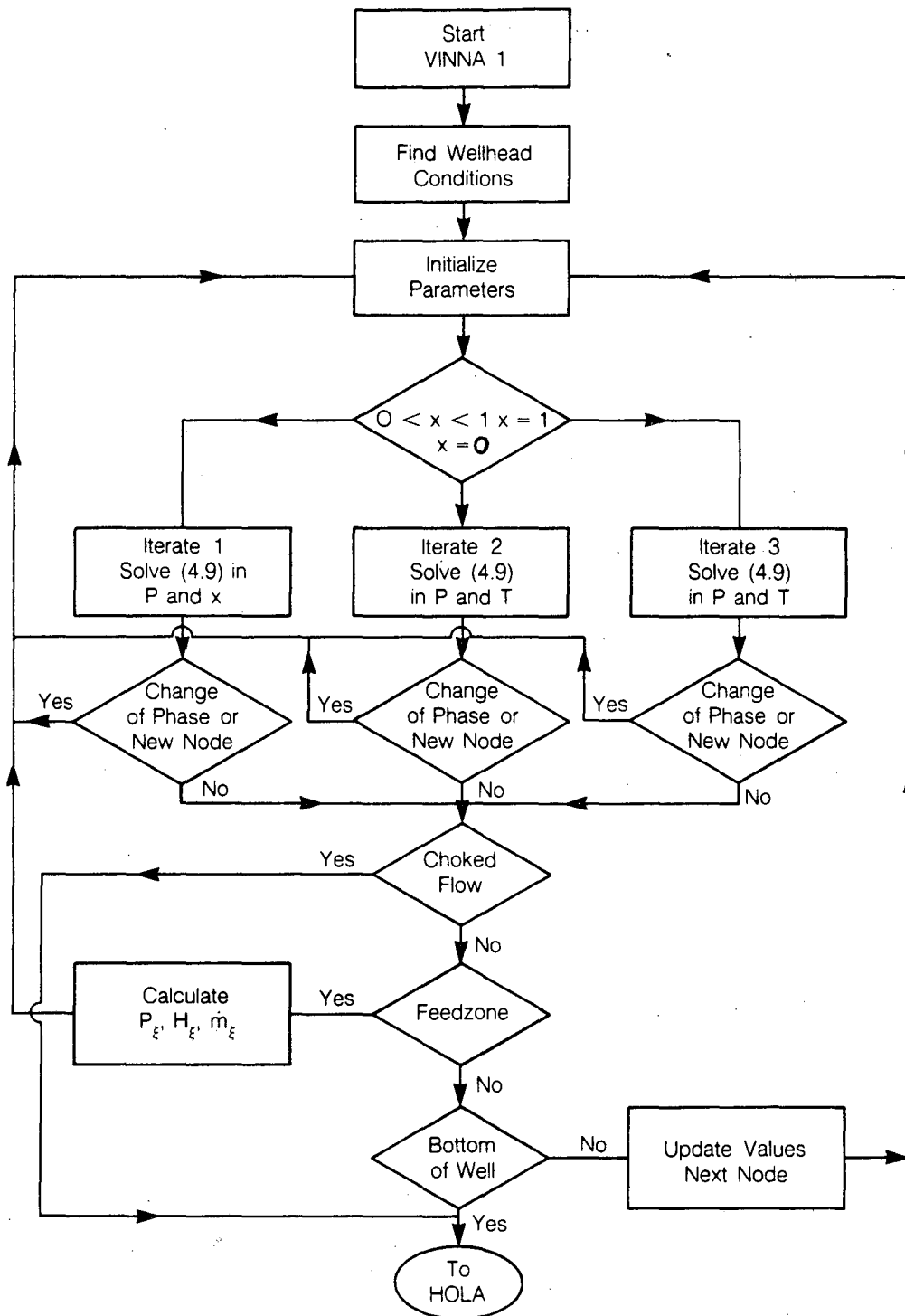
XBL 874-10131

Figure 4.2 The six possible flow cases at a feedzone in the well. ξ is an imaginary node defined in Figure 4.1.



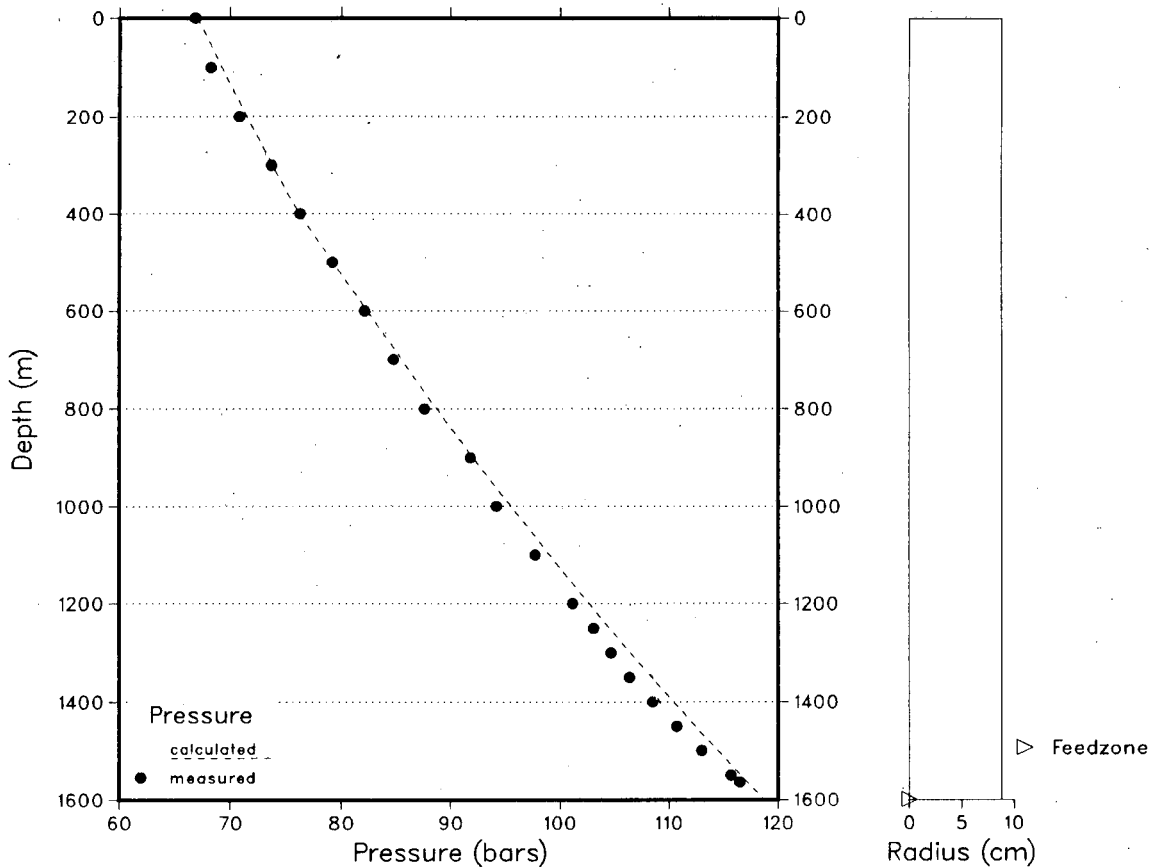
XBL 874-10129

Figure 4.3 A flow diagram for the main routine HOLA.



XBL 874-10133

Figure 4.4 Flow diagram for the subroutine VINNA1



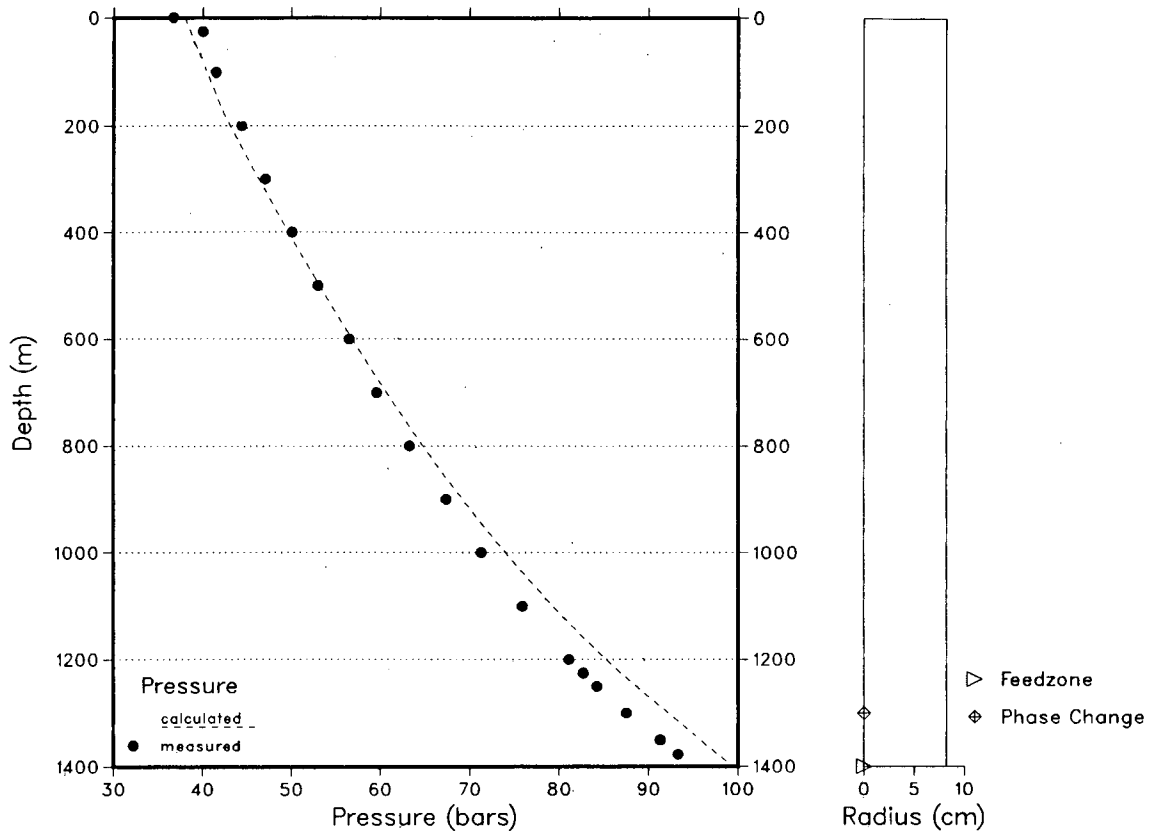
CERRO PRIETO, Well M-51
 Wellbore calculations during discharge
 Measurements from feb-20-1978

Wellhead pressure (bar abs.) : 67.00
 Wellhead temperature (C) : 282.84
 Wellhead dryness : 0.222
 Wellhead enthalpy (kJ/kg) : 1590.00
 Wellhead total flow (kg/s) : 33.00

Feedzone no:	Depth (m)	Flow (kg/s)	Enthalpy (kJ/kg)
1	1600.0	33.00	1622.8

XBL 874-1967

Figure 5.1 Calculated and measured pressures in well M-51, Cerro Prieto.



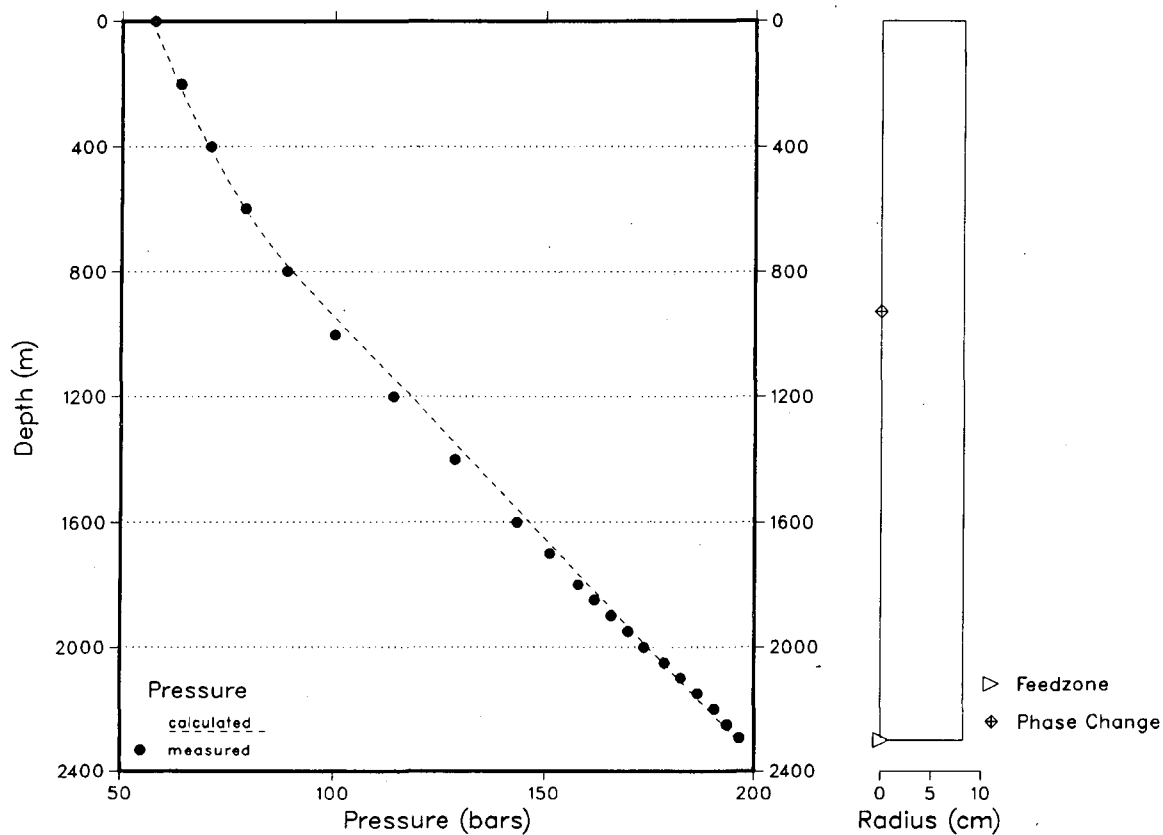
CERRO PRIETO, Well M-90
 Wellbore calculations during discharge
 Measurements from FEB-28-1976

Wellhead pressure (bar abs.) : 38.00
 Wellhead temperature (C) : 247.31
 Wellhead dryness : 0.160
 Wellhead enthalpy (kJ/kg) : 1350.00
 Wellhead total flow (kg/s) : 40.00

Feedzone no:	Depth (m)	Flow (kg/s)	Enthalpy (kJ/kg)
1	1400.0	40.00	1374.7

XBL 874-1968

Figure 5.2 Calculated and measured pressures in well M-90, Cerro Prieto.



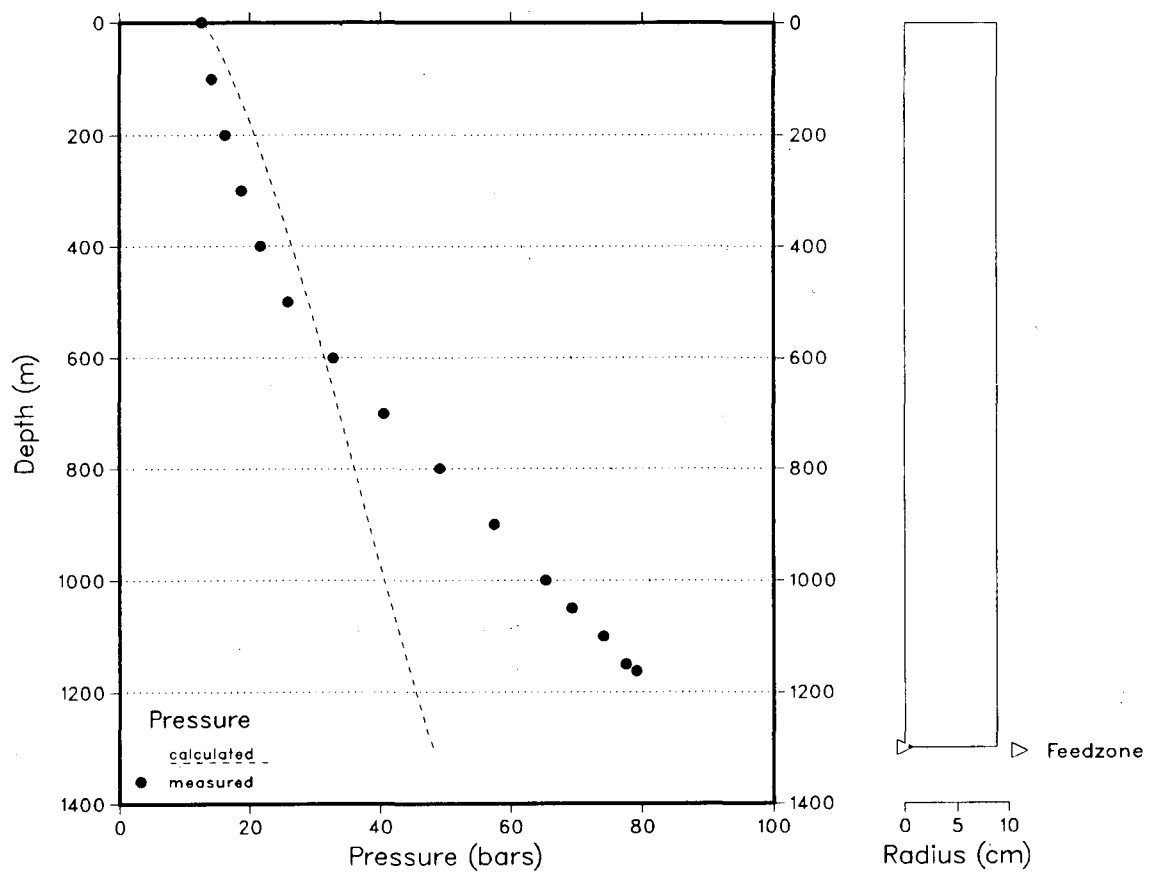
CERRO PRIETO, Well M-91
 Wellbore calculations during discharge
 Measurements from FEB-8-1976

Wellhead pressure (bar abs.) : 57.00
 Wellhead temperature (C) : 272.22
 Wellhead dryness : 0.115
 Wellhead enthalpy (kJ/kg) : 1380.00
 Wellhead total flow (kg/s) : 34.00

Feedzone no:	Depth (m)	Flow (kg/s)	Enthalpy (kJ/kg)
1	2300.0	34.0000	1417.9

XBL 874-1966

Figure 5.3 Calculated and measured pressures in well M-91, Cerro Prieto.



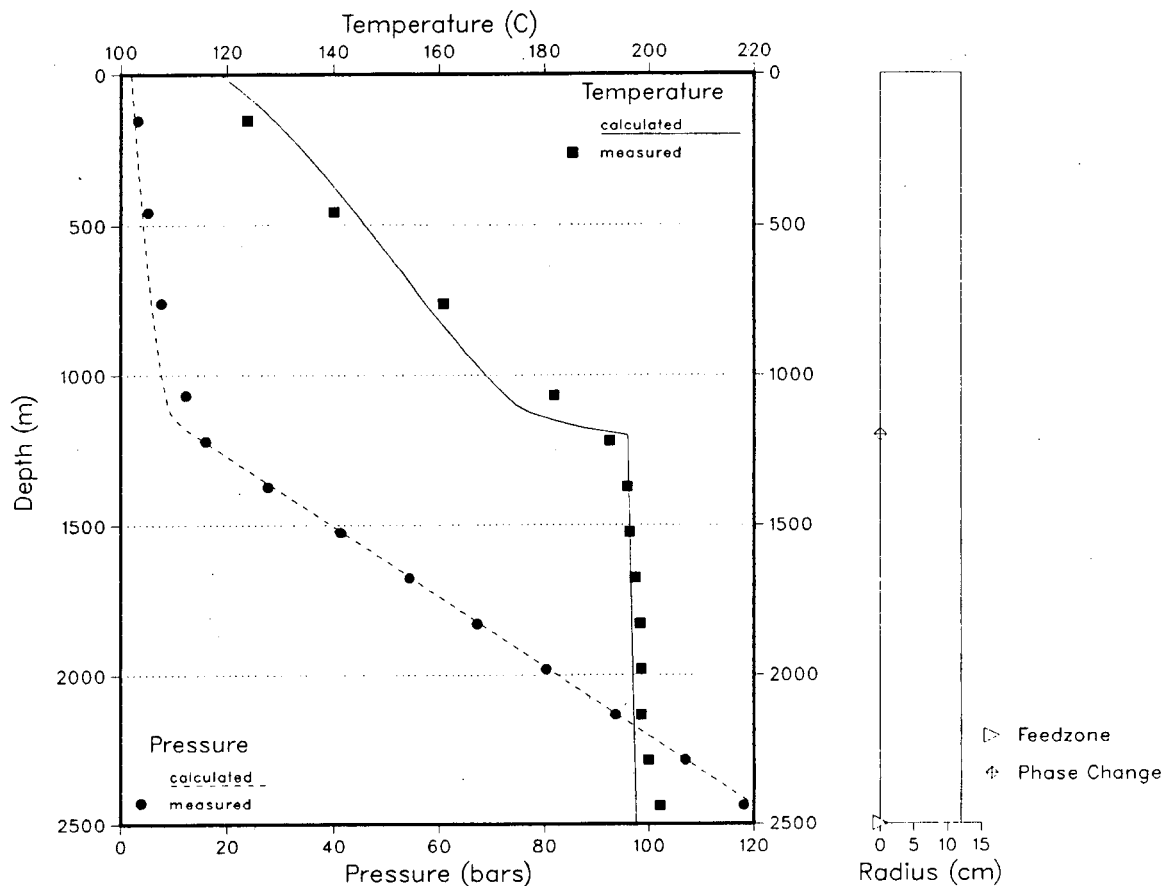
CERRO PRIETO, Well M-39
 Wellbore calculations during discharge
 Measurements from apr-26-1976

Wellhead pressure (bar abs.) : 13.00
 Wellhead temperature (C) : 191.61
 Wellhead dryness : 0.287
 Wellhead enthalpy (kJ/kg) : 1380.00
 Wellhead total flow (kg/s) : 45.00

Feedzone no:	Depth (m)	Flow (kg/s)	Enthalpy (kJ/kg)
1	1300.0	45.00	1402.4

XBL 874-1969

Figure 5.4 Calculated and measured pressures in well M-39, Cerro Prieto.



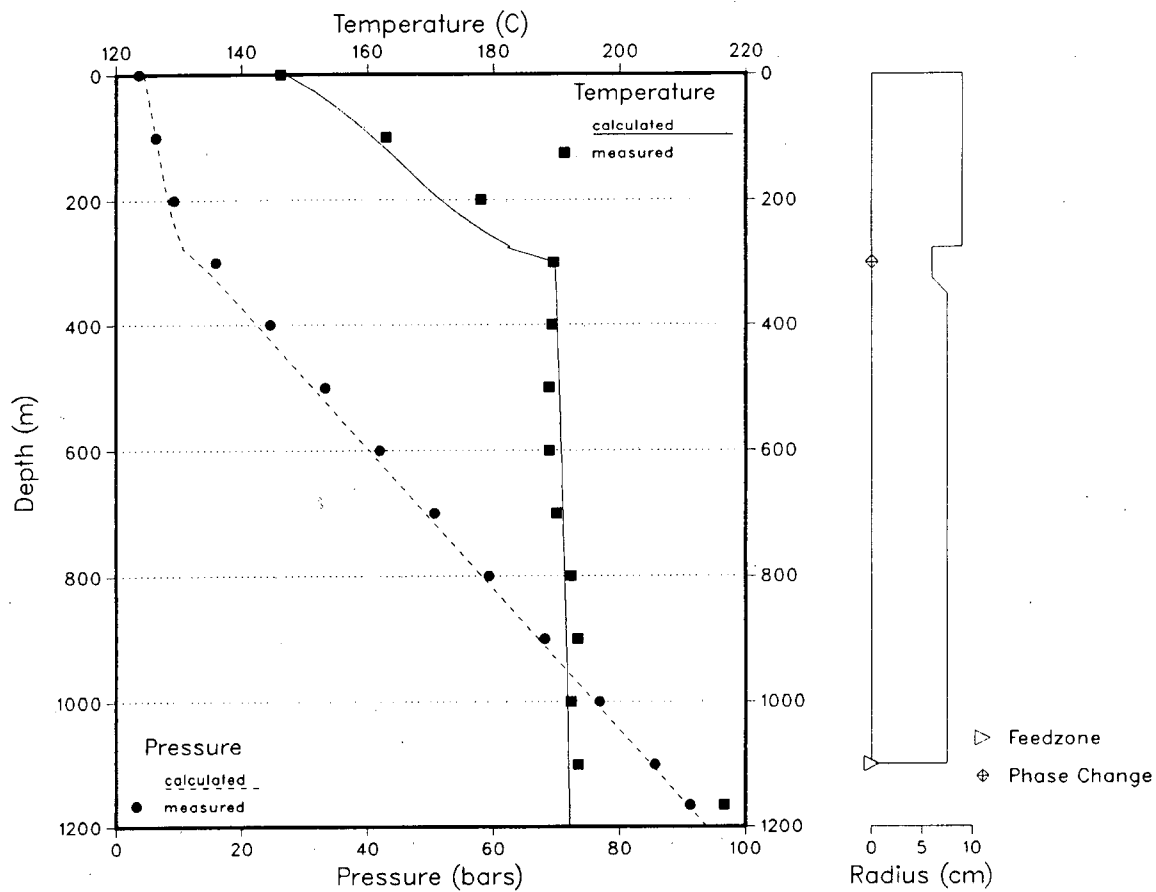
Mesa, Well 6-1
 Wellbore calculations during discharge
 Measurements from jan 1973

Wellhead pressure (bar abs.) : 1.50
 Wellhead temperature (C) : 111.37
 Wellhead dryness : 0.159
 Wellhead enthalpy (kJ/kg) : 820.00
 Wellhead total flow (kg/s) : 15.80

Feedzone no:	Depth (m)	Flow (kg/s)	Enthalpy (kJ/kg)
1	2500.0	15.80	850.4

XBL 874-1954

Figure 5.5 Calculated and measured downhole profiles in well 6-1, East Mesa



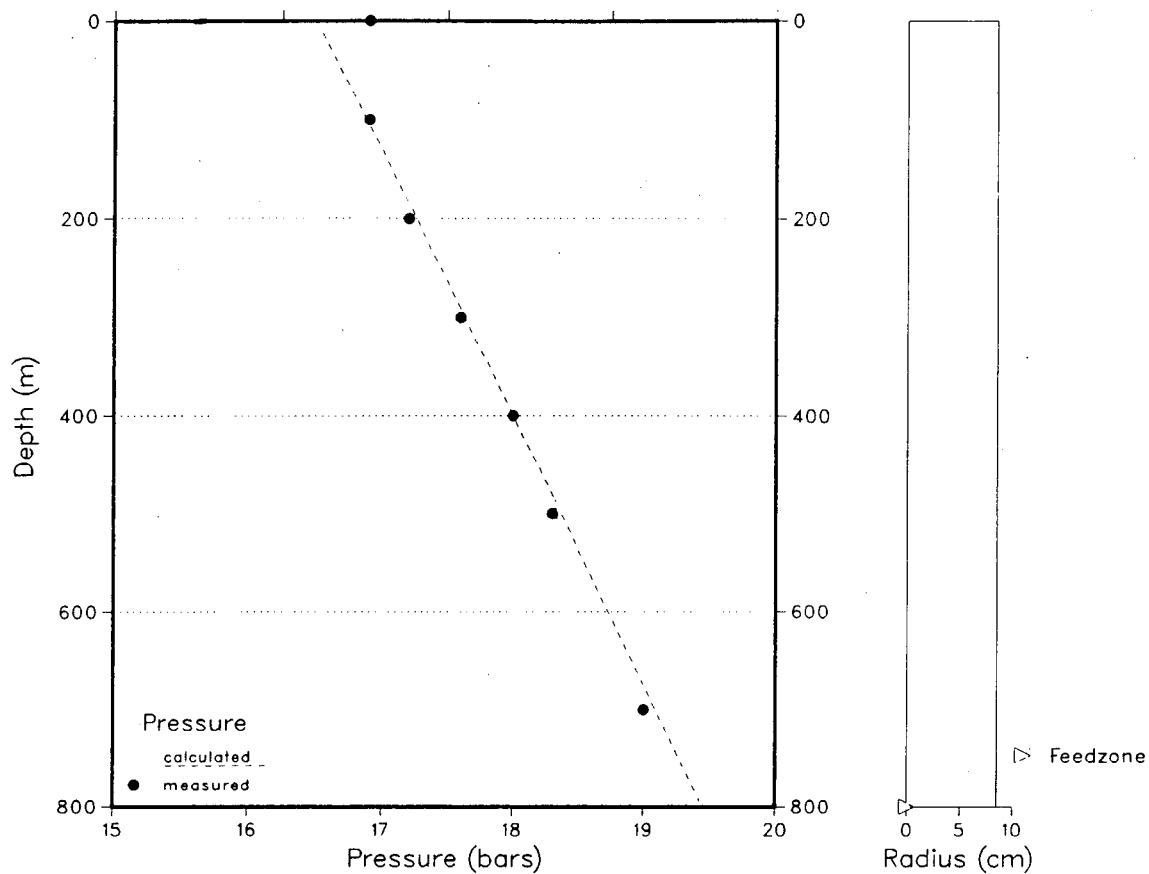
Krafla , well 2
 Pressure and enthalpy during discharge
 30-jul-1978

Wellhead pressure (bar abs.) : 4.40
 Wellhead temperature (C) : 147.09
 Wellhead dryness : 0.085
 Wellhead enthalpy (kJ/kg) : 800.00
 Wellhead total flow (kg/s) : 25.00

Feedzone no:	Depth (m)	Flow (kg/s)	Enthalpy (kJ/kg)
1	1200.0	25.00	820.5

XBL 874-1961

Figure 5.6 Calculated and measured downhole profiles in well KW-2, Krafla.



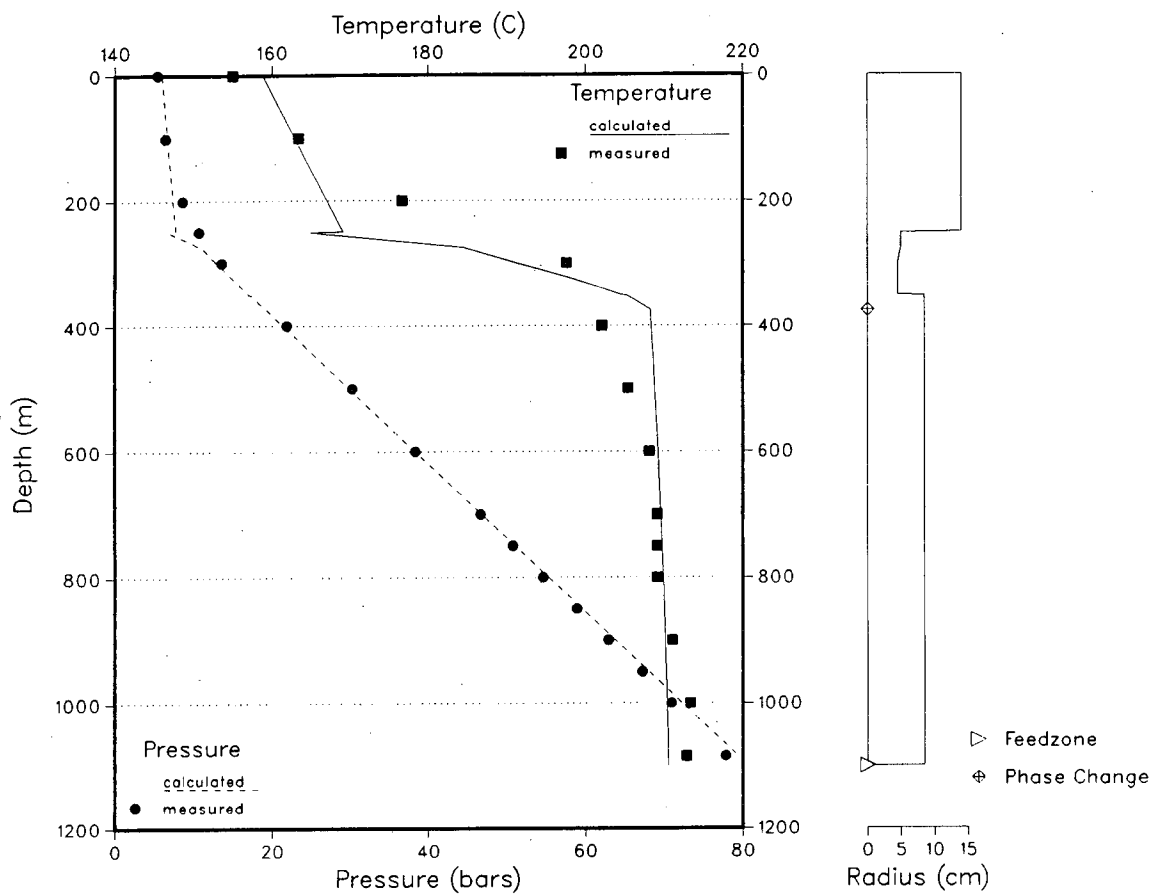
Krafla , well 7
 Pressure and temperature during discharge
 P-measurement from 1-aug-78

Wellhead pressure (bar abs.) : 16.50
 Wellhead temperature (C) : 205.44
 Wellhead dryness : 1.000
 Wellhead enthalpy (kJ/kg) : 2800.00
 Wellhead total flow (kg/s) : 4.60

Feedzone no:	Depth (m)	Flow (kg/s)	Enthalpy (kJ/kg)
1	800.0	4.60	2825.8

XBL 874-1962

Figure 5.7 Calculated and measured downhole profiles in well KJ-7, Krafla.



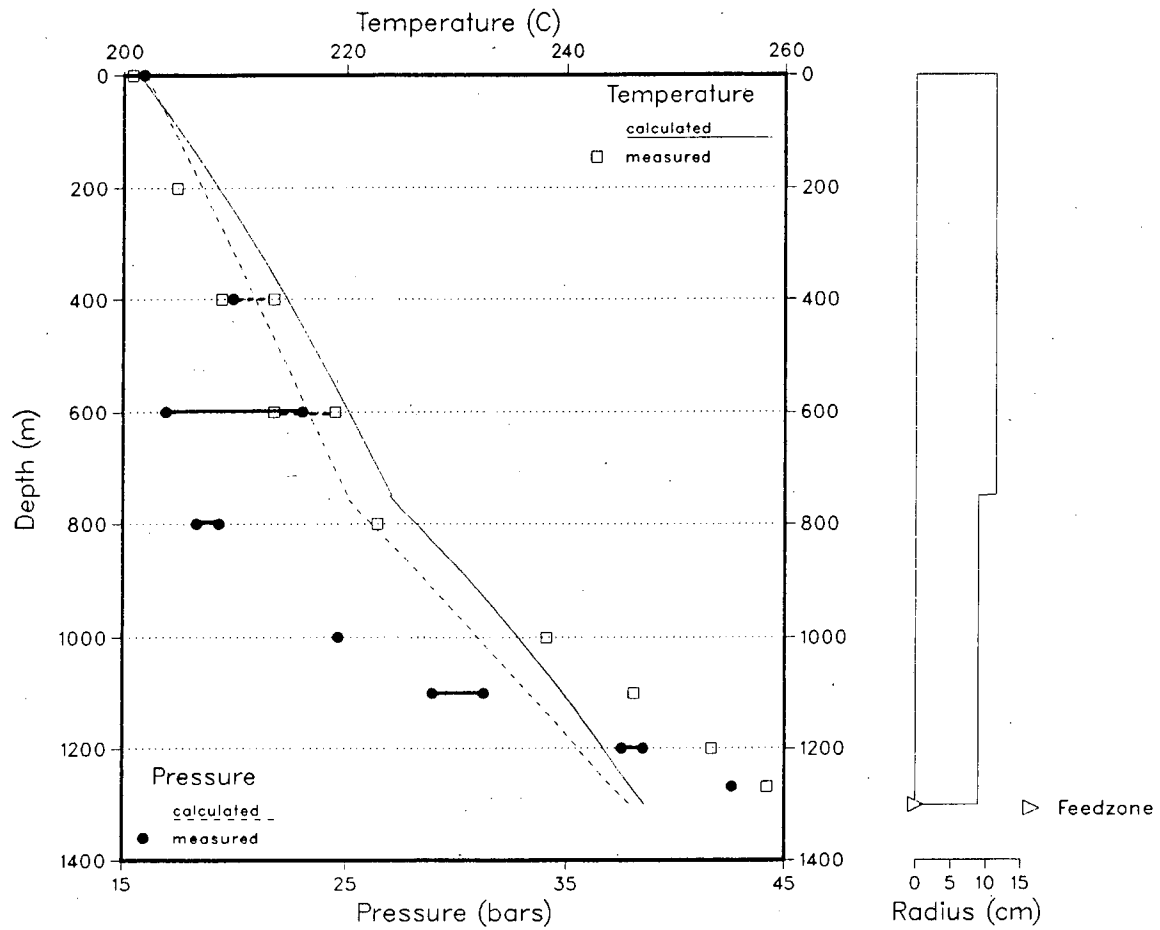
Krafla , well 9
 Pressure and enthalpy during discharge, scaling tap at 275-350 m
 10-feb-1977

Wellhead pressure (bar abs.) : 6.00
 Wellhead temperature (C) : 158.84
 Wellhead dryness : 0.101
 Wellhead enthalpy (kJ/kg) : 880.00
 Wellhead total flow (kg/s) : 16.40

Feedzone no:	Depth (m)	Flow (kg/s)	Enthalpy (kJ/kg)
1	1100.0	16.40	902.2

XBL 874-1963

Figure 5.8 Calculated and measured downhole profiles in well KJ-9, Krafla.



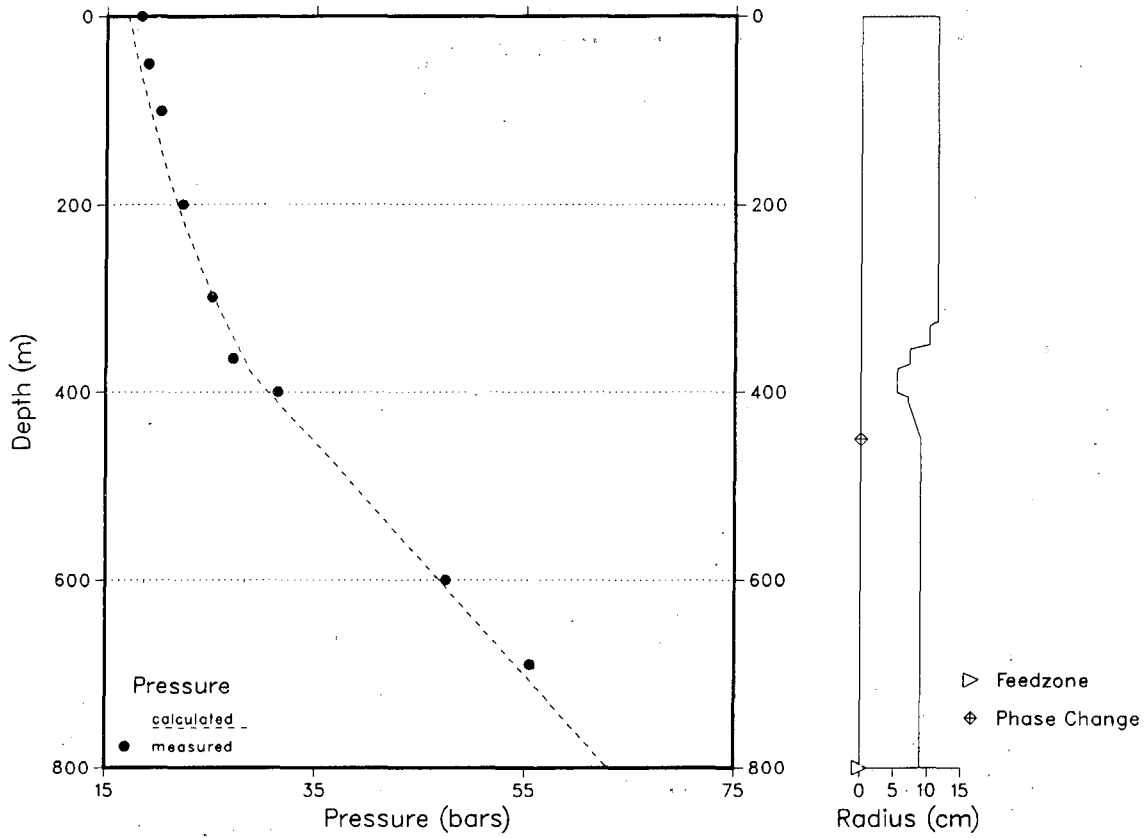
Nesjavellir, well NJ-14
 Pressure and enthalpy during discharge
 30-may-1986

Wellhead pressure (bar abs.) : 16.00
 Wellhead temperature (C) : 201.37
 Wellhead dryness : 0.249
 Wellhead enthalpy (kJ/kg) : 1340.00
 Wellhead total flow (kg/s) : 24.00

Feedzone no:	Depth (m)	Flow (kg/s)	Enthalpy (kJ/kg)
1	1300.0	24.00	1362.9

XBL 874-1964

Figure 5.9 Calculated and measured downhole profiles in well NJ-14, Nesjavellir. Solid lines in between data points at each depth indicate the range of measured pressures, dashed lines are for the range in measured temperatures.



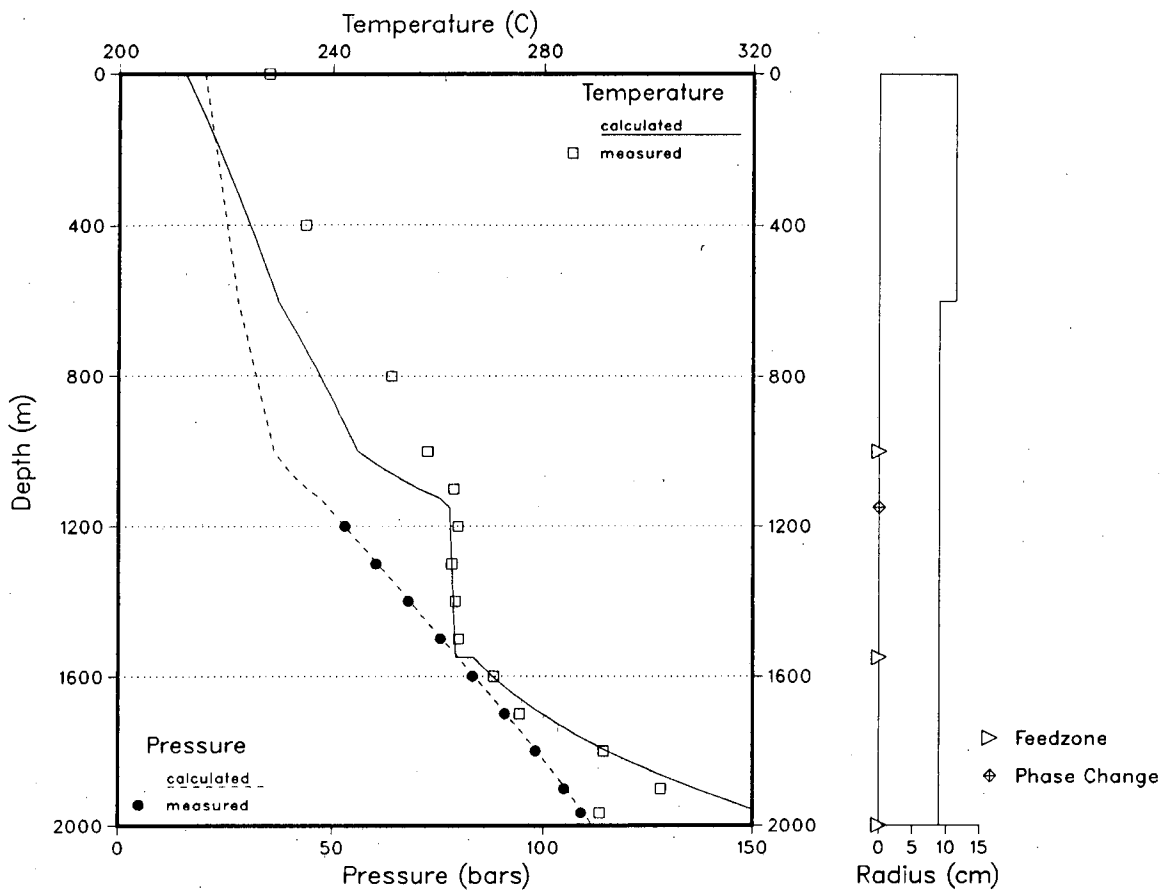
Svartsengi, well 4
 Wellbore calculations during discharge
 Measurements from dec-1976

Wellhead pressure (bar abs.) : 17.00
 Wellhead temperature (C) : 204.31
 Wellhead dryness : 0.082
 Wellhead enthalpy (kJ/kg) : 1030.00
 Wellhead total flow (kg/s) : 30.00

Feedzone no:	Depth (m)	Flow (kg/s)	Enthalpy (kJ/kg)
1	800.0	30.00	1043.5

XBL 874-1965

Figure 5.10 Calculated and measured pressure in well no. 4, Svartsengi.



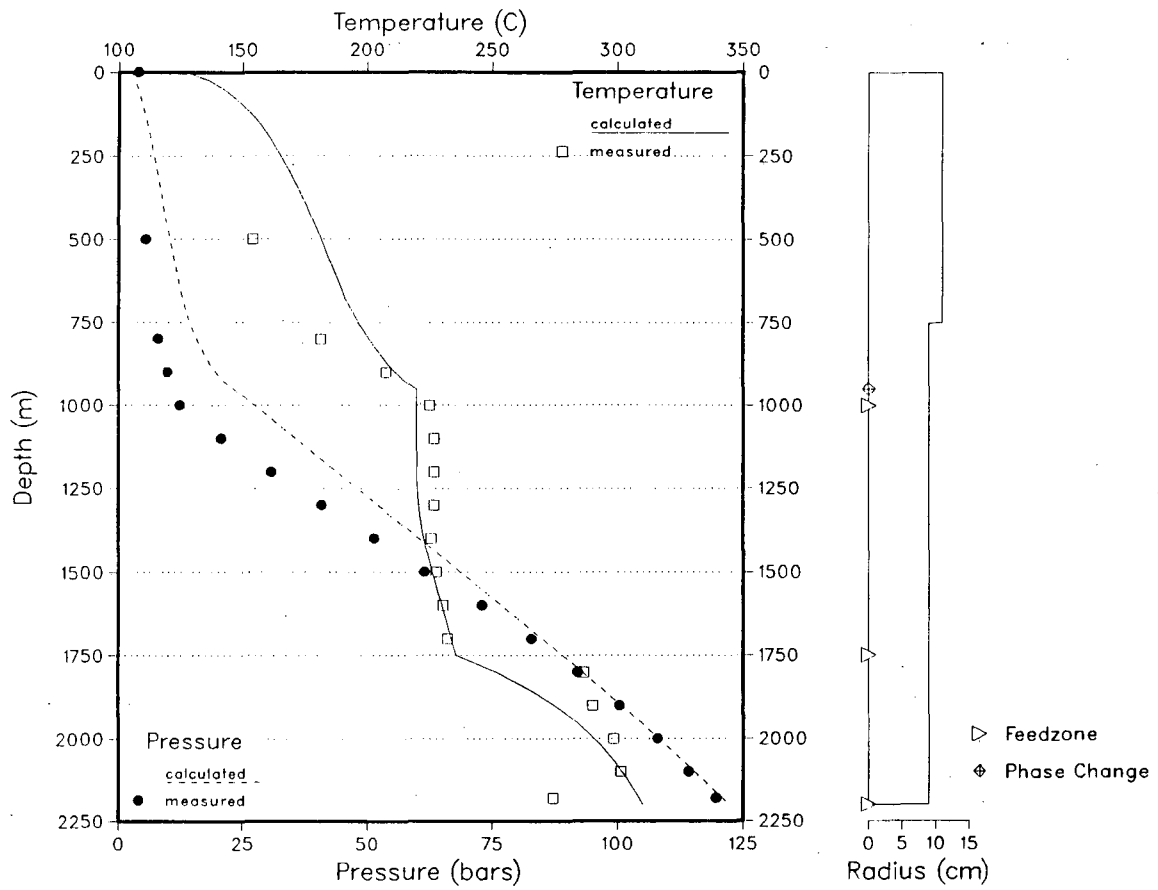
Nesjavellir, well NJ-7
 Pressure and enthalpy during discharge
 6-feb-1986

Wellhead pressure (bar abs.) : 20.00
 Wellhead temperature (C) : 212.37
 Wellhead dryness : 0.239
 Wellhead enthalpy (kJ/kg) : 1360.00
 Wellhead total flow (kg/s) : 23.00

Feedzone no:	Depth (m)	Flow (kg/s)	Enthalpy (kJ/kg)
1	1000.0	14.50	1500.0
2	1550.0	8.40	1150.6
3	2000.0	0.10	1526.2

XBL 874-1958

Figure 6.1 Calculated and measured downhole profiles in well NJ-7, Nesjavellir.



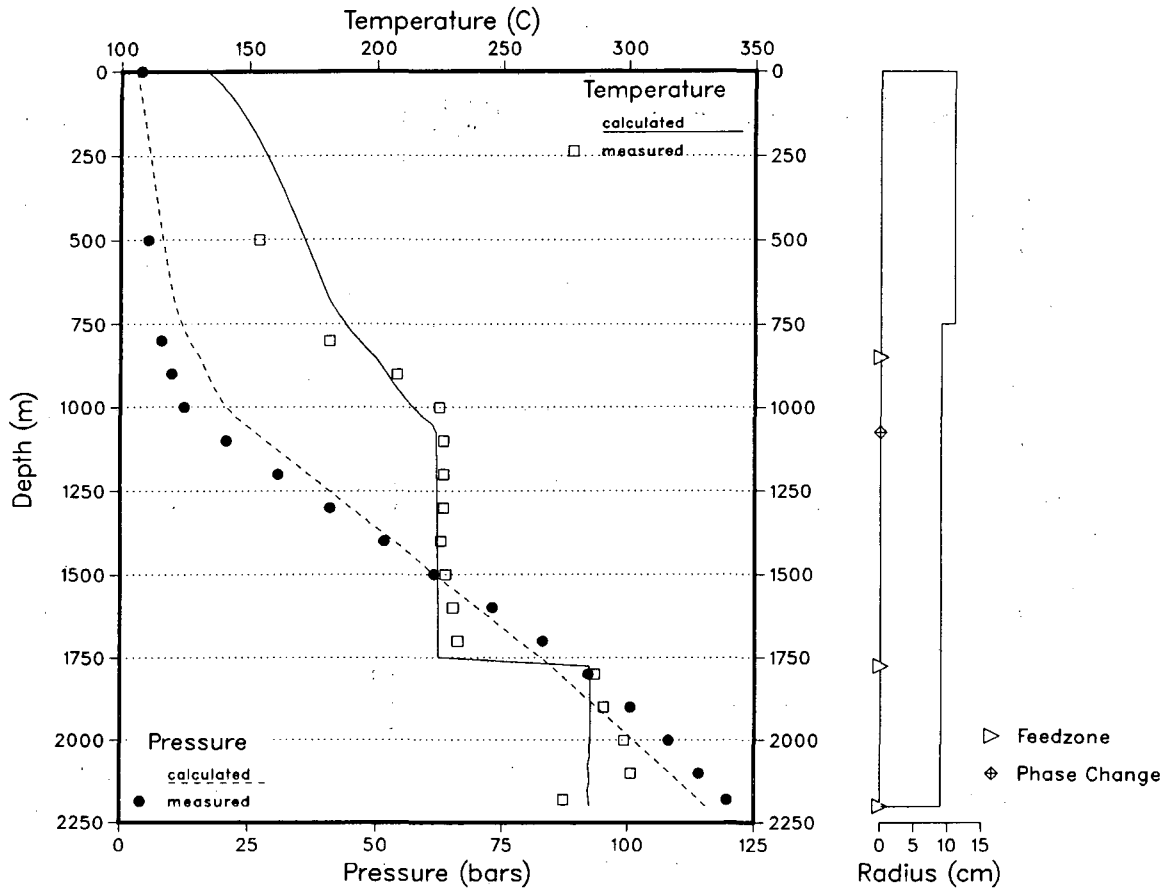
Krafla , well 11
 Wellbore calculations during discharge
 Measurements from FEB-16&17-1977

Wellhead pressure (bar abs.) : 2.50
 Wellhead temperature (C) : 127.43
 Wellhead dryness : 0.181
 Wellhead enthalpy (kJ/kg) : 930.00
 Wellhead total flow (kg/s) : 38.00

Feedzone no:	Depth (m)	Flow (kg/s)	Enthalpy (kJ/kg)
1	1000.0	40.0000	943.1
2	1750.0	-1.8000	1018.0
3	2200.0	-0.2000	1398.5

XBL 874-1957

Figure 6.2 Calculated and measured downhole profiles in well KJ-11, Krafla. Negative flowrates are present in the lower part of the well.



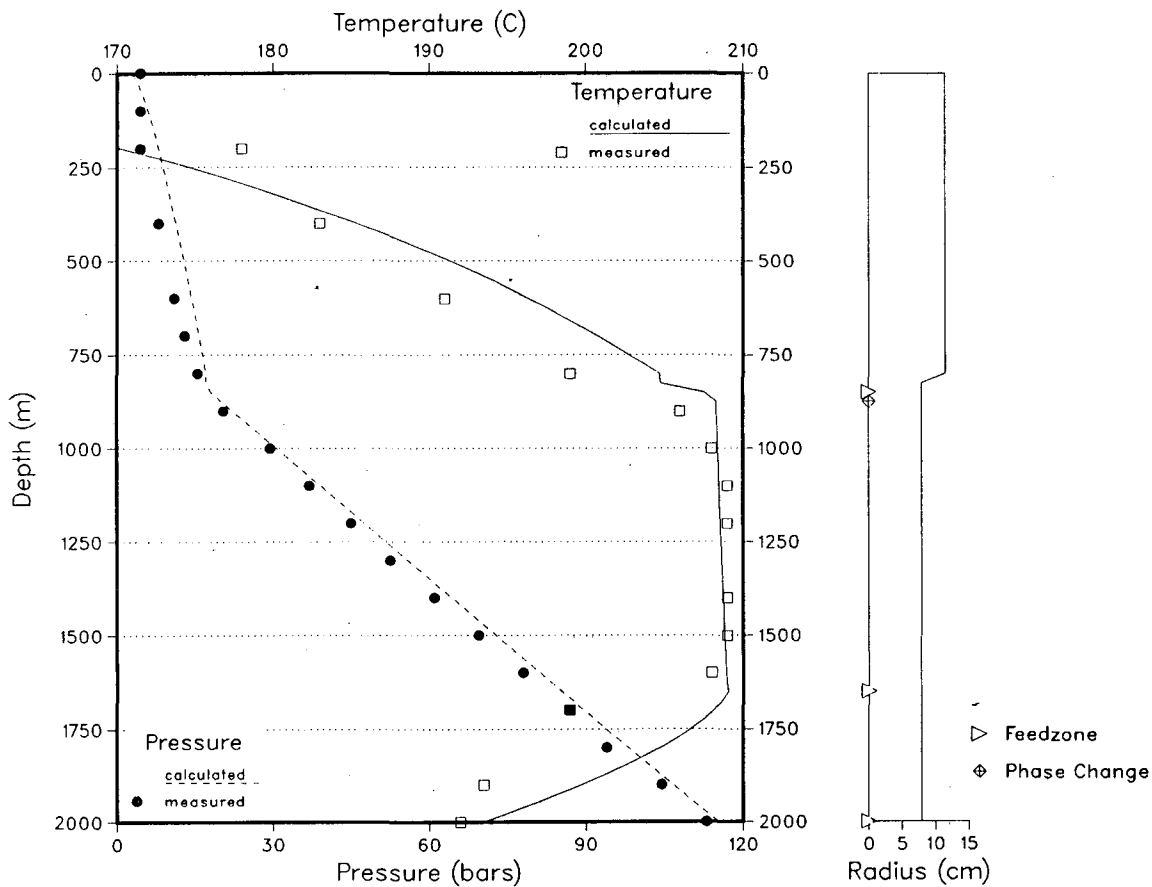
Krafla, well 11
 Wellbore calculations during discharge
 Measurements from FEB-16&17-1977

Wellhead pressure (bar abs.) : 3.00
 Wellhead temperature (C) : 133.54
 Wellhead dryness : 0.143
 Wellhead enthalpy (kJ/kg) : 870.00
 Wellhead total flow (kg/s) : 30.00

Feedzone no:	Depth (m)	Flow (kg/s)	Enthalpy (kJ/kg)
1	850.0	7.80	670.0
2	1775.0	21.00	951.0
3	2200.0	1.20	1340.6

XBL 874-1960

Figure 6.3 Calculated and measured downhole profiles in well KJ-11, Krafla. Positive flowrates are found in the well and the feedzones.



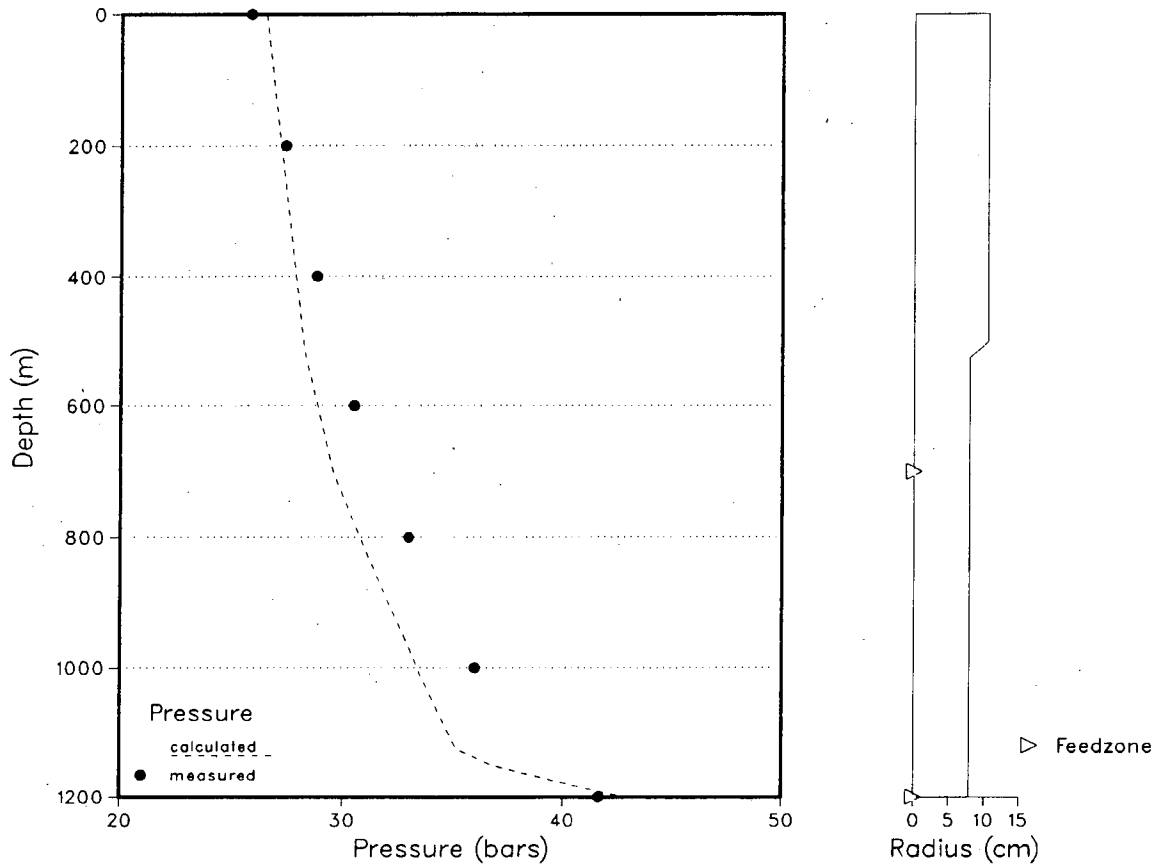
Olkaria, well OW-201
 Wellbore calculations during discharge
 Measurements from 22-oct-1984

Wellhead pressure (bar abs.) : 3.00
 Wellhead temperature (C) : 133.54
 Wellhead dryness : 0.332
 Wellhead enthalpy (kJ/kg) : 1280.00
 Wellhead total flow (kg/s) : 35.50

Feedzone no:	Depth (m)	Flow (kg/s)	Enthalpy (kJ/kg)
1	850.0	33.0000	1330.0
2	1650.0	2.8000	901.6
3	2000.0	-0.3000	827.7

XBL 874-1959

Figure 6.4 Calculated and measured downhole profiles in well OW-201, Olkaria.



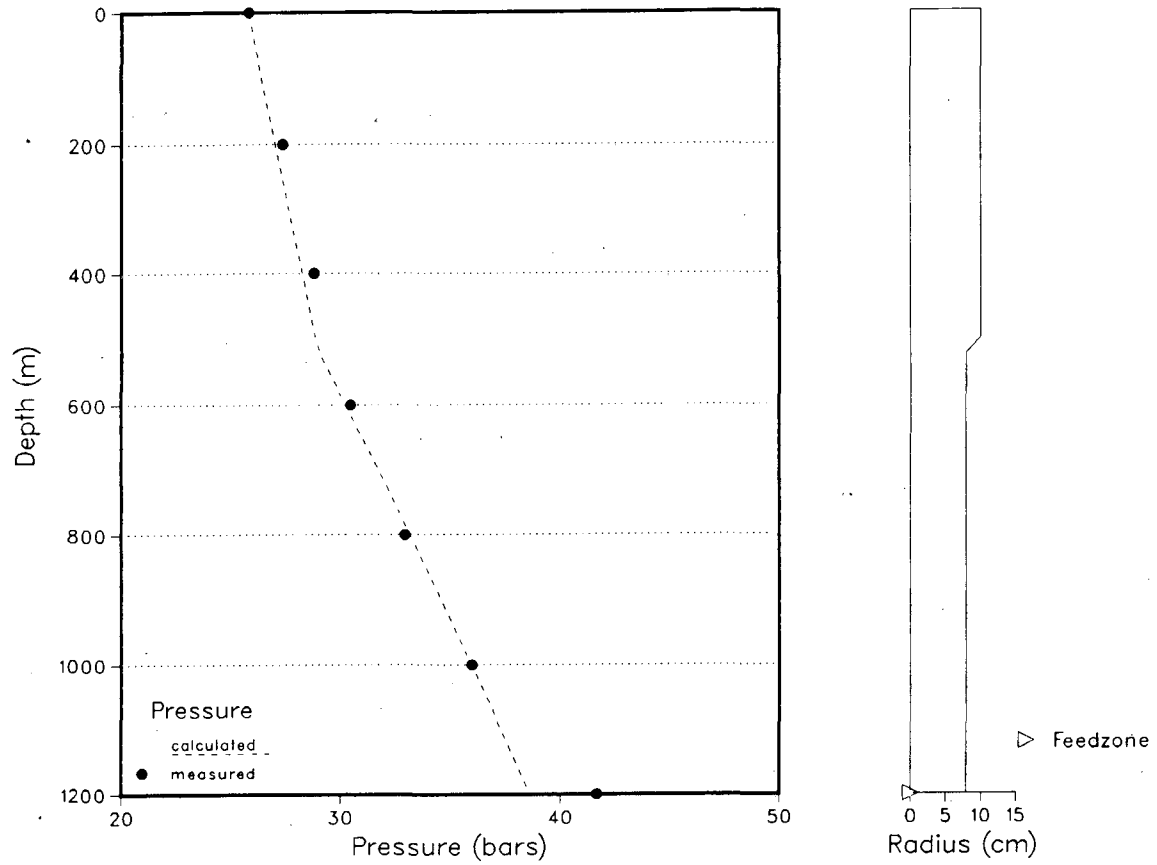
Olkaria, well OW-15
 Wellbore calculations during discharge
 Measurements from 22-oct-1984

Wellhead pressure (bar abs.) : 26.50
 Wellhead temperature (C) : 227.06
 Wellhead dryness : 0.670
 Wellhead enthalpy (kJ/kg) : 2200.00
 Wellhead total flow (kg/s) : 4.70

Feedzone no:	Depth (m)	Flow (kg/s)	Enthalpy (kJ/kg)
1	700.0	3.8460	2400.0
2	1200.0	0.8540	1341.8

XBL 874-1956

Figure 6.5 Calculated and measured downhole profiles in well OW-15, Olkaria. Two feedzones are assumed for the well.



Olkaria, well OW-15
 Wellbore calculations during discharge
 Measurements from 22-oct-1984

Wellhead pressure (bar abs.) : 25.80
 Wellhead temperature (C) : 225.62
 Wellhead dryness : 0.672
 Wellhead enthalpy (kJ/kg) : 2200.00
 Wellhead total flow (kg/s) : 8.00

Feedzone no:	Depth (m)	Flow (kg/s)	Enthalpy (kJ/kg)
1	1200.0	8.0000	2212.4

XBL 874-1955

Figure 6.6 Calculated and measured downhole profiles in well OW-15, Olkaria. Single feedzone is assumed for the well.

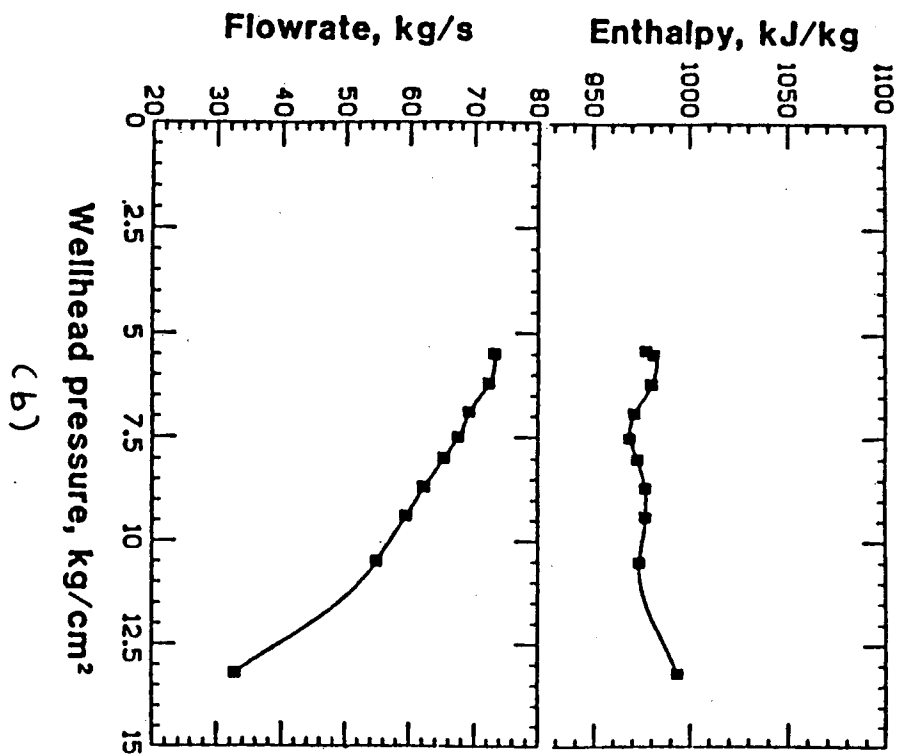
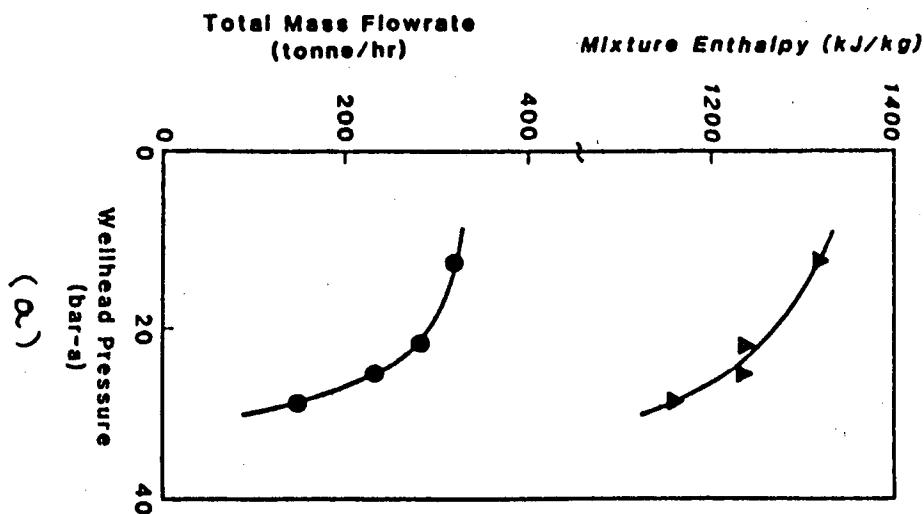
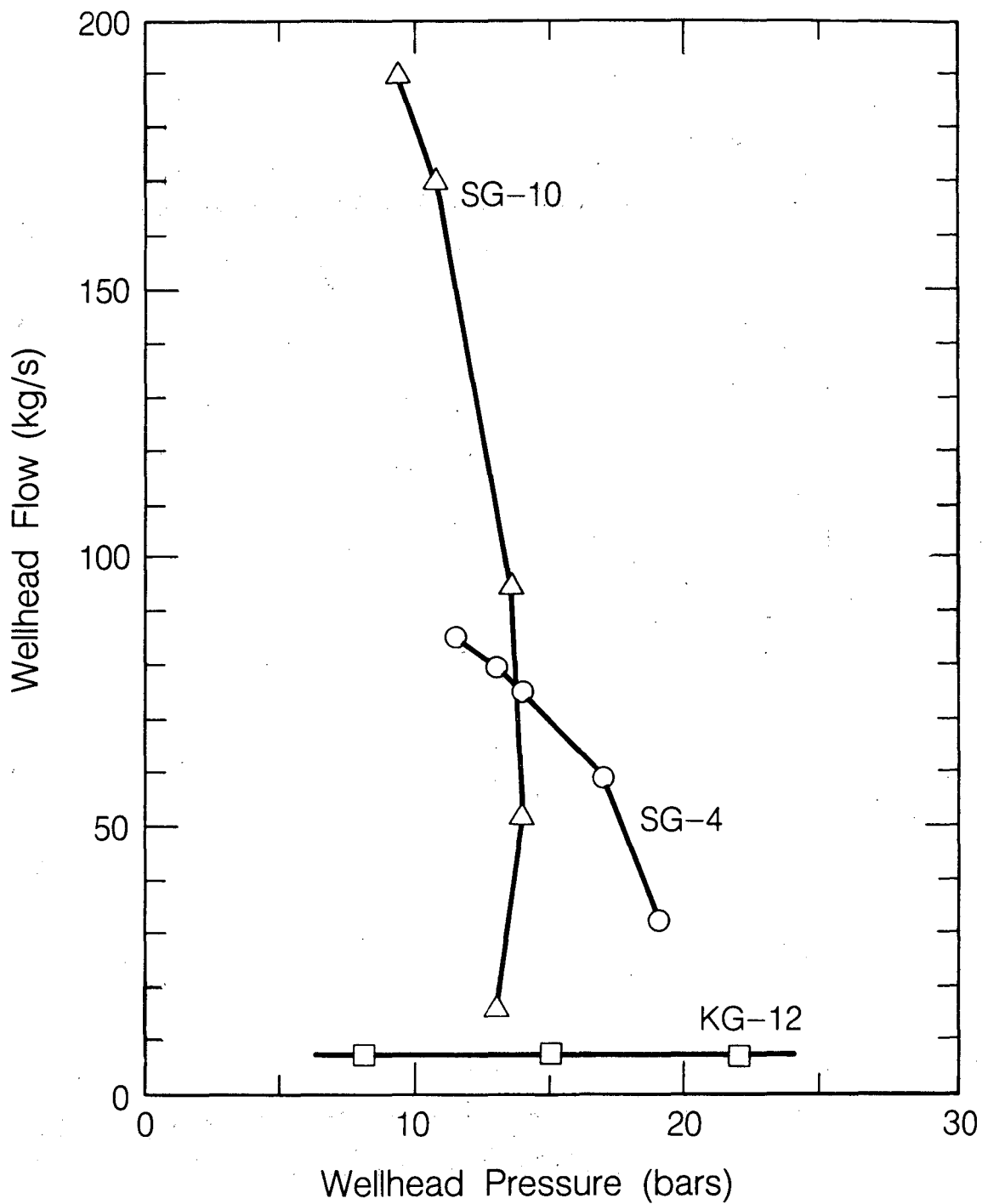


Figure 7.1 Wellhead output curves for (a) well 2 in the Loz Azufres field, Mexico and (b) from well 1 in the Miravalles field, Costa Rica (from Gudmundsson, 1986.)



XBL 874-10137

Figure 7.2 Wellhead delivery curves for wells in the Svartsengi (SG-4, SG-10) and Kráfla (KG-10) fields (from Palmason 1983, Parlaktuna 1985, and Sigurdsson 1985).

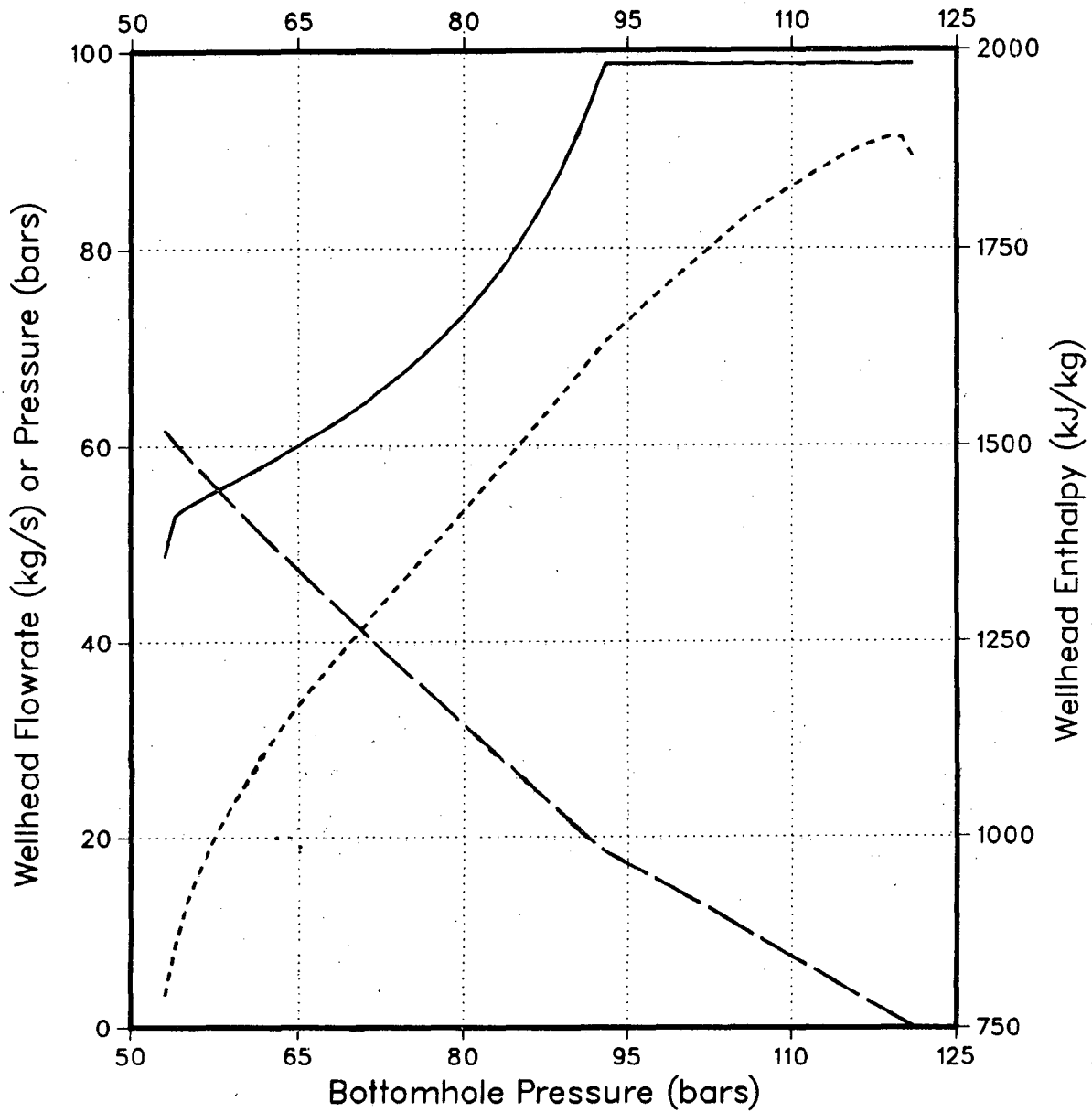


Figure 7.3 Calculated wellhead conditions as a function of bottomhole pressure for the standard well discussed in text. Wellhead pressure is indicated by dotted line, wellhead enthalpy by solid line and wellhead flowrate by dashed line.

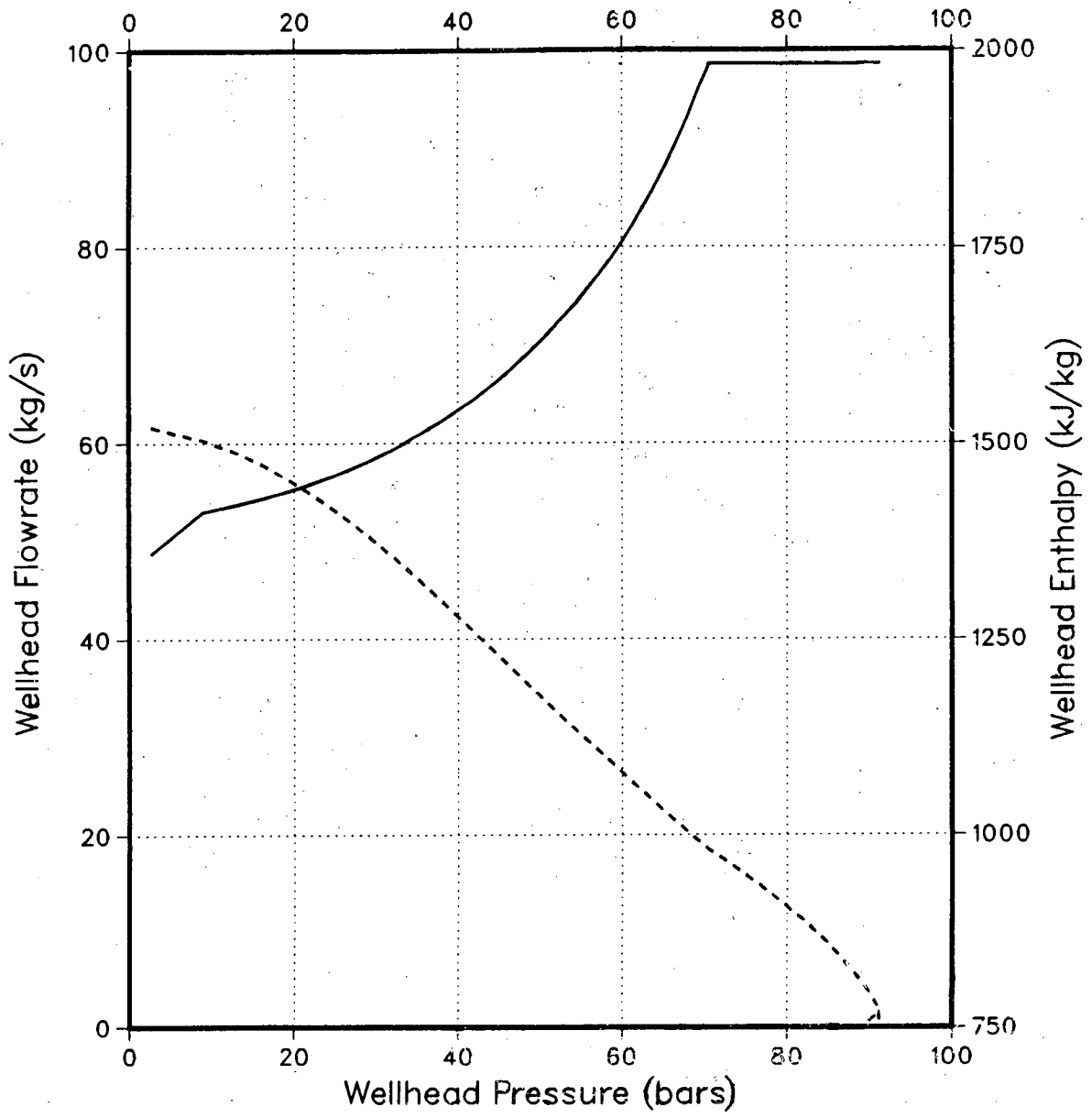


Figure 7.4 Wellhead output curves for the standard well discussed in text. The wellhead enthalpy is indicated by solid line and the wellhead flowrate by dotted line.

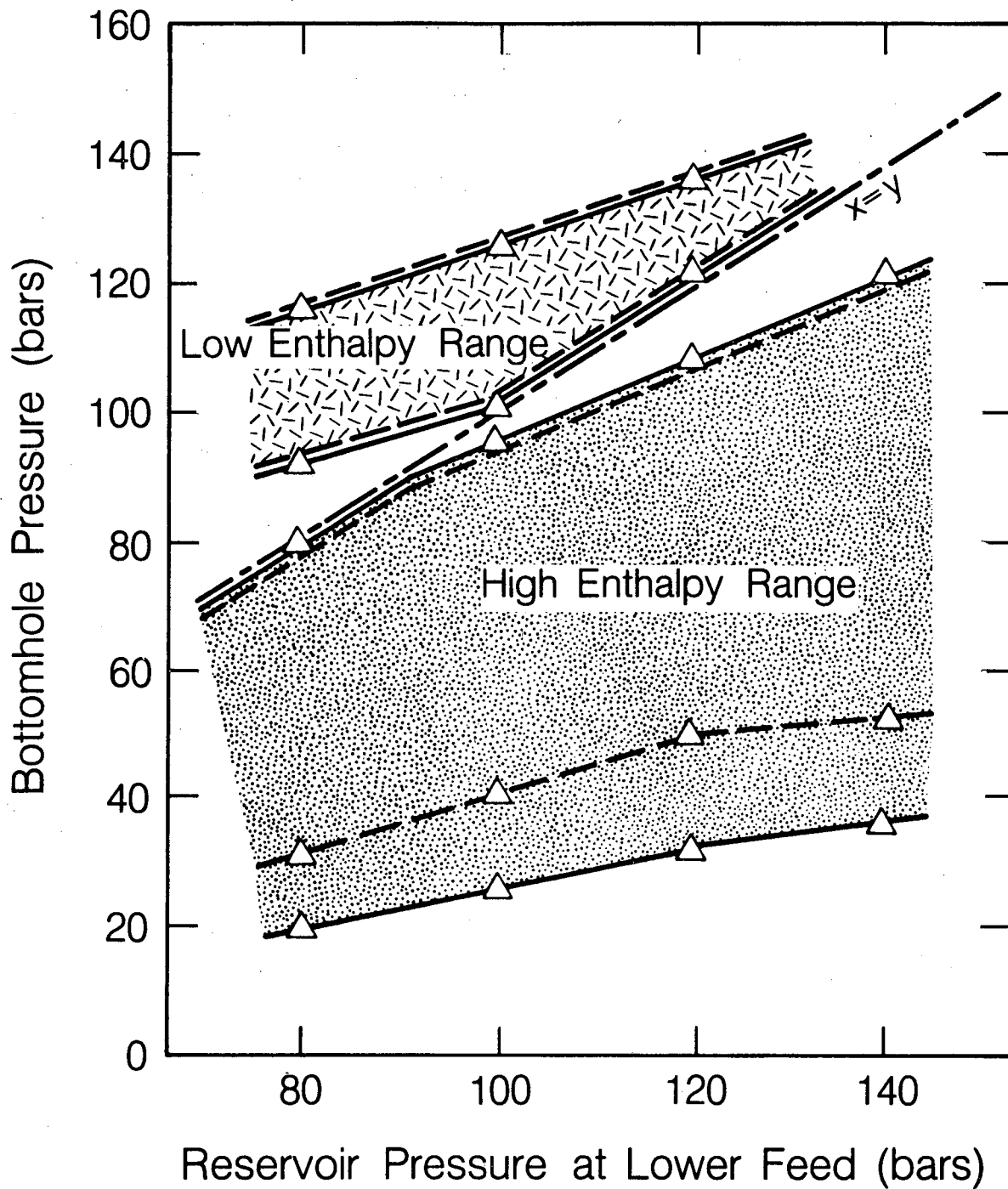


Figure 7.5 Discharge ranges for the standard well. The reservoir pressure at the upper feedzone is 80 bars. Dashed lines indicate solution boundaries for $1 \times 10^{-12} \text{ m}^3$ feedzone productivity indices, whereas the solid lines are for $5 \times 10^{-13} \text{ m}^3$ productivity indices.

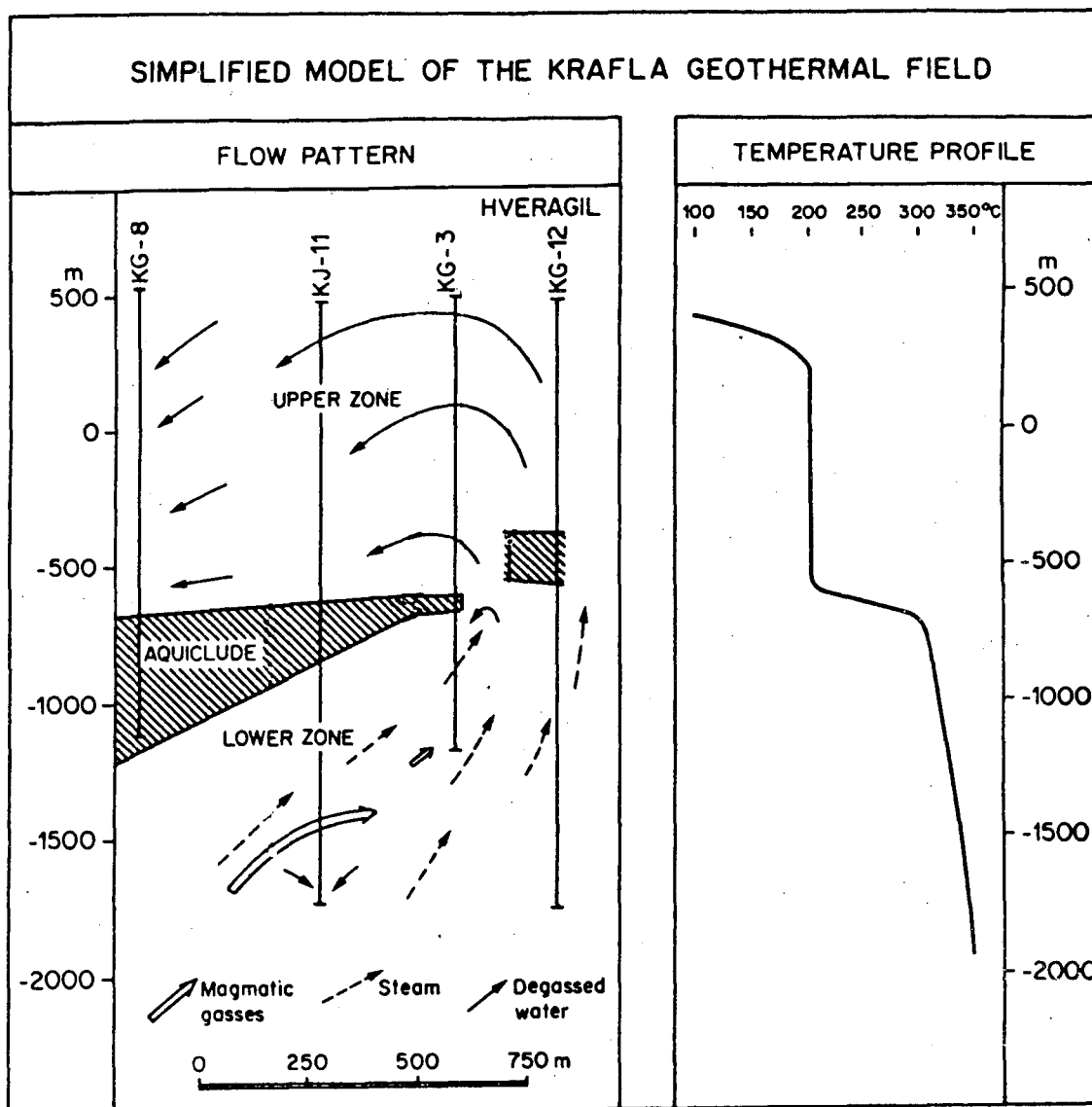
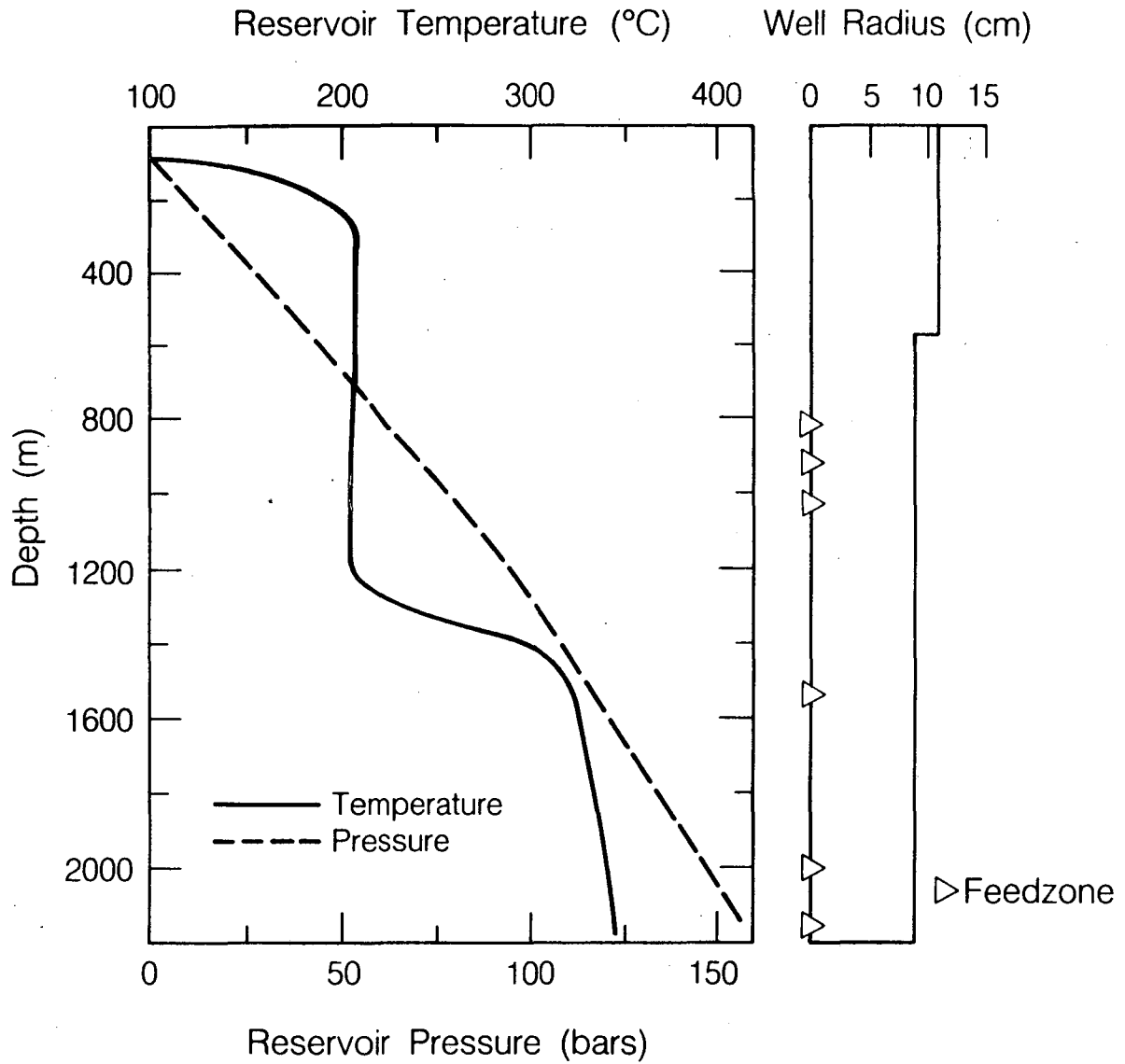


Figure 7.6 . A simplified model of the Krafla reservoir (from Stefansson, 1981).



XBL 874-10144

Figure 7.7 Estimated reservoir temperatures and pressures in the vicinity of well KJ-11. The geometry of the well and location of feedzones for the well are also shown (from Steingrímsson, 1986, personal communication).

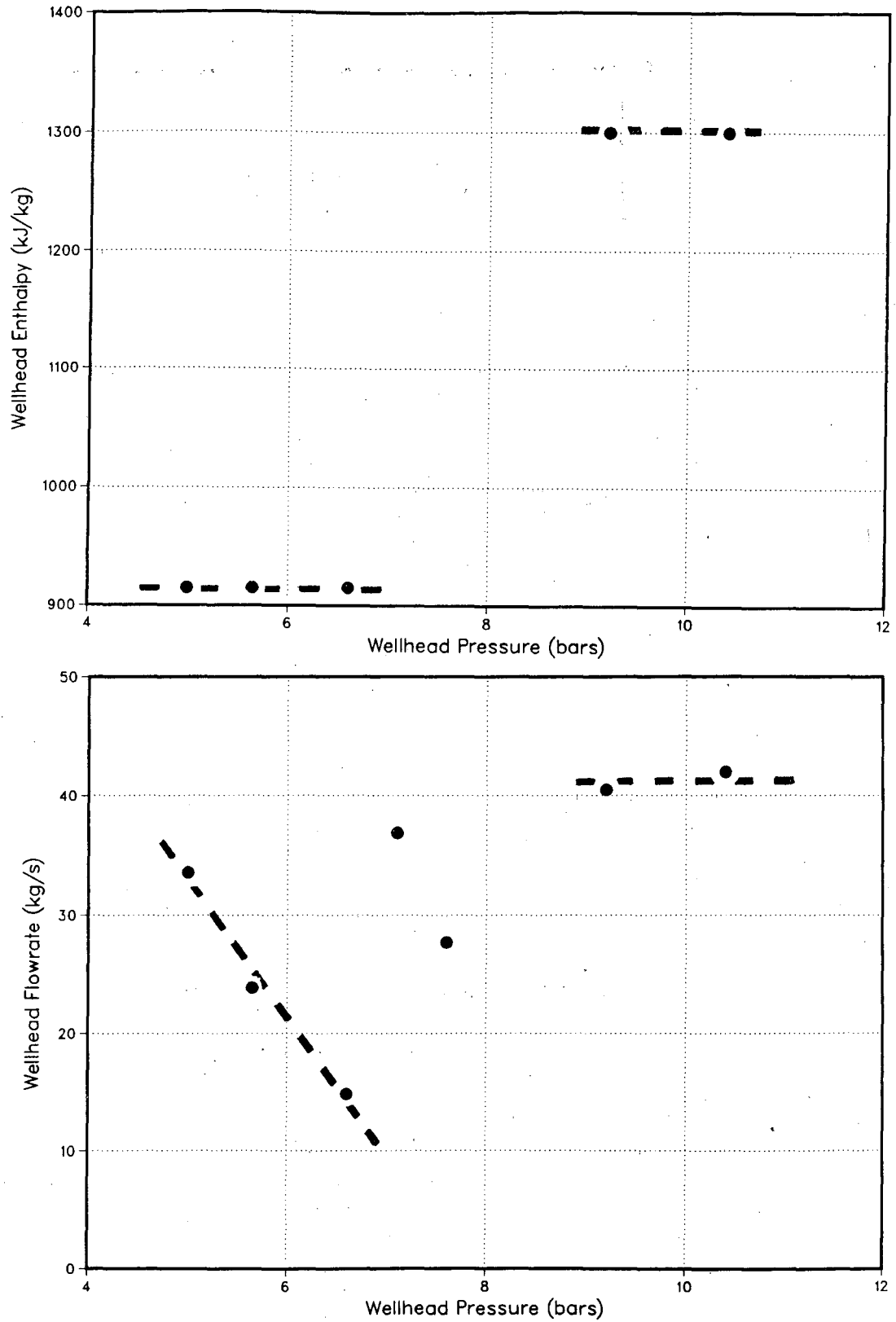


Figure 7.8 Measured wellhead output curves from well KJ-11 (from Stefansson and Steingrimsen, 1980).

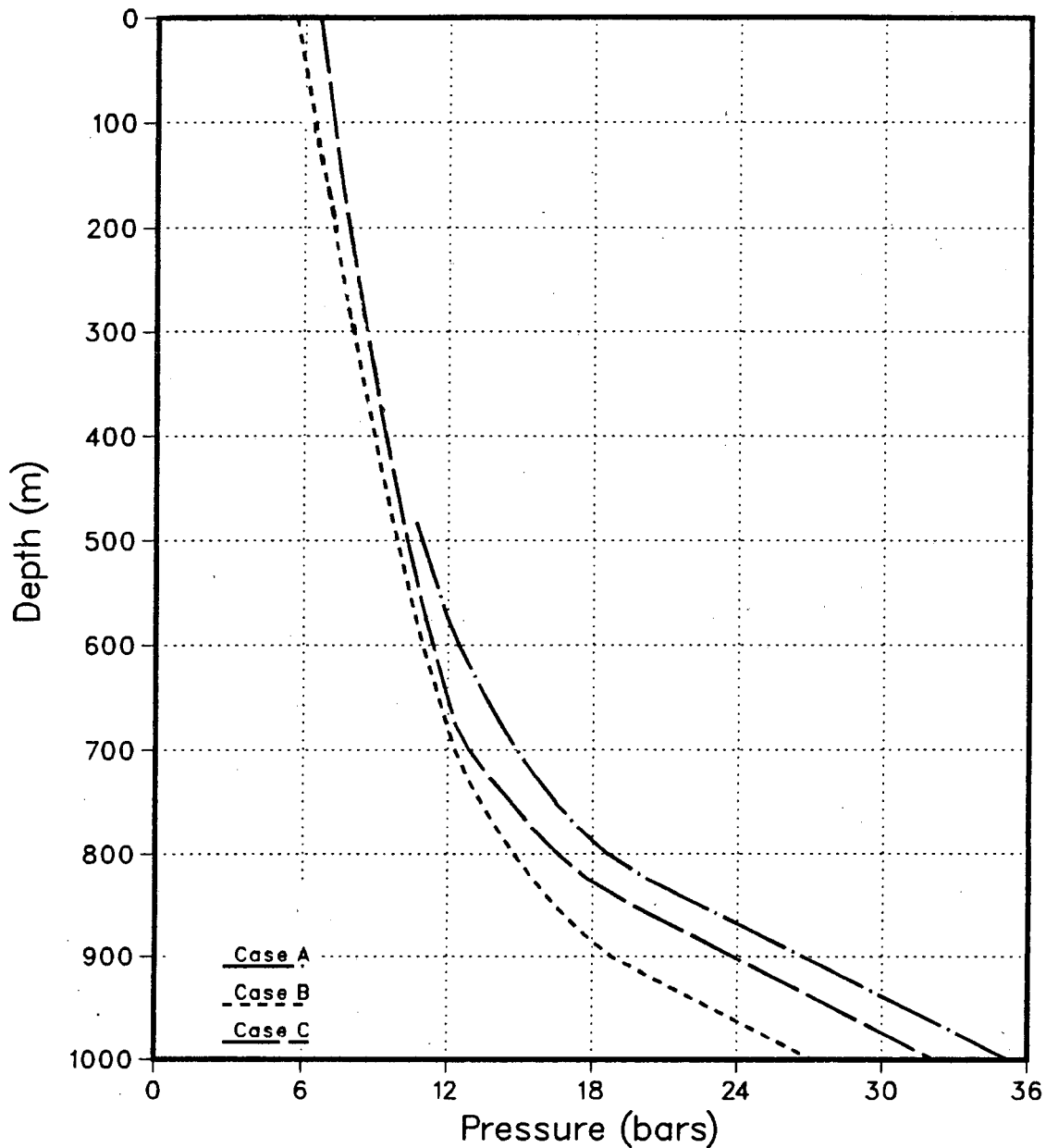


Figure 7.9 Calculated downhole pressures in well KJ-11, using the measured wellhead data in Figure 7.8. Case A represents 5.0 bars wellhead pressure and 34 kg/s flowrate, Case B is for 5.6 bars and 23.8 kg/s and Case C is for 6.6 bars and 14.9 kg/s. The wellhead enthalpy is 915 kJ/kg for all cases.

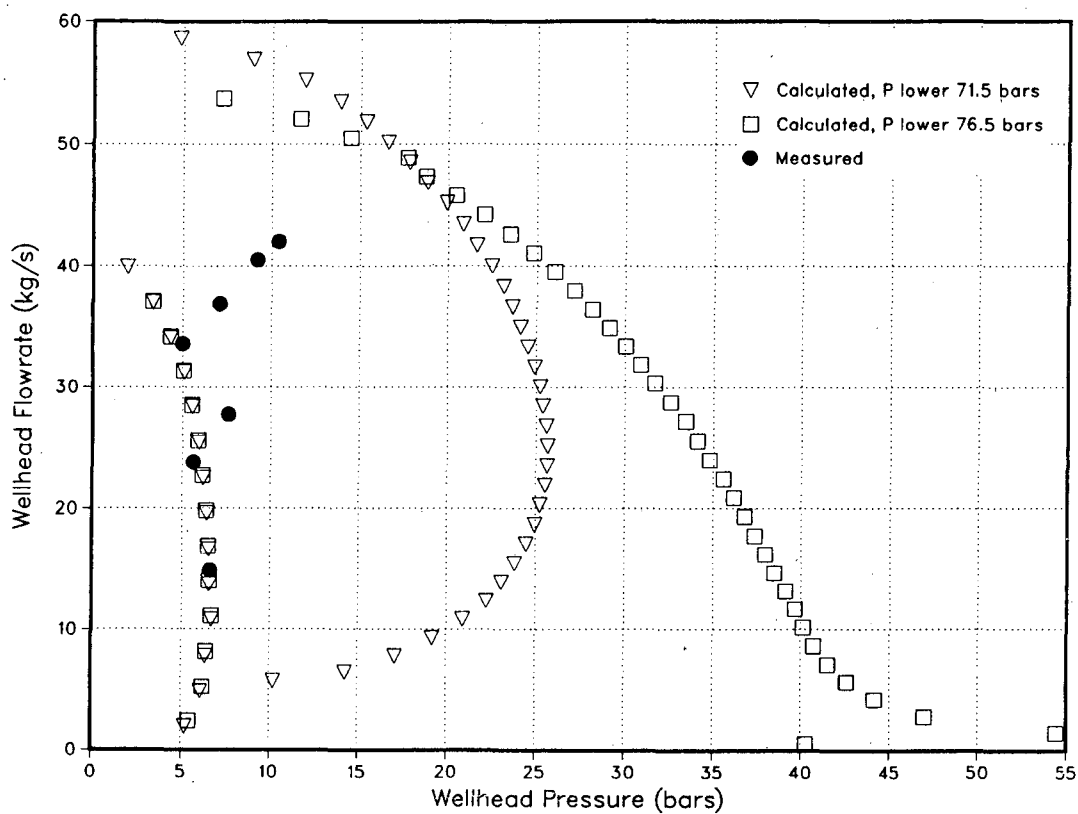
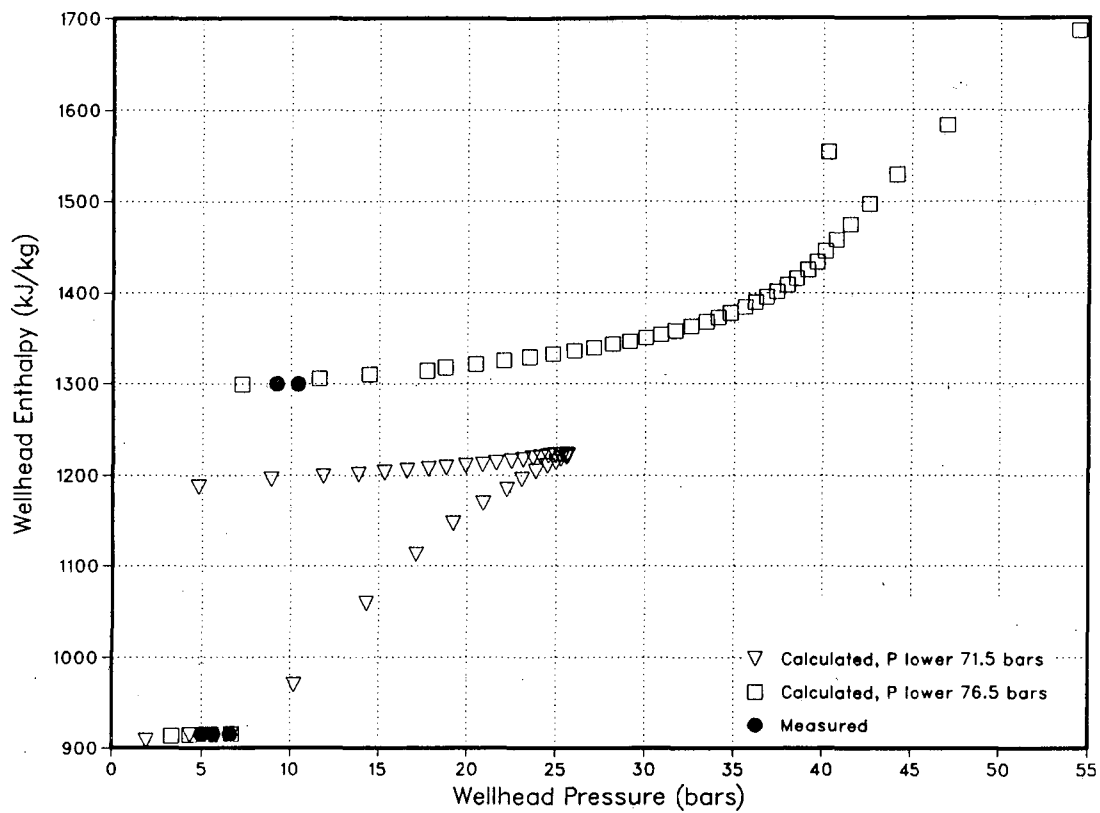


Figure 7.10 Measured and calculated wellhead output curves for well KJ-11. The lower feedzone is at 1600 m depth. See Table 7.1 for the feedzone parameters.

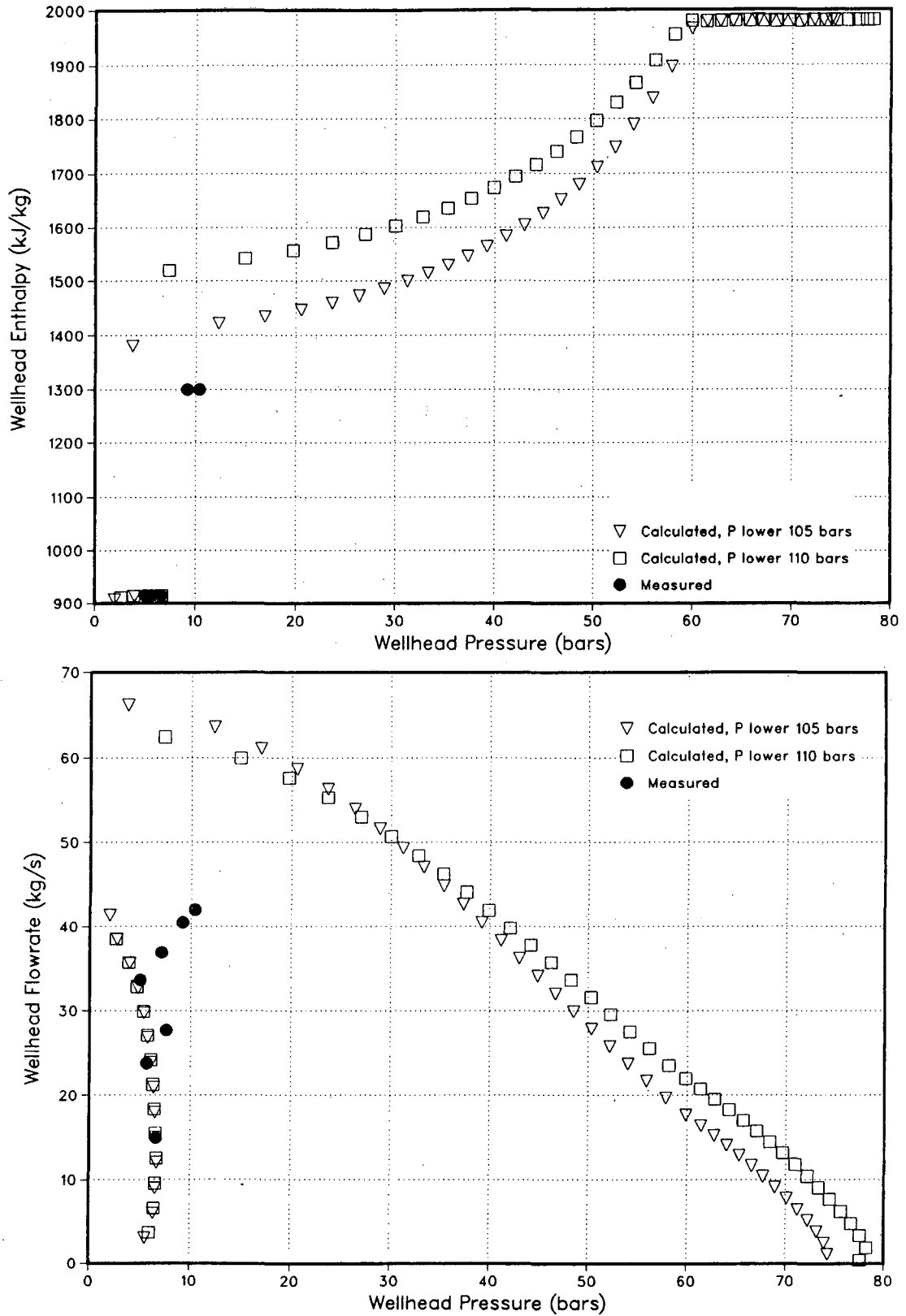


Figure 7.11 Measured and calculated wellhead output curves for well KJ-11. The lower feedzone is at 2000 m depth. See Table 7.1 for the feedzone parameters.

APPENDIX A

Input Data for HOLA

TABLE A1 An example of input file for HOLA, if one wants to calculate wellbore conditions for given wellhead parameters and given flowrate and enthalpy at every feedzone except the lowest one. The number of grid nodes is the only limit to the number of feedzones. Uses VINNA1.FOR.

Block	Numerical values	Explanation	Format
1	Textline " "		A80 " "
2	3.E+05 150. 30. 900.E+03	Wellhead pressure, Pa Wellhead temperature (not used in 2ph flow), kg/s Wellhead total mass flow, kg/s Wellhead total enthalpy, J/kg	F15.0 " " "
3	2000. 0. 2800. 1000. 1.E+05 100.	Total length of well, m Thermal conductivity, W/m/°C Rock density, kg/m ³ Heat capacity, J/kg/°C Time from initial discharge Output at x-m intervals	" " " " " "
4	800., 0.11, 0.0001, 25. 1., 0.09, 0.0001, 1. 24., 0.09, 0.0001, 24. 1175., 0.09, 0.0001, 25. 0.	1st section of well: length, radius, roughness, Δz (m) 2nd section " " " " " " 3rd section " " " " " " 4th section " " " " " " Empty line	4F10.0 " " " 4f10.0
5	3 0., 10. 1000., 200. 2000., 300.	Number of reservoir temperature data points Depth (m), temperature (°C) " " " " " "	I3 2F12.0 " "
6	0. 1. 3 850, 7.8, 700.E+03 2000, 21., 950.E+03	VELT, Armand coefficients used for phase velocities ANS, No PI-indexes, feedzone flow and enthalpy given Number of feedzones; below are feedzone properties Depth m, Flowrate kg/s, Enthalpy J/kg Depth m, Flowrate kg/s, Enthalpy J/kg	F15.0 " I3 5F14.0 "

TABLE A2 An example of input file for HOLA, if one wants to find flow conditions in a multi-feedzone well for a required wellhead pressure. Only positive flowrates but feedzones allowed at every node except the top one. Uses ITHHEAD.FOR. The zero value for the initial bottomhole pressure will used the default initial pressure, which occurs if the well is filled with 10 °C column of water.

Block	Numerical values	Explanation	Format
	Textline		A80
1	"		"
	"		"
	0.E+05	Initial wellbottom pressure, Pa	F15.0
2	0.E+05	Required wellhead pressure, Pa	"
	0.1	Allowed fractional error in wellhead pressure	"
	10.E+05	Step size in wellbottom iterations, Pa	"
	2000.	Total length of well, m	"
	0.	Thermal conductivity, W/m/ ° C	"
3	2800.	Rock density, kg/m ³	"
	1000.	Heat capacity, J/kg/ ° C	"
	1.E+05	Time from initial discharge	"
	100.	Output at x-m intervals	"
	750., 0.11, 0.0001, 25.	1st section of well: length, radius, roughness, Δz (m)	4F10.0
	1., 0.09, 0.0001, 1.	2nd section " " " " " "	"
4	24., 0.09, 0.0001, 24.	3rd section " " " " " "	"
	125., 0.09, 0.0001, 25.	4th section " " " " " "	"
	1100., 0.09, 0.0001, 50.	5th section " " " " " "	"
	0.	Empty line	4f10.0
	3	Number of reservoir temperature data points	I3
5	0., 10.	Depth (m), temperature (° C)	2F12.0
	1000., 200.	" " "	"
	2000., 300.	" " "	"
	0.	VELT, Armand coefficients used for phase velocities	F15.0
	0.	ANS, then PI-indexes, nnodes feeds and posit. or zero flow	"
6	1	Number of feedzones; below are feedzone properties	I3
	2000,110.E+05,2000.E+03,2.9E-12	Depth m, Pres. Pa, Enthalpy J/kg, PI-index m ⁸	5F14.0

TABLE A3 An example of input file for HOLA, if one wants to calculate all possible flow conditions in a two-feedzone well, with either positive or negative flowrates in feedzones and the well. The zero value for the initial bottomhole pressure, will use the default initial pressure which occurs at the bottom of the well if it is filled with 10 ° C water. Uses ITHEAD2.FOR.

Block	Numerical values	Explanation	Format
	Textline		A80
1	"		"
	"		"
	0.E+05	Initial wellbottom pressure, Pa	F15.0
2	0.E+05	Required wellhead pressure, Pa	"
	0.1	Allowed fractional error in wellhead pressure	"
	10.E+05	Step size in wellbottom iterations, Pa	"
	2000.	Total length of well, m	"
	0.	Thermal conductivity, W/m/ ° C	"
3	2800.	Rock density, kg/m ³	"
	1000.	Heat capacity, J/kg/ ° C	"
	1.E+05	Time from initial discharge	"
	100.	Output at x-m intervals	"
	750., 0.11, 0.0001, 25.	1st section of well: length, radius, roughness, Δz (m)	4F10.0
	1., 0.09, 0.0001, 1.	2nd section " " " " " "	"
4	24., 0.09, 0.0001, 24.	3rd section " " " " " "	"
	125., 0.09, 0.0001, 25.	4th section " " " " " "	"
	1100., 0.09, 0.0001, 50.	5th section " " " " " "	"
	0.	Empty line	4F10.0
	3	Number of reservoir temperature data points	I3
5	0., 10.	Depth (m), temperature (° C)	2F12.0
	1000., 200.	" " "	"
	2000., 300.	" " "	"
	0.	VELT, Armand coefficients used for phase velocities	F15.0
	-1.	ANS, then PI-indexes, 2 feeds in the well and ± flow	"
6	2	Number of feedzones; below are feedzone properties	I3
	1000, 70.E+05, 925.E+03, 1.3E-12	Depth m, Pres. Pa, Enthalpy J/kg, PI-index m ³	5F14.0
	2000, 110.E+05, 2000.E+03, 2.9E-12	Depth m, Pres. Pa, Enthalpy J/kg, PI-index m ³	5F14.0

TABLE A4 An example of input file for HOLA, if one wants to find wellbore conditions at a given, positive wellhead flowrate. Only two-feedzones possible and positive or zero flowrates in the well and in the feedzones. Uses ITHEAD3.FOR.

Block	Numerical values	Explanation	Format
	Textline		A80
1	"		"
	"		"
	57.E+05	Initial wellbottom pressure, Pa	F15.0
2	20.	Required wellhead flowrate, kg/s	"
	0.1	Allowed fractional error in wellhead flow	"
	5.E+05	Step size in wellbottom iterations, Pa	"
	2000.	Total length of well, m	"
	0.	Thermal conductivity, W/m/°C	"
3	2800.	Rock density, kg/m ³	"
	1000.	Heat capacity, J/kg/°C	"
	1.E+05	Time from initial discharge	"
	100.	Output at x-m intervals	"
	800., 0.11, 0.0001, 25.	1st section of well: length, radius, roughness, Δz (m)	4F10.0
	1., 0.09, 0.0001, 1.	2nd section " " " " " "	"
4	24., 0.09, 0.0001, 24.	3rd section " " " " " "	"
	1175., 0.09, 0.0001, 25.	4th section " " " " " "	"
	0.	Empty line	4F10.0
	3	Number of reservoir temperature data points	I3
5	0., 10.	Depth (m), temperature (°C)	2F12.0
	1000., 200.	" " "	"
	2000., 300.	" " "	"
	0.	VELT, Armand coefficients used for phase velocities	F15.0
	4.	ANS, then PI-indexes and required pos. wellhd flow	"
6	2	Number of feedzones; below are feedzone properties	I3
	1000, 70.E+05, 925.E+03, 1.3E-12	Depth m, Pres. Pa, Enthalpy J/kg, PI-index m ³	5F14.0
	2000, 110.E+05, 2000.E+03, 2.9E-12	Depth m, Pres. Pa, Enthalpy J/kg, PI-index m ³	5F14.0

TABLE A5 An example of input file for HOLA, if one wants to find feedzone flowrates when single-phase fluid is injected at the wellhead at a given flowrate. Only two-feedzones possible and negative or zero flowrates in the well and in the feedzones. Uses ITHEAD4.FOR.

Block	Numerical values	Explanation	Format
	Textline		A80
1	" "		" "
	5.E+05	Step size in wellbottom iterations, Pa	F15.0
2	0.1	Allowed fractional error in wellhead flowrate	"
	80.E+03	Wellhead enthalpy, J/kg	"
	-20.	Required wellhead flowrate, kg/s	"
	2000.	Total length of well, m	"
	2.5.	Thermal conductivity, W/m/°C	"
3	2800.	Rock density, kg/m ³	"
	1000.	Heat capacity, J/kg/°C	"
	1.E+05	Time from initial discharge	"
	100.	Output at x-m intervals	"
	800., 0.11, 0.0001, 100.	1st section of well: length, radius, roughness, Δz (m)	4F10.0
	1., 0.09, 0.0001, 1.	2nd section " " " " " "	"
4	99., 0.09, 0.0001, 99.	3rd section " " " " " "	"
	1100., 0.09, 0.0001, 100.	4th section " " " " " "	"
	0.	Empty line	4F10.0
	3	Number of reservoir temperature data points	I3
5	0., 10.	Depth (m), temperature (°C)	2F12.0
	1000., 200.	" " "	"
	2000., 300.	" " "	"
	0.	VELT, Armand coefficients used for phase velocities	F15.0
	5.	ANS, then PI-indexes and required neg. wellhd flow	"
6	2	Number of feedzones; below are feedzone properties	I3
	1000, 70.E+05, 925.E+03, 1.3E-12	Depth m, Pres. Pa, Enthalpy J/kg, PI-index m ³	5F14.0
	2000, 110.E+05, 2000.E+03, 2.9E-12	Depth m, Pres. Pa, Enthalpy J/kg, PI-index m ³	5F14.0

*LAWRENCE BERKELEY LABORATORY
TECHNICAL INFORMATION DEPARTMENT
UNIVERSITY OF CALIFORNIA
BERKELEY, CALIFORNIA 94720*